UNSTEADY FLUID FLOW AROUND CERTAIN BLUFF BODIES

by

Sisira J Polpitiye

This thesis is submitted to the University of
Leicester as a   partial fulfilment of
the degree of Doctor of Philosophy

July 1986.

UMI Number: U001373

UMI

Dissertation Publishing

ProQuest

ABSTRACT

It is shown in this thesis that fluid dynamic forces on unsteadily moving bluff bodies depend on the history of motion as much as on the velocity and acceleration of motion. An empirical relationship between the motion of the body and the resulting force is obtained by analysing the effect of the history of motion on the fluid dynamic force at any instant.

The fluid dynamic force, velocity and acceleration are obtained as functions of time, by oscillating test models in water while they are being towed at constant speed. The test models used are:
1. a two-dimensional circular cylinder,
2. a rectangular block with square frontal area and fineness ratio of 3:1,
3. a cruciform parachute canopy with arm ratio of 4:1, and
4. a ring-slot parachute canopy.

The functions by which the history of flow affects the future forces, are evaluated by using the Convolution Integral. The results show that the effects due to history of both velocity and acceleration are by no means negligible, that is the velocity and the acceleration at a specific time prior to any instant is so domineering that the fluid dynamic force can approximately be expressed as being delayed by this period of time. This 'time-delay', or time lag (as opposed to phase-lag) in the part of the measured force is found to be independent of the frequency of excitation. In the light of this evidence, a prediction model is suggested for estimating unsteady fluid forces. The data required for the application of this prediction model are obtained experimentally.

Chapter One of this thesis gives a brief explanation of the historical background of unsteady fluid dynamics. The effects of acceleration on the fluid dynamic force, in both ideal and real fluids, are discussed in Chapter Two. Explained in Chapter Three are the techniques used for building the force prediction model, and data acquisition. The experimental procedure is explained in Chapter Four. Chapter Five gives the empirical form of the prediction model, and some data that are used in association with this model.

Dedicated to my Parents

ACKNOWLEDGEMENT

OBJECTIVES

The main objectives of the research programme leading to the production of this thesis are:

1. To consider a relationship for forces on bluff bodies moving unsteadily through real fluids,

2. To develop a model form of the relationship, based on experimental results for a limited number of test models, and to discuss the advantages of and the limitations on the applications of this model,

3. To provide experimental data for modelling forces on bluff bodies moving unsteadily through real fluids, with dynamics of parachutes being the main field of application, and

4. To discuss the nature of future experiments that should be conducted for widening the scope of application of the empirical relationship.

NOMENCLATURE

A   -   Characteristic area of the submerged body.

a   -   Radius of circle or cylinder.

$A_i ; B_j$ -   Coefficients of the Fourier Series($i=0,1,2,....$; $j=1,2,....$).

A_n -   Acceleration number ($\dot{U}L/U^2$)

C_H -   Coefficient of history-dependent force (of eq. 1.5).

C_M -   Inertia coefficient (The coefficient of acceleration-dependent force component of the fluid moving past a stationary body.)

C_N -   Coefficient of velocity-dependent force component in the lateral (normal) direction: force in the lateral direction non-dimensionalised by the group $0.5\rho AU|U|$, where U is the total velocity of the body.

C_R -   Coefficient of velocity-dependent force component (the velocity-dependent force non-dimensionalised by the group $0.5\rho AU|U|$).

C_T -   Coefficient of velocity-dependent force component, in the axial direction: force in the axial direction non-dimensionalised by the group $0.5\rho AU|U|$, where U is the total ve.ocity of the body.

C_{total} -   Coefficient of the total fluid dynamic force (the total force non-dimensionalised by the group $0.5\rho AU|U|$)

D   —   Diameter of cylinder.

d_i —   Inside diameter

d_o —   Outside diameter

E   —   Young's Modulus.

F   —   Froude number.

F(t)   —   Total fluid dynamic force on a submerged body.

G   —   Rigidity Modulus.

G(t)   —   Impulse Response Function (IRF).

g   —   Acceleration of gravity.

h   —   Depth (distance from the surface of the ship tank to the centre of the test model).

I   —   Second moment of area.

I(t)   —   An input function (of time).

J   —   Polar moment of area.

k   —   Added mass coefficient (The coefficient of acceleration-dependent force component on a submerged body moving through a fluid which is stationary at infinity.); stiffness of the test sting.

k_{ij} —   Added mass coefficient in the ith direction due to acceleration in the jth direction.

K-C   —   Keulegen-Carpenter number ($U_m T/D$).

L   —   Characteristic length of the submerged body; length of test sting.

M   —   Mass of body.

m   —   Mass per unit length (of rod).

n   —   Normal unit vector to surface S; Vortex shedding frequency.

R_e —   Reynolds number based on the relative velocity

between the submerged body and the surrounding fluid.

r	–	Corner radius of a square cylinder.
S	–	Surface vector.
S_t	–	Strouhal number.
t	–	Time.
T	–	Period of oscillation.
T_f	–	Total kinetic energy of the fluid in the flow field.
$U; U_i$	–	Velocity.
U_m	–	Maximum velocity in sinusoidal motion.
$U(t)$	–	Velocity as a function of time.
$\dot{U}$	–	Acceleration (dU/dt).
U_N	–	Peak value of the oscillatory component of lateral velocity.
U_0	–	Peak value of the oscillation component of axial velocity.
U_T	–	Velocity of translation of the towing carriage.
$w(z)$	–	Complex potential function.
z	–	Complex variable, $z = x+iy$.
z_k	–	Co-ordinates of the core of the kth vortex $(z_k = x_k + iy_k)$.
$\bar{f}(z)$	–	Complex conjugate of the function $f(z)$.
α	–	Angle of attack.
α_{ij}	–	Added mass tensor $(i=1,2,..,6; j=1,2,..,6)$.
ϕ	–	Velocity potential function; phase angle.

μ   –   Dynamic viscosity of fluid.

ϱ   –   Density of fluid.

Γ   –   Circulation of fluid.

σ   –   Standard deviation.

τ   –   A time constant; the dummy variable in the convolution integral.

υ   –   Kinematic viscosity of fluid.

V   –   Reference volume; Volume of fluid displaced by the submerged body.

θ   –   Crank angle of oscillation test rig

ω   –   frequency.

Ψ   –   Phase angle.

CONTENTS

LIST OF TABLES

Chapter Five

Appendix D

Appendix E

LIST OF FIGURES

CHAPTER ONE

SURVEY OF LITERATURE RELATING TO FLUID DYNAMIC FORCES ON BODIES DUE TO UNSTEADY MOTION

INTRODUCTION

Submerged bodies in unsteady flow pose an interesting as well as a challenging problem to the fluid dynamicist. Demand for theoretical knowledge, and for data for application are increasing, for both analytical and practical reasons. Common examples of applications are: the dynamics of parachutes, airships, submarines and ships. Further applications include design of offshore structures and high-sided vehicles where engineers are required to evaluate the maximum possible fluid dynamic forces under severe loading conditions and loading frequencies.

The total fluid dynamic force acting on a submerged body is given by the vectorial sum of the pressure distribution and the skin friction over the entire surface. Such forces, for incompressible, infinite fluids, depend on a number of parameters:

1. the geometric shape of the body and its attitude of motion;

2. the nature of motion of the body and that of the surrounding fluid: whether linear, angular or oscillatory;

3. the magnitudes of the velocity and the acceleration of the body and those of the surrounding fluid; and

4. the Reynolds number of the flow.

Effects of free stream disturbances, fluid surfaces and other nearby boundaries may also occur under special circumstances. It is required for analytical and design purposes to estimate these forces using either theoretical or experimental model expressions.

The fluid dynamic force on a particular shape of body with a certain attitude of motion is commonly considered to consist of two components:

1. velocity-dependent force:

   This force component is a function of the relative velocity between the body and the surrounding fluid. It is common to relate this force, in non-dimensional forms, to, the Reynolds number of flow.

2. acceleration-dependent force:

   This component of the total force is a function of the acceleration of the body and that of the free stream. The kinetic energy of the fluid which is otherwise undisturbed is increased by the presence of a submerged body. This increase of kinetic energy due to the submerged body continuously changes if the motion of the body is unsteady. In such state the acceleration-dependent force is associated with the rate of change of energy imparted by the body to the surrounding fluid. These forces are normally related to non-dimensional form of acceleration and oscillation. They may also depend on the Reynolds number of flow.

If the fluid at infinity is not at rest, the acceleration of the free stream produces a pressure gradient[1a] analogous to the force of buoyancy due to the acceleration of gravity. In the case of an accelerated free stream the presence of this buoyancy force, enhances the acceleration-dependent force. Correspondingly it reduces this force for a decelerating free-stream.

If the fluid dynamic force is considered to consist of two components as stated above, it is logical to model both velocity-dependent and acceleration-dependent components of this force by suitable coefficients introduced in each term. It then remains to determine these coefficients either theoretically of experimentally for various shapes of bodies so that for unsteady motion by using these determinations the total force on these bodies can be predicted at any instant in time. Experimental methods of determining these coefficients normally include measuring total forces on submerged bodies by imparting known modes of motion.

Since for any particular direction of motion there are two empirical coefficients involved they can be determined from experimental results only if either one or both of them are assumed to be constants. These coefficients can then be used under similar circumstances to predict the fluid dynamic forces. The reliability of the numerical values obtained for these coefficients depends on their consistency in correlation with various independent parameters, such as Reynolds number or non-dimensional acceleration (acceleration number) or the effect of flow history.

The parameters influencing the fluid dynamic force due to unsteady motion are discussed in the first two chapters of the thesis. In Chapter Five the coefficients involved in the prediction models are correlated with these parameters.

SURVEY OF LITERATURE RELATING TO FLUID DYNAMIC

FORCES ON BODIES DUE TO UNSTEADY MOTION

1.1 INTRODUCTION

Under steady conditions, incompressible fluid dynamic forces on submerged bodies are developed because of circulation of fluid in the vicinity of the body. In potential flow fields these forces can be derived analytically but in real fluid motion the analytical approach fails because the exact circulation of the surrounding fluid is not known. This circulation arises, partly as a result of dissipation due to the boundary layer and flow separation, and partly due to the asymmetry of the flow field as illustrated by the flow around aerofoils. The analytical methods of deriving forces on submerged bodies where there is flow separation are known to be complicated and inaccurate. Therefore, the forces are normally determined by experimental methods. The experimentally measured forces are suitably non-dimensionalised by the group $0.5\rho U^2 A$, where U is the relative velocity between the body and the free stream and A the characteristic area, to obtain a coefficient C_R. For most geometric shapes correlations between C_R in steady flow and Reynolds number have successfully been achieved in the past. Numerous examples can be found in reference [13].

The mechanics of accelerated flow past solid bodies have been studied by many authors although success in extending the analysis beyond potential flow theory has been somewhat limited. Consequently, the demand of data for practical applications is yet to be fulfilled.

The unsteady forces depend on acceleration, as much as on velocity of motion. The total force F(t) can be expressed by a function f, such that[12]

$$F(t) = f(\varrho, L, \upsilon, U, \dot{U}) \qquad (1.1)$$

For arbitrary modes of motion the parameters on the right hand side of equation (1.1) at any instant in time are independent of each other. Hence dimensional analysis permits:

$$\frac{F(t)}{0.5\varrho U^2 A} = f\left(\frac{\varrho UL}{\upsilon}, \frac{\dot{U}L}{U^2}\right) \qquad (1.2)$$

However, unlike steady motion, there are numerous different ways of imparting acceleration to a body. e.g. purely accelerated motion, motion started from rest and oscillatory motion with or without mean velocity. The flow field produced by each mode of motion is often different from others, even at instants when the velocity and acceleration from one mode of motion are identical to those of another. Thus, the fluid dynamic forces for these conditions can differ from each other substantially. Therefore, compared with steady flow, the number of

parameters involved is substantially more than those equations (1.1) and (1.2) show, and the analyses become relatively harder. Assumptions and approximations made, in order to simplify the analysis and correlate data, vary from one researcher to another.

This substantial increase in complexity is mainly due to the forces that are acceleration-dependent. Although the existence of the acceleration-dependent forces has been known for more than a century, experimental data available are hardly adequate for predicting such forces.

1.1.1 Acceleration-Dependent Force and The Concept of Added Mass

A solid body in motion in a fluid also sets the surrounding fluid in motion. Acceleration-dependent forces arise because of either the increasing or the decreasing velocity of the body. This in turn either increases or decreases the rates at which both the kinetic energy and the momentum are imparted to the surrounding fluid. The rates at which the kinetic energy and the momentum of the fluid increase, demand additional work and forces to be applied to the moving body.

The effect of acceleration-dependent force on a submerged body is significant (a) at velocities where the magnitude of the acceleration-dependent force is comparable with the velocity-dependent force and (b) when the mass of the submerged body is similar in magnitude to that of the displaced fluid, thus the inertia of the body is comparable with that of the fluid around it.

1.1.1.1 Acceleration-Dependent Forces in Potential Flow

By integrating over the entire flow field the kinetic energy of the fluid disturbed by a moving submerged body, Lamb[25] showed that, in a potential flow field, the rate of change of kinetic energy of the disturbed fluid is a finite quantity proportional to that of the body itself. Thus, the whole effect of the presence of the fluid can be effectively replaced by a mass proportional to that of either the displaced fluid or a reference volume of fluid, the proportionality constant being a function of the geometric shape of the body and its attitude of motion. This increased mass is commonly known as the 'added mass' and is equal to $k\rho V$ where ρ is the density of the fluid, V a reference volume which usually is the volume of fluid displaced by the body and k the coefficient of acceleration-dependent force or the coefficient of added mass. For some bodies, e.g. parachute canopies, the volume of fluid which they displace is not readily determinable and it is for this reason that an arbitrary reference volume is defined. Since k, in potential flow, depends on the geometric shape of the body and its attitude of motion only, the concept of added mass becomes a useful method of avoiding the complicated process of deriving the fluid dynamic force by analysing the pressure distribution around the body.

An analogous term, 'drift mass' which is equal to the added mass was introduced by Darwin[10] who analysed the mass of the fluid displaced by a moving solid object (fig.1.1).

For fluids accelerating over bodies rather than bodies accelerating in fluids which are otherwise at rest, the acceleration-dependent force is further increased by a force equal to $\rho \dot{V}U$ due to the pressure gradient in the free stream. The coefficient of acceleration-dependent force thus becomes, C_M = k + 1.0. Details of more general forms of motion in which both the body as well as the surrounding fluid have accelerations, can be found in page 24 of the paper by Hogben[14].

The complex potential function in an ideal fluid can be established analytically because the potential flow field around a certain body is unique. In the case where a body is moving in an otherwise undisturbed fluid, it depends only on the shape and attitude of the body and the instantaneous velocity of the body relative to the surrounding fluid. The velocity at any point in the fluid, for unit relative velocity of the body, is invariant. Therefore, the kinetic energy of the surrounding fluid is always proportional to that of the body. i.e. the added masses in potential flow are unique and they can be derived analytically. For defined reference axes they depend only on the body shape and its direction of motion: linear or angular.

Given in table 1.1 are values of coefficients of added mass in potential flow for some common geometric shapes[16,33].

1.1.1.2 Acceleration-Dependent Forces in Real Fluids

Forces on moving bodies in potential flow fields can conveniently be calculated analytically because the corresponding complex potential functions can be determined. The flow fields associated with real fluids, however, are different from those of ideal fluids because of the boundary layer developed around the immersed body and the resulting flow separation. Therefore, for bluff bodies for example, the added masses based on potential flow analysis often have little or no practical relevance. Where analytical methods of determining added masses fail, recourse is made to experimental methods. Consequently, in order to estimate the fluid dynamic forces due to unsteady motion fluid dynamicists and engineers are required to depend on published experimental data.

1.2 EXPERIMENTAL RESULTS FOR UNSTEADY FLOW AROUND BODIES

Because of their viscous properties real fluids behave differently from ideal fluids. Thus the real fluid flow around submerged bodies are often very different from those in potential flow. Nevertheless, there are specific circumstances under which similarities can be observed between flows of real and ideal fluids around bodies.

1.2.1 Similarities Between Real Fluids and Potential Flow

Past experimental results have shown that in certain modes of motion, the added mass for a real fluid can be very similar in magnitude to that for an ideal fluid.

Keulegan and Carpenter[22] conducted experiments by measuring forces on stationary cylinders due to waves. At low amplitudes of oscillation the experimental coefficient of acceleration-dependent force was found to be very close to the potential flow value. Sarpkaya's[36] experimental results for unseparated flow around cylinders have shown that the total fluid dynamic force consists, almost entirely, of the acceleration-dependent force only. Such resemblances between theoretical and experimental values will occur under certain circumstances:

1. Around stream-lined bodies real flow is not dissimilar to that in potential flow. Therefore, the fluid dynamic forces for such bodies are close to those in ideal fluid.

2. In low amplitude oscillatory motion of either the submerged body or the surrounding fluid the amplitude of oscillation may not be sufficiently large for flow separation to occur. The flow field, therefore, remains similar to that in potential flow, and

3. During early stages of motion started from rest, sufficient time will not have elapsed for flow separation to occur.

For such cases since real flow fields around bodies without sharp edges are similar to those of potential flow, experimental values of fluid dynamic forces are very similar to the theoretical ones.

1.2.2 Flow Around Bluff Bodies

However, if the actual flow field is very different from potential flow, the experimental results discussed above have little practical relevance. This is often the case for flow around bluff bodies. By nature, bluff bodies differ from stream-lined bodies, because over a large region of the body surface there is flow separation, making the flow field substantially different from those in potential flow. Therefore, any analysis of the fluid dynamic forces must be based on appropriate experimental data. Thus, experimental data are required in order that forces on bluff bodies may be estimated, for practical applications.

1.3 A RELATIONSHIP FOR FORCES IN UNSTEADY MOTION

In the present text it will be considered that the fluid dynamic forces on submerged bodies occur due to two reasons: (a) the effect of circulation in the flow field around the body. As von Karman and Sears[21] have shown the corresponding force is given by the rate of change of total momentum associated with the circulation, and (b) the effect due to added mass. The former is normally associated with the relative velocity between the submerged body and the surrounding fluid. The latter is effective when there is acceleration of either the body or the fluid. Therefore, by considering the fluid dynamic force to be of two components, one that is velocity-dependent and the other that is acceleration-dependent, it can be expressed using a formula of the type given by Morison's wave equation[28] as

$$F(t) \; . \; = \; C_R \; 0.5 \varrho A \; U|U| \; + \; k \varrho V \; dU/dt \qquad (1.3)$$

where, $|U|$ is the modulus of the velocity. The non-dimensional parameters C_R and k are the coefficient of velocity-dependent component and the coefficient of acceleration-dependent component of the total force. In real fluids these coefficients must be determined from experimental results. The data are then applied for estimating forces on submerged bodies at various stages of their unsteady motion.

1.4 RELATIVE IMPORTANCE OF THE MAXIMUM FLUID DYNAMIC FORCE AND THE INSTANTANEOUS FORCE

The nature of the data required for predicting forces in unsteady motion depends very much on the applications of such data. In designing offshore structures, for example, the emphasis is on the maximum forces, and the frequencies of loading. For ships submarines, airships and parachutes instantaneous forces rather than the maxima are relevant, because the dynamics of such bodies continuously depend on the external forces at any instant in time. Thirdly, in analysing the stability of a high-sided vehicle, subjected to lateral gusts, one is interested not only on the maximum values of the forces, but the period over which such forces are sustained.

An investigation was conducted by the author at the early stages of the present research programme, to estimate fluid dynamic forces on transportation vehicles, and to

analyse the relative magnitude of the acceleration-dependent force component. The investigation included deriving the fluid dynamic forces on high-sided road vehicles, due to lateral gusts. The gust velocity was idealized by a sine function for convenient calculation procedures. Figure 1.2 shows the variation of the fluid dynamic force due to the lateral gust, based on average values of experimentally determined force coefficients. The immediate significance of the graph is that although the acceleration-dependent force is relatively high, being about 23% of the maximum value of the force for low velocities, it has very little effect on the maximum force of the gust (about 6%). The main reason is that the maximum value of the fluid dynamic force is dominated by the velocity of flow. At points where the velocity is maximum, the acceleration is zero. Therefore, the effect of the acceleration-dependent component can be ignored when analysing the fluid dynamic forces on high-sided vehicles, without seriously affecting their stability.

Although forces on either ships or submarines due to sea waves have characteristics similar to those of gusts, the overall effect is somewhat different. The peak values of forces do have a bearing on the stability and structural loading on these vessels. Forces during stages other than the peak force have continuous effects on their motion, both in direction and magnitude. Furthermore, the frequencies of loading may lock-in with the natural frequencies of vibration or vortex shedding, and therefore, require

attention. This argument applies, not only to ships, but to airships and parachutes.

In general, wherever external forces continuously affect the motion, both velocity and acceleration-dependent force components are significant. Thus, data for predicting forces due to unsteady flow are used in two fundamentally different applications:

1. to estimate the maximum fluid dynamic forces and the natural frequencies. (e.g. gusts loading on high-sided vehicles; wave loading on offshore structures). The objective is to analyse the structural stability under various loading conditions;

2. to predict dynamic behaviour and to evaluate dynamic stability of airships, parachutes, ships and submarines and to analyse the continuous effects of forces arising from the movements due to manoeuvring and external disturbances.

Therefore, the nature of data published by various authors tend to be different from one to another, because of the different interests they pursue in terms of applications. For example, in purely translational motion instantaneous acceleration number has been considered as a suitable independent parameter to which the force coefficients can be related[17]. On the other hand Keulegan and Carpenter[22] related coefficients of forces produced by waves on cylindrical components, to the ratio of 'amplitude of wave motion/diameter of cylinder'. The applications of these

published data can be limited to the circumstances under which the experimental results have been acquired.

1.5 ACQUISITION OF EXPERIMENTAL DATA FOR FORCE COEFFICIENTS

Equation (1.3) has been used in many forms in order to analyse forces on the bodies submerged in real fluids in time dependent motion. Experimental methods used for deriving non-dimensional force coefficients date back to early parts of this century. Outlined briefly in the following sections of this chapter are certain developments in unsteady fluid dynamics, leading up to the present study of research.

1.5.1 Evaluating Force Coefficients from Experimental Results

An expression such as Morison's equation (eq.1.3) used to represent forces in unsteady motion includes two unknowns: C_R and k. i.e. experimental values of F(t), U and dU/dt lead to simultaneous equations. Unless predetermined values are substituted for either C_R or k, these equations can be solved to evaluate these coefficients only if either one or both are assumed to be constants (with respect to time). Therefore, any experimental method by which the coefficients in equation (1.3) are evaluated, must be accompanied by suitable assumptions in order to simplify the process of evaluating these coefficients.

1.5.2 Quasi-steady Assumption

A quasi-steady expression is defined by a model such as Morison's equation, in which the coefficient of velocity-dependent force C_R is assumed to possess a value equal to that in steady flow. This assumption substantially simplifies the process of deriving the coefficients of acceleration-dependent force, because steady flow data for most geometric shapes of bodies are readily available from publications such as that of Hoerner[13]. Consequently, the only unknown in equation (1.3) is calculated by measuring forces on submerged bodies, due to known velocities and accelerations involved in the unsteady motion.

Using steady flow values of C_R for spheres moving through water, Frazer and Simmons[12] obtained coefficients of acceleration-dependent force that varied from 0.87 (for low velocities) to 3.4, (for high velocities), compared with 0.5 for potential flow. Iversen and Balent[17], using circular plates moving perpendicular to their planes, obtained coefficients which were much higher than their theoretical values. Furthermore, as can be seen in figure 1.3 the uncertainty of these coefficients for low acceleration numbers (A_n) was considerable. Experimental values obtained by Relf and Jones[32] were 87% higher than corresponding theoretical values for spheres, and up to 40% higher for streamlined airship models. Using a torsional pendulum immersed in various liquids Yu[44] obtained the added mass of circular discs and short cylinders. The experimental values of added mass for circular discs were

found to be 28% higher than the corresponding potential flow values.

These higher values of acceleration-dependent force, obtained by different experiments show that the added masses involved in real fluids, derived using quasi-steady assumption, are generally greater than those in an ideal flow. This additional added mass may occur as a result of the attached boundary layer and the downstream wake due to flow separation, thus increasing the mass of fluid 'attached' to the body.

This quasi-steady mathematical model has was used for evaluating acceleration-dependent force coefficients of fully inflated parachutes[43,42,8]. The steady values of velocity-dependent force coefficients for various angles of attack were evaluated by towing model parachutes in fluids, at constant speeds. Typical data for added mass coefficients for parachute canopy models are shown in figure 1.4.

1.5.3 Average Force Coefficients in Oscillatory Flow

An alternative method of determining the coefficients in equation (1.3) is to assume that for a given type of motion both C_R and k are constants.

Studies of wave forces on offshore structures led Keulegan and Carpenter[22] to calculate average force coefficients in oscillatory flow. They investigated the case in which the velocity and the acceleration of fluid in the region where the body is submerged are considered to be sinusoidal. Thus the acceleration of flow always leads the

velocity by 90 degrees. The velocity-dependent and the acceleration-dependent components of the total force were separated by Fourier Transformation and the coefficients of the Fourier series were used to derive the average values of force coefficients.

Having found no correlation between the Reynolds number of flow and the force coefficients, Keulegan and Carpenter introduced the periodic parameter which relates the amplitude of oscillation induced by waves to the characteristic length of the submerged body. This non-dimensional parameter, $U_m T/D$ is now commonly known as the Keulegan-Carpenter number (U_m: maximum velocity of the cycle; T: period of sinusoidal oscillation; D: characteristic length.) Figures 1.5a and 1.5b show some typical values of force coefficients given by Keulegan and Carpenter. The correlation between the Keulegan-Carpenter number and the force coefficients was also confirmed by later researchers. A comprehensive review of average force coefficients obtained by different authors can be found in reference [15]. It is now popular to present, mainly for design applications in offshore structures, experimental data showing force coefficients correlated with Keulegan-Carpenter number. Since these data were determined using simple harmonic motion their application may well be limited.

Bearman et al[2] conducted experiments using square cylinders with different corner radii. The sinusoidal motion was imparted using a U-tube filled with water. The force coefficients of velocity-dependent force and

acceleration-dependent force were correlated with Keulegan-Carpenter number. They concluded that the effect of the corner radius r, for square cylinders of width D is such that the minimum value of the coefficient of velocity-dependent force occurs when the ratio r/D is about 0.3. By contrast, in steady flow the coefficient of fluid dynamic force is a minimum when r/D is equal to 0.5 - i.e. for circular cylinder[13].

1.5.4 Application of Potential Flow Coefficients

Assuming that the coefficient of acceleration-dependent force is equal to that in potential flow and using Morison's equation (eq. 1.3), Maull and Milliner[26] estimated the instantaneous values of velocity-dependent forces on circular cylinders in oscillatory flow. The coefficients of velocity-dependent force were calculated using experimentally obtained forces in equation (1.3). They used water oscillating in a U-tube as their working medium. The oscillatory forces were based on purely sinusoidal flow, with no mean velocity. One significant phenomenon seen in their results is that the maximum value of velocity-dependent force occurs not when the velocity in the cycle is maximum but at a time just after this maximum velocity. Maull and Milliner extended their studies by relating the velocity-dependent component of the force to the movements of the vortices shed by the cylinder. Considering a control volume, around which the total circulation of fluid is zero, they derived a

relationship between the circulation around the cylinder and its fluid dynamic force. Using this relationship they argued that it is possible for the velocity-dependent in-line force to reach its maximum at an instant after the maximum velocity of the cyclic motion. Furthermore, the experimental results showed that the coefficients of velocity-dependent force at points near the extreme ends of the cyclic motion can have negative values.

Sarpkaya and Garrison[35,37] modelled the forces on a circular cylinder due to flow started impulsively from rest to a constant speed. Using the rate of change of momentum of the vortices in the flow field and considering three stages of flow development - start of separation; shedding of symmetric vortices; and shedding of asymmetric vortices - they were able to model force coefficients that agreed with the experimental results (see fig.1.6).

Von Karman and Sears[21] analysed lift forces on aerofoils in non-uniform flow by analysing the circulation around the body and that around the trailing vortices. They represented the total lift force by three components:

1. a component due to the added mass,

2. a quasi-steady lift force analogous to the steady flow lift force and

3. a component that depends explicitly on the vorticity distribution in the wake.

Effects on the fluid dynamic force due to the vortices in the flow field are discussed in Chapter Two of this thesis.

1.5.5 Application of Experimentally Obtained Data

As discussed in the previous section, numerous methods have been used to obtain the force coefficients in unsteady motion. A summary of published data based on experimental methods, is given in Table 1.2. There are discrepancies among data for certain coefficients obtained by different authors. Whether these results are reliable for engineering applications is open to question, because of these discrepancies. Undoubtedly, more experimental work is required to build a bank of 'consistent' data, so that unsteady fluid dynamic forces under a variety of conditions can be modelled with confidence. Furthermore, experimental methods are important because fluid dynamicists should understand better the physics involved in unsteady flow of real fluids.

1.6 EFFECT OF FLOW HISTORY

The model relationship given by equation (1.3) on which the experiments mentioned in Section 1.5, were based, has two essential features:

1. It implies that the fluid dynamic force at any instant in time consists of two components: (a) a velocity-dependent force, and (b) an acceleration-dependent force.

2. The instantaneous fluid dynamic force depends only on the values of velocity and of acceleration at that instant.

The way in which the motion is imparted does not appear in equation (1.3). It fails to recognise that real fluids possess a 'memory' effect, due to their viscous properties, that would have some influence at subsequent instants. i.e. the velocity and acceleration at previous stages of motion are known to affect the fluid dynamic force at later stages. Vortices in the wake, for example, which have certain influence on the circulation around the submerged bodies have been shed at previous instants. Since the fluid dynamic force on the body strongly depends on the circulation around it, the history of motion should be included in any form of expression designed to model these forces. By doing so the physics of unsteady flow is more appropriately represented.

1.6.1   Flow History Effects in Stokes Flow

Theoretical analysis of the effects due to history of motion on fluid dynamic force was made as early as 1851, by Stokes[40], and later by Basset[1] and by Lord Rayleigh[31]. The analysis was valid only for Stokes flow (i.e. very low Reynolds number flow), where the flow is laminar. The flow field in laminar flow can be solved using the Navier-Stokes equation. The fluid dynamic forces can be derived analytically by neglecting the convective terms. The total force on a sphere as expressed by Lord Rayleigh[31] consists of the following components.

1. The velocity-dependent component, analogous to that in steady flow, which is a function of the relative

velocity between the body and the fluid, (hence the Reynolds number of flow).

2. The acceleration-dependent force which consists of two components:

(a) the force due to the motion of the fluid surrounding the body, which would be the same when the fluid is inviscid, and

(b) the force due to the history effect of flow which would vanish either when the fluid is inviscid or when there had been no acceleration for a long period of time.

Rayleigh[31] expressed the total force on a sphere of diameter D, in very low Reynolds number flow as:

$$F(t) = \rho V \left\{ \frac{18\upsilon}{D^2} U + \frac{1}{2} \frac{dU}{dt} \right.$$
$$\left. + \frac{9}{D} \sqrt{(\upsilon/\pi)} \int_{-\infty}^{t} \frac{\dot{U}(\tau)}{\sqrt{(t-\tau)}} d\tau \right\} \qquad (1.4)$$

where U(t) is the free-stream velocity and τ is a dummy variable.

Equation (1.4) has since been used by Brush et al[7], Ordar and Hamilton[29] and Karanfilian and Kotas[20] in the modified form given in equation (1.5) in which the velocity-dependent component was replaced by a term which is proportional to the free stream dynamic pressure.

$$F(t) \quad . \quad = \quad C_R \; 1/2\rho AU|U| + C_M \rho V\dot{U}$$

$$+ \; C_H L^2 \; \sqrt{(\pi\mu\rho)} \int_{-\infty}^{t} \frac{\dot{U}(\tau)}{\sqrt{(t-\tau)}} d\tau \qquad (1.5)$$

where, C_R, C_M and C_H are the respective coefficients of velocity, acceleration and history dependent components of the total force. This modification was included so that the expression could be used for moderate and high Reynolds number.

The Reynolds number range, for spheres, in experiments of Brush et al[7] was 1.0 to 540. After claiming satisfactory correlations between the experimental results and the model form given by equation (1.5) Brush et al emphasized the need for more studies in unsteady flow. In simple harmonic motion of spheres, Odar and Hamilton[29] used steady flow coefficients of velocity-dependent force to derive the coefficient of acceleration-dependent component, for instants during the cycle when the history effect is expected to be zero. The coefficient of the history-dependent force component was then evaluated using these values of C_R and k. The maximum Reynolds number for these experiments was 62. Using simple harmonic motion for spheres, Karanfillian and Kotas[20] obtained experimental results for Reynolds numbers in the range 100 to 10,000. They used published data of steady flow force coefficients, to evaluate the coefficients of history-dependent force by considering instants at which the acceleration dependent force is zero. They concluded that the average values of

the coefficients of acceleration-dependent force and history effects were similar to their theoretical values of 0.5 and 1.5 respectively.

The author is unaware of any industrial applications of either these results or the model relationship given by equation (1.5).

1.6.2 Functional Analysis Applied in Unsteady Motion

Applying linear theory in ship dynamics, Bishop et al.[4,5,6] related the motion, as a function of time, to the fluid dynamic force on scaled ship models. The velocity of the ship model was expressed as a series of impulses. The total force on the ship was modelled by adding the 'effect of each impulse of motion'. If the force due to a unit impulse of velocity is given by G(t), the total force due to the velocity U(t), and its history was expressed, using the convolution integral, as

$$F(t) \quad = \quad \int_{-\infty}^{t} G(t-\tau) \ U(\tau) \ d\tau \qquad\qquad (1.6)$$

where, function G(t), known as the Impulse Response Function (IRF) was determined from experimental results. This function accounts for the whole time history of U(t). The analysis was simplified by assuming slow motion derivatives, thus ignoring the effects of higher order derivatives of the velocity of the ship models.

Strictly speaking equation (1.6) is applicable only for linear systems where the total force due to a certain

function of motion is made up of the vectorial sum of the elemental forces due to the elemental velocities that make up the function of motion. i.e. if the force due to the motion $X_1(t)$ is $Y_1(t)$ and that due to $X_2(t)$ is $Y_2(t)$, then the force due to $X_1(t)+X_2(t)$ must be equal to $Y_1(t)+Y_2(t)$. Using experimental results, Bishop et al[5] concluded that this method was capable of very accurate specification of forces, even though linear theory was applied to a practical problem which normally requires non-linear representation.

Cummins[9] made a theoretical analysis of the use of the Impulse Response Function in ship dynamics and derived the equations representing the response of a ship hull. The author is unaware of any comparisons made between the Cummins' mathematical model and experimental results.

1.7 COMMENTS ON PUBLISHED DATA

Despite the large amount of experimental work carried out up to now on unsteady motion in fluids, the results available are deficient in certain aspects. The shapes of bodies for which data are available are limited. There are serious conflicts and uncertainties regarding the reliability of published data. Engineering applications of these published data are made inconvenient because of certain discrepancies in the results obtained by different methods. The only possible exception applies to the force coefficients obtained by Keulegan and Carpenter[22]. Their data, nevertheless, have strictly limited applications: only for sinusoidal oscillatory flow with zero mean velocity.

Fundamental questions regarding the variations in the flow coefficients and the effects of flow history remain yet unanswered.

FINENESS RATIO		0.25	0.5	1.0	2.0	4.0	8.0	*
Elliptical Cylinder	k(axial)	4.0	2.0	1.0	0.5	0.25	0.125	0.0
	k(rotational)	1.65	0.45	0.0	0.45	1.65	3.81	*
Rectangular cylinder	k(axial)		2.14	1.19	0.67			
	k(rotational)		0.57	0.55	0.57			
Ellipsiods	k(axial)			0.5	0.209	0.0816	0.0292	0.0
	k(normal)			0.5	0.702	0.862	0.934	1.0
	k(rotational)			0.0	0.24	0.61	0.84	1.0
Rankine Ovoids	k(axial) *			0.5	0.27	0.12	0.047	0.0
Circular disc	k(axial)	0.637 of sphere with equivalent diameter						
Hemispherical shell with pinhole at leading point	k(axial)	1.5 of included mass						
Hemispherical cup	k(axial)	2.137 of included mass						
circular cylinder open along leading edge	k(axial)	2:0 of included mass						
	k(normal)	2.0 of included mass						
	k(rotational)	1.33 of included moment of inertia about apex						

Table 1.1 Potential flow coefficients of added mass (k(axial) and k(normal)) and coefficients of added moment of inertia (k(rotational)) for common geometric shapes, as a fraction of mass and moment of inertia, respectively of the displaced volume of fluid.

AUTHOR (year)	TEST MODEL	C_R	k (or C_M)	EXPERIMENTAL METHOD	REMARKS
Cowley & Levy (1918) [8a]	Stream-lined body of fineness ratio = 4:1		≈ 0.04	Stream-lined body falling through water under gravity	Graphs of added mass vs. fineness ratio
Relf & Jones (1918) [32]	sphere airships: fineness ratio = 6:1 fineness ratio = 8:1 fineness ratio = 10:1		0.83 longitudinal: 0.1 lateral: 1.06 logitudinal: 0.185 lateral: 1.28 longitudinal: 0.265 lateral: 1.32	small oscillations in still water	
Frazer & Simmons (1919) [12]	Sphere		0.87-3.4	Spheres falling through liquid under gravity	
Yu(1942)[44]	Circular disc		0.814	Oscillation of circular discs using torsional pendulum	The added mass as a factor of mass displaced by sphere of equivalent diameter
Iversen & Balent (1950) [17]	circular disc		0.637 - 4.0(+)	disc moving normal to its plane	The uncertainity range of added mass for low acceleration numbers is very high; approaches potential flow value (0.637) for high acc. moduli
Keulegan & Carpenter (1959) [22]	circular cylinder	1.2-2.2	(0.75-2.5)	Sinusoidal oscillatory flow around cylinders	force coefficients correlated with Keulegan-Carpenter number
Bearman (1984) [2]	square cylinder	1.6-3.3	(2.3-3.4)	Sinusoidal osc. flow around square cylinders	force coefficients correlated with Keulegan-Carpenter number

Table 1.2 Experimental values of coefficients of acceleration-dependent for various shapes bodies.
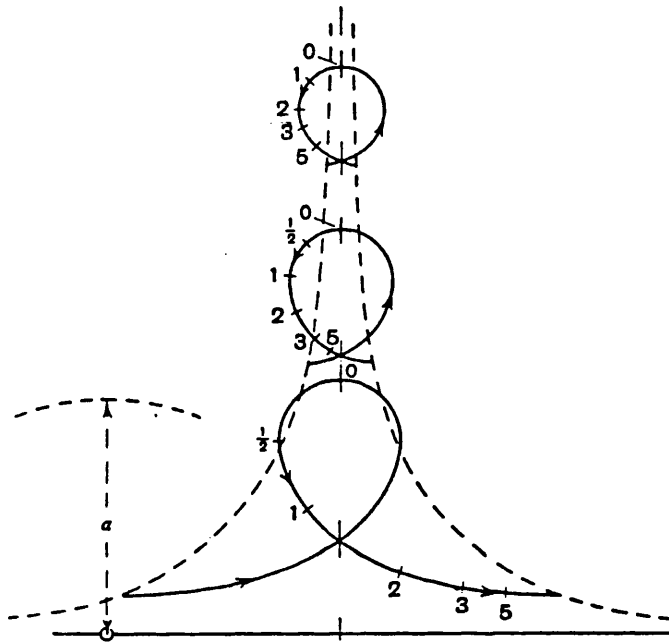
Figure 1.1   Drift   mass   of   a   circular cylinder
with radius a.
The   broken   lines   show   the   initial   and   final
positions   of   the   fluid   particles   moved   by   the
circular cylinder.   The drift mass is given by the
fluid enclosed by the two broken lines[10].
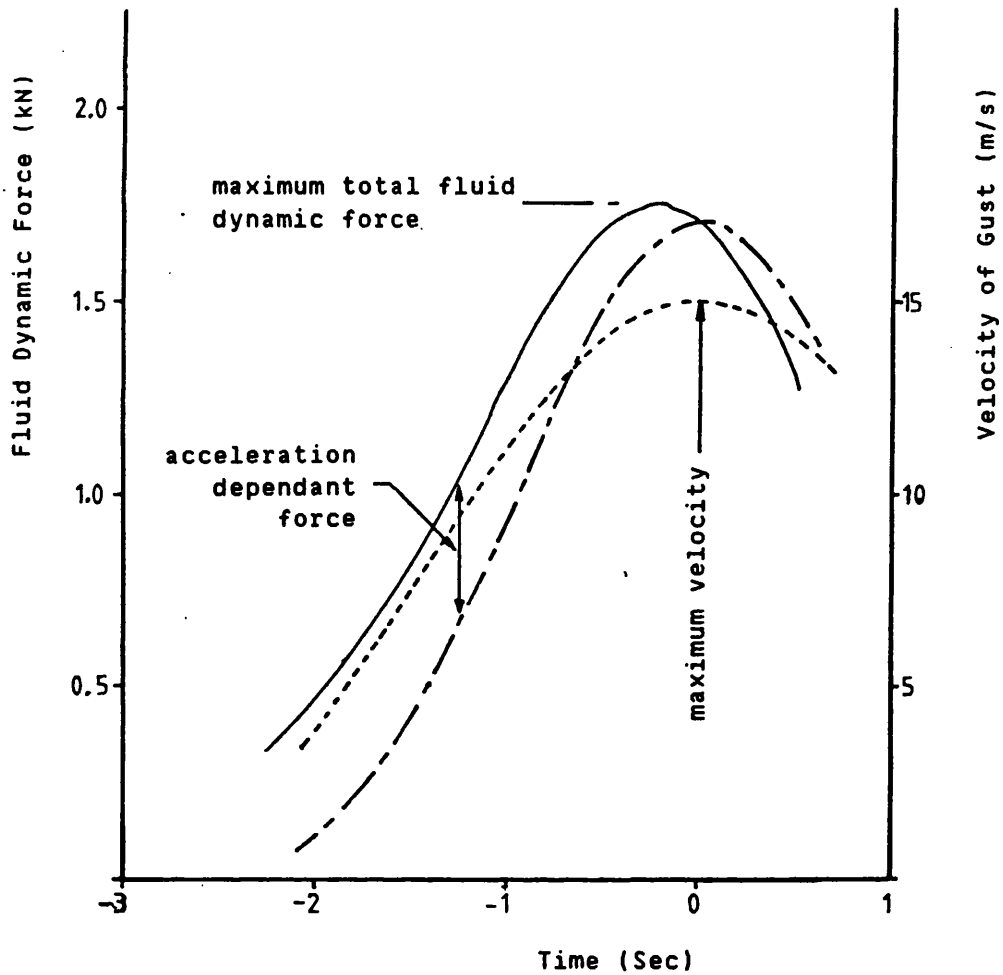
Figure 1.2   Forces   on   a   high   sided   road
vehicle   due   to a lateral gust, idealised as a
sine wave.
-------------- velocity of the lateral gust
--------------- component of velocity dependant
                force
---------------- total fluid dynamic force
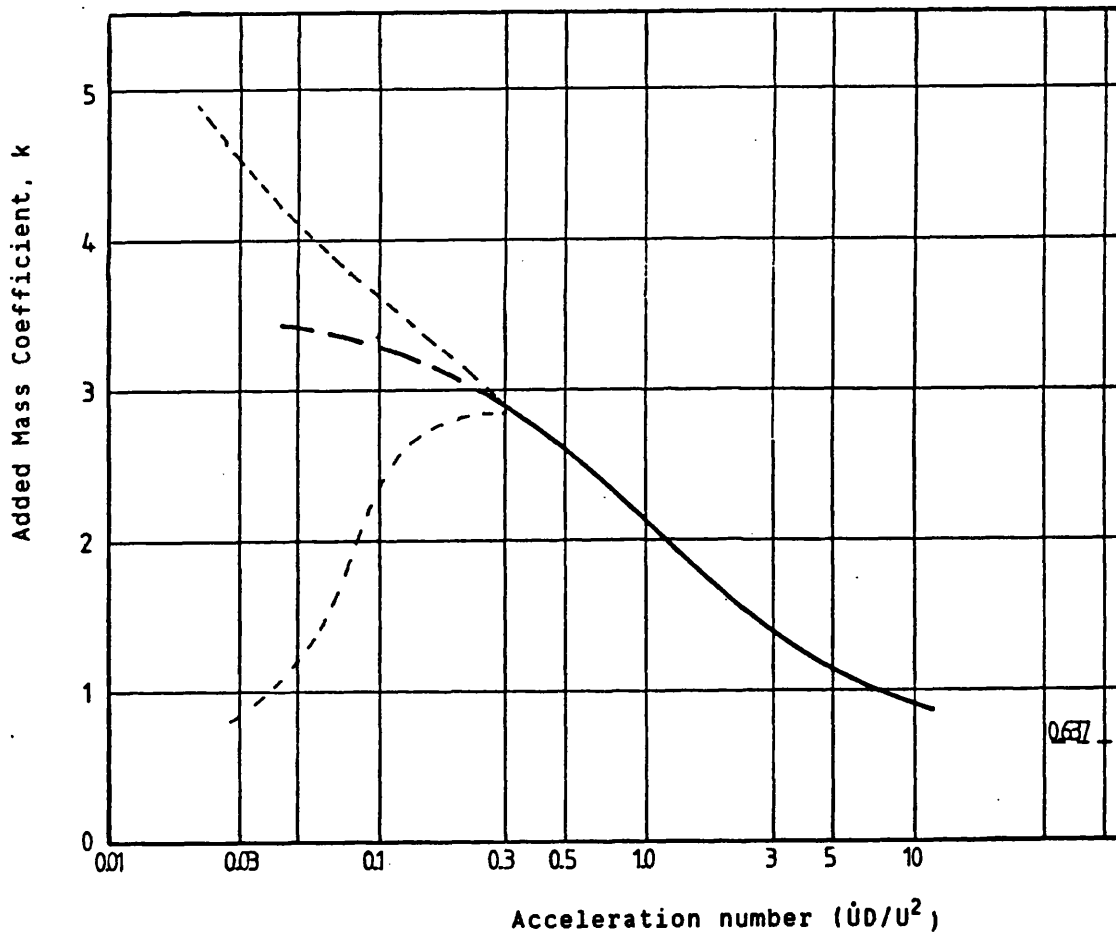
Figure 1.3 Graph of the coefficient of added mass versus the acceleration number for a circular disc moving through water parpendicular to its plane[17].

34
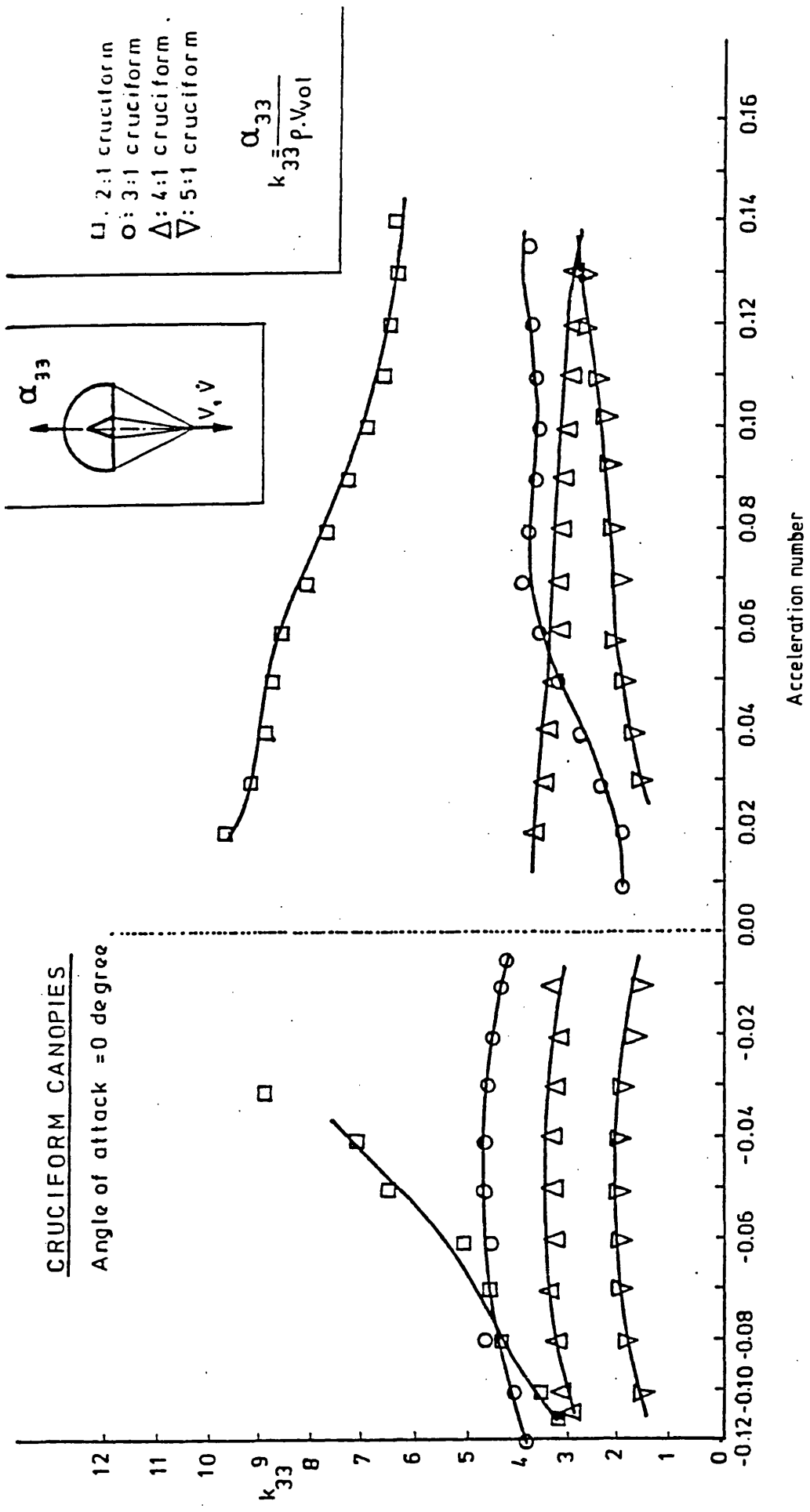
Figure 1.4 Graphs of the coefficients of acceleration-dependent force versus acceleration number for cruciform parachute models of various arm-ratios[42].
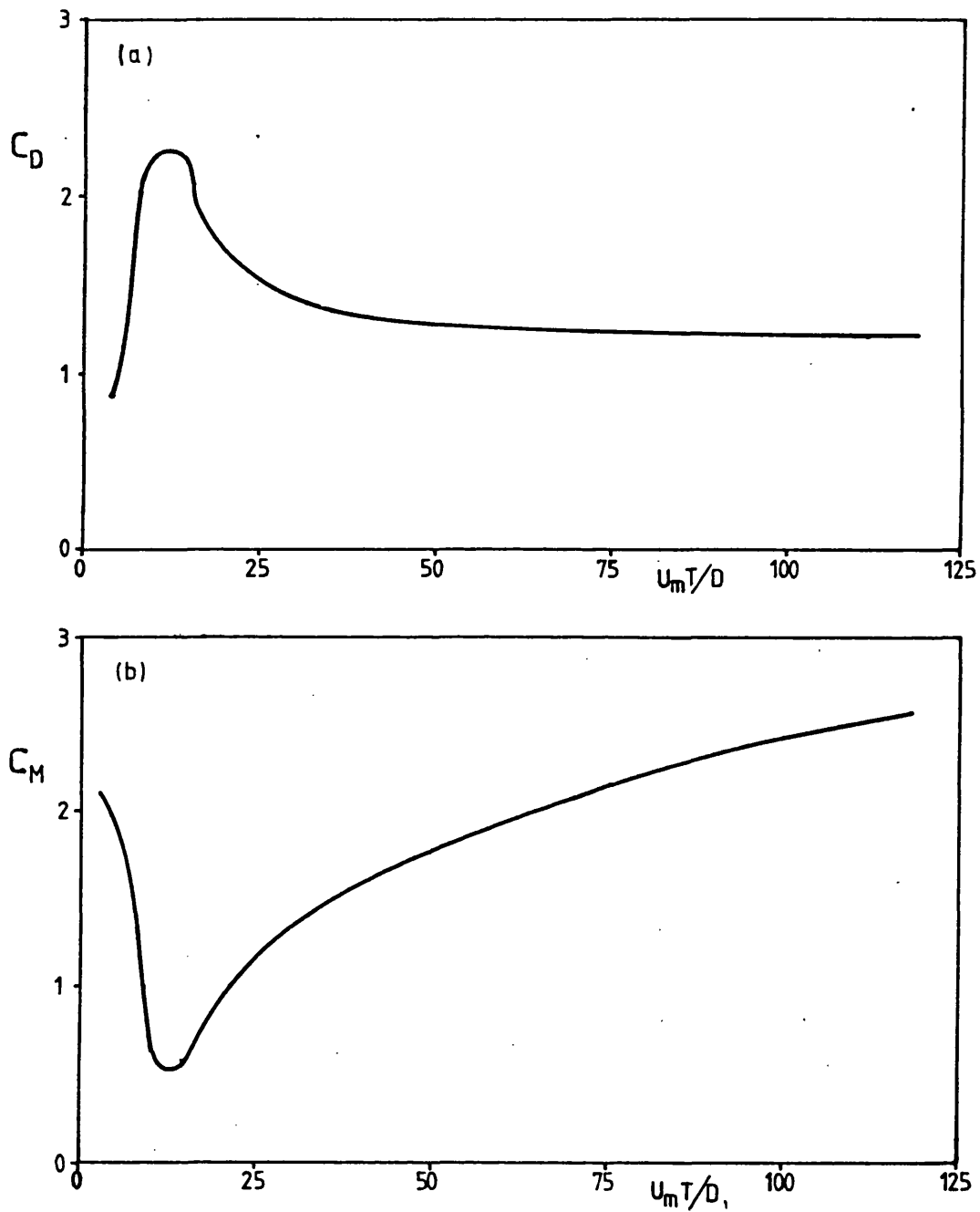
Figure 1.5a & 1.5b   Graphs   of velocity-dependent
force   coefficient C_D, and acceleration-dependent
force   coefficient C_M,   versus   the   periodic
parameter U_mT/D for   circular   cylinders   in
sinusoidally   oscillating   flow[22].   (These   data
have been revised by later researchers.)
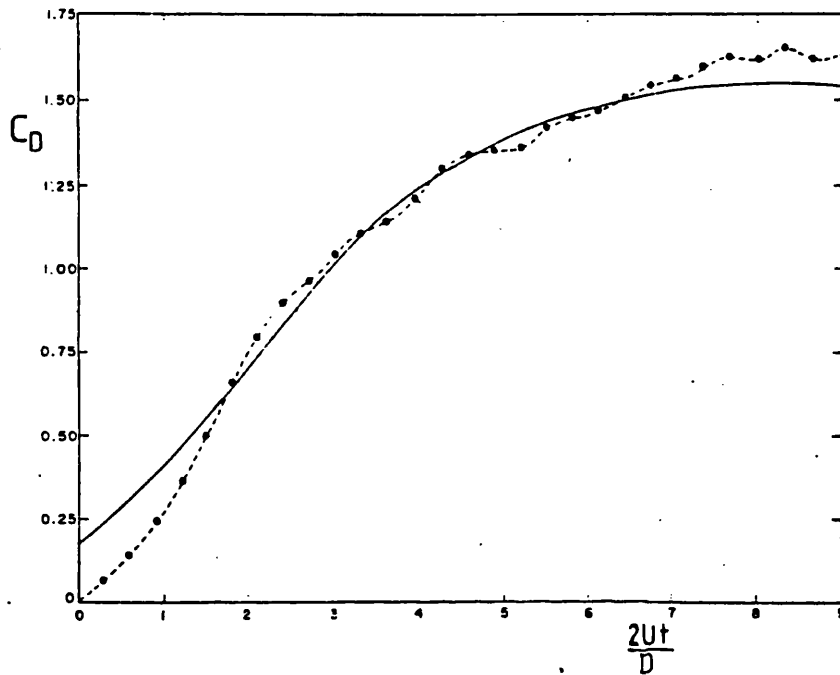
Figure 1.6   Coefficient   of   velocity-dependent
force   on   a   circular   cylinder   due   to   flow
impulsively   started   from   rest   to   a   constant
velocity U[37].
———————————— experimental
—•———•———•—— model   based   on   the   circulation
              around   the   cylinder   derived   using
              the   movements   of the   surrounding
              vortices.

CHAPTER TWO

THEORIES IN UNSTEADY FLOW

THEORIES IN UNSTEADY FLOW

2.1 INTRODUCTION

The phenomenon of added mass is widely used in relating the acceleration of submerged bodies and the resulting fluid dynamic force, because in unsteady motion it avoids the much more complicated process of deriving the pressure distribution around the submerged body. A submerged body in motion imparts velocity to the particles of fluid around it. In a potential flow field these particle velocities, per unit velocity of the body, depend only on the shape of the body and the co-ordinates of the considered locations with respect to the body.

The added mass of a body in a potential flow field, can be derived by analysing the rate of change of either the momentum or the kinetic energy of the surrounding fluid. The disadvantage in the momentum method is that the integral of momentum of the fluid around the body diverges with increasing distance from the body[3], often leading to indeterminate functions. Therefore, the added mass is usually evaluated by the kinetic energy method.

A brief description of the procedure involved in determining the added mass in potential flow is included in this chapter. Certain parameters that strongly influence

the unsteady force on the bodies in real fluids are also discussed.

2.2   ADDED MASS TENSOR

A solid body moving through an infinite fluid continuously imparts energy to the surrounding medium. If the fluid possess a velocity potential ϕ, its kinetic energy in general can be given as:

$$T_f = \frac{1}{2}\rho \int \phi(\partial\phi/\partial n)dS \qquad (2.1)$$

where n is the outward normal to the surface S. Since there are six degrees of freedom of motion: three for the linear directions and three for the angular directions, the velocity potential function of the flow field ϕ can be described by the vectorial sum of the components for each direction as:

$$\phi = U_i \phi_i$$
$$= U_1 \phi_1 + U_2 \phi_2 + \ldots + U_6 \phi_6 \qquad (2.2)$$

U_i represents the component of velocity in the ith direction of motion, and ϕ_i the corresponding velocity potential for unit velocity. The added mass tensor α_{ij}, is defined such that the total kinetic energy of the surrounding fluid is given by:

$$T_f = 0.5\alpha_{ij} U_i U_j$$

where, i=1,2,...,6 and j=1,2,...,6.

Substitution of equation (2.2) in equation (2.1)[38], gives

$$\frac{2T_f}{U_i U_j} = \alpha_{ij} = \rho \int \phi_i \frac{\partial \phi_j}{\partial n} dS \qquad (2.3)$$

The coefficients of the added mass tensor k_{ij} are obtained by dividing the added mass tensor α_{ij} by the mass of a reference volume V, of fluid, which conventionally is the volume displaced by the submerged body.

$$k_{ij} = \alpha_{ij}/\rho V \qquad (2.4)$$

With i=1,2,...,6 and j=1,2,...,6, there are 36 possible components of the added mass tensor: 9 for translation, 9 for rotation and 18 result from the interaction between directions. Since $\alpha_{ij} = \alpha_{ji}$ and therefore $k_{ij} = k_{ji}$, the number of components reduces to 6 for translation, 6 for rotation and 9 for interaction, the total being 21.

These coefficients k_{ij}, for ideal fluids, are independent of time as well as the magnitudes of velocities and accelerations in the linear and angular directions. In the case of fluids of which the boundaries are at infinity they depend only on the geometric shape of the body inclusive of its attitude.

2.3 APPLICATIONS AND LIMITATIONS OF APPLYING POTENTIAL FLOW

VALUES OF ADDED MASS TO REAL FLUIDS

Added mass coefficients for ideal fluids k_{ij}, given by equation (2.4), generally differ from those in real fluids because they do not consider the real fluid phenomena of boundary layer and flow separation. Therefore, as discussed in Section 1.2 of the previous chapter, application of these coefficients to real fluids has strict limitations. Generally, real fluid flow fields around bluff bodies are not at all similar to ideal flow fields, because of flow separation and the formation of a wake downstream of the body. The equations associated with such flow fields cannot be accurately derived by analytical methods. Therefore, it is not possible to make a theoretical approach for evaluating the real fluid added masses.

If, however, a set of equations based on either experimental or theoretical considerations could be written to represent a real fluid flow field such that the velocity at any point in such a flow field could be calculated using these equations, then the added masses and the fluid dynamic forces could be derived analytically. Certain parameters that could be considered in writing equations to represent a real fluid flow field are discussed in the following section. The difficulties encountered, in formulating such equations for accurate representation of the dynamics of real fluids, also are discussed.

2.4 MODELLING SEPARATED FLOW AROUND A CIRCULAR CYLINDER

As an example a circular cylinder submerged in an infinite fluid, the free stream of which is undisturbed, can be considered for this purpose.

At some distance away, and upstream, the effect of a submerged body on the surrounding fluid is negligible. In this region a real fluid would behave as if it were inviscid. In a real fluid a region of vorticity is formed in the boundary layer and downstream of the body. These vortices would 'create' a set of image vortices which are equal in strength but opposite in direction, thus representing the effect of the presence of the body. The co-ordinates of the image vortices, as shown in figure 2.1, depend on the curvature of the body surface. . The circulation around and the force on the body due to each vortex in the flow field can be calculated from the circulation and the location of each vortex and the linear velocity of its core, such that each image vortex would satisfy the conditions on the surface of the body. Therefore, separated flow over a circular cylinder can be approximately modelled by superimposing a family of vortices, representing the boundary layer and the wake, in an otherwise inviscid flow field, as shown in figure 2.2. A circular cylinder is considered as an example because the complex potential function of the flow around it can be derived with relative ease using the Circle Theorem given by Milne-Thomson[27]. Once the complex potential function has been derived the principle of the analysis used for deriving

the forces on the cylinder can be applied to other shapes of bodies also.

Now, in an incompressible and infinite fluid the force on a stationary submerged body due to the free stream velocity U(t), can be considered as two components:

1. In a potential flow field the fluid dynamic force on a submerged body due to the free stream acceleration is equal to $C_M \rho V (dU/dt)$ where C_M, for a circular cylinder, is equal to 2.0.

2. The circulation of fluid around a submerged body at any instant in time produces a force equal to the rate of change of momentum due to this circulation. The momentum of circulation of a pair of vortices is given by the product of the density of the fluid, the circulation around each vortex and the linear distance between the pair. Thus the instantaneous circulation, hence the fluid dynamic force on the submerged body can be evaluated if the location and the circulation of each vortex in the flow field are known.

In such an analysis the fluid is treated as inviscid. The boundary layer and the downstream wake is considered as a group of vortices for which potential flow theory can be applied.

2.4.1 Complex Potential Function of Flow Around a Circular Cylinder

Let the complex potential function of a two-dimensional flow field be f(z) where z = x + iy.

Using the Circle Theorem given by Milne Thomson[27], this flow function can be modified to accommodate a circular cylinder, the centre of which is at the origin of the z-plane of the two dimensional flow field:

$$w(z) \quad = \quad f(z) \quad + \quad \bar{f}\left(\frac{a^2}{z}\right) \qquad (2.5)$$

where $\bar{f}(z)$ is the complex conjugate of the function $f(z)$. For example, the complex potential function of circular cylinder in a uniform stream of velocity U is

$$w \quad = \quad -U\left(z + a^2/z\right)$$

2.4.2 Complex Potential Function of Vortices in the Flow Field

The complex potential for a vortex of circulation Γ at the origin of the z-plane is given by:

$$w \quad = \quad i(\Gamma/2\pi)\ln z$$

The potential function of the kth vortex with its centre at the point z_k, therefore, is:

$$w_k \quad = \quad i(\Gamma_k/2\pi)\ln(z-z_k)$$

where $z_k = x_k + iy_k$

Using equation (2.5) it can be shown that the presence of a circular cylinder at the origin as shown in figure 2.3, leads to:

$$w_k \quad = \quad i(\Gamma_k/2\pi)\ln(z-z_k) - i(\Gamma_k/2\pi)\ln(a^2/z - \bar{z}_k)$$

and $\ln(a^2/z-\bar{z}_k) \quad = \quad \ln(z-a^2/\bar{z}_k) - \ln z + \ln(-\bar{z}_k)$

Physically this represents two vortices one being at z=0. This could be removed still giving a solution to the problem. Of these two expressions we choose that which models the physical situation under investigation. The difference is between vortices being generated by the cylinder and vortices already existing and being convected past the cylinder. This latter situation requires the presence of the vortex at the centre whereas in the former case it would be removed. Thus the velocity potential function for a flow field with m vortices is given by

$$w(z) = U(z + \frac{a^2}{z}) + i(1/2\pi) \sum_{k=1}^{m} \Gamma_k \ln(z - z_k)$$

$$- i(1/2\pi) \sum_{k=1}^{m} \Gamma_k \ln(z - \frac{a^2}{z_k}) \qquad (2.6)$$

2.4.3 The Forces on the Cylinder Due to a Flow Field Described by the Complex Function w(z)

Using Blasius' theorem as generalized by Milne-Thomson[27] the lift(L) and drag(D) forces on a submerged body due to a flow field w(z) are given by

$$D - iL = i(\rho/2) \oint (dw/dz)^2 dz$$

$$- i\rho (\partial/\partial t) \oint \bar{w} d\bar{z} \qquad (2.7)$$

The fluid dynamic force on the submerged body can be ·derived using equation (2.7) if the complex potential function of the flow field around that body is known.

Examples of such applications can be found in published literature[27,37]. However, the algebra involved in such analysis is rather lengthy and complex. Besides, the solutions of such methods are often inaccurate because insufficient data are available to represent the vortices in real fluids adequately.

In the present text, the author wishes to avoid this lengthy algebraic procedure by considering the momentum of vortices in the flow field, as suggested by von Karman and Sears[21]. In this method, as described earlier in this chapter, the momentum of a pair of vortices is expressed by the product of the density of fluid, the circulation of each vortex and the linear distance between them. The force applied on the submerged body is thus given by the rate of change of this momentum of vortices.

By considering a two dimensional vortex of strength Γ_k at point z_k, and its image, to satisfy the boundary condition at the surface of the cylinder, at point a^2/z_k one can write the momentum of the vortex as,

$$\text{Momentum} = - \varrho \Gamma_k (z_k - a^2/\bar{z}_k)$$

Writing the force on the submerged body as given by the rate of change of momentum, and bearing in mind the presence of the pressure gradient due to the free stream acceleration, one gets,

$$D - iL = - \sum_{k=1}^{m} i\varrho \; \Gamma_k (u_k - iv_k)$$

$$+ 2\pi\varrho a^2 \; (\partial U/\partial t)$$

$$- i\varrho \sum_{k=1}^{m} (z_k - \frac{a^2}{z_k}) \; \frac{\partial \Gamma_k}{\partial t} \qquad \bullet$$

$$+ i\varrho \sum_{k=1}^{m} \Gamma_k \; \frac{\partial}{\partial t} (\frac{a^2}{z_k}) \qquad (2.8)$$

The velocity (u_n, v_n) of the core of the nth vortex is given by[37]:

$$-u_n + iv_n = - U + U\frac{a^2}{z_n^2} + \frac{i}{2\pi} \sum_{k=1}^{m} \frac{\Gamma_k}{z_n - z_k}$$

$$+ \frac{i}{2\pi} \sum_{k=1}^{m} \frac{\Gamma_k}{z_n - a^2/\bar{z}_k} \qquad (2.9)$$

The mathematical model given by equations (2.8) and (2.9) can effectively be used to evaluate the fluid dynamic force only if the co-ordinates of the vortices, their velocities, circulation and rates of either growth or diffusion are known. Neither a theoretical nor a practical method is known to the author for obtaining these details. Until such data are available this analytical approach is limited to merely a discussion of what the actual physics might be, in the light of the given parameters.

2.4.4 Forces Due to an Isolated Vortex

The effect of the circulation of fluid in the vicinity of the submerged cylinder, on the fluid dynamic

force applied on it, can be discussed with relatively less complexity by considering the effect of an isolated vortex. Assuming circulation to be constant with time, and leaving the effects due to the movements of the image vortex and the force due to the acceleration of the free stream, the fluid dynamic force in equation (2.8) due to the kth vortex (fig. 2.2) can be written as

$$D_k \qquad = \qquad - \varrho \, \Gamma_k \, V_k \qquad (2.10)$$

In the case of vortex produced by the flow separation over the cylinder surface, the drag force on the cylinder would be positive if the vortex moves away from the x-axis. Conversely, if the vortex moves towards the x-axis this would produce a negative drag on the cylinder.

Using potential flow theory it can be shown that, due to accelerated flow, the pressure at any point on the submerged cylinder is given by $2a\varrho(dU/dt)Cos\theta$. It can be seen therefore, that at the 'rear stagnation point' (on the surface at $\theta=\pi$) the pressure is decreased (the magnitude may be somewhat different for real fluids) for accelerated flow, and increased for decelerated flow. The vortices behind the cylinder can thus expected to be forced either towards or away from the x-axis due to this additional pressure gradient normal to the free stream acceleration.

2.5 SUMMARY: Accelerated Motion in Read Fluids

In unsteady fluid dynamics the flow fields associated with separated flow change from one state to

another depending on the variations in the free stream velocity and acceleration. Therefore, the coefficients of velocity-dependent component and acceleration-dependent component of the total force continuously change with the shape of the flow field.

In separated flow, the vortices in the wake downstream of the body move towards the axis of symmetry of the main stream when the acceleration is positive. Therefore, the width of the wake is reduced. Furthermore, the effect of accceleration in the free stream is to shift the point of separation downstream, thus increasing the region of attached flow and thus reducing the width of the wake. In negative acceleration the reverse occurs.

Since the velocity-dependent force in the direction of the free stream is substantially dependent on the characteristics of the downstream wake, the effect free stream acceleration on the fluid dynamic force can be summed up as in Table 2.1.

	for acceleration	for deceleration
width of the wake	decreases	increases
velocity-dependent force coefficient	lower than the steady flow value	higher than the steady flow value

Table 2.1 The effect of free stream acceleration on the flow field and the velocity-dependent force.

Given these characteristics, when the velocity-dependent component of the total force in accelerated fluids is compared with the force in steady flow for corresponding velocities the former shows the characteristic of 'trying to catch up with' the latter. i.e. when there is acceleration in the free stream the continuously increasing velocity-dependent component of the force on the submerged body at any instant, is always less than the force in steady flow for the corresponding velocity. Similarly, if the flow is decelerated, the continuously decreasing velocity-dependent force is always greater than the corresponding force in steady flow. This specific characteristic of the velocity-dependent force is present because the wake downstream of the body becomes narrower when the acceleration is positive, and wider when the acceleration is negative.

If, for example, the unsteady motion of the body is such that the mean velocity of the body is always greater than the fluctuations in the velocity, then the flow field will be such that the vortices generated due to flow separation always lie downstream of the body. In such a case the behaviour of the flow field can be described by the properties given in Table 2.1. Therefore, in an experiment where there is no 'flow reversal', the measured force would show the characteristic of continuous 'lagging' behind the quasi-steady model. This behaviour would occur because of the movements of the vortices, which have been shed at previous instants and the widening and the narrowing of the downstream wake. It also shows that the velocities and

accelerations at previous times of motion would play a significant role, in the fluid dynamic force in separated flow.
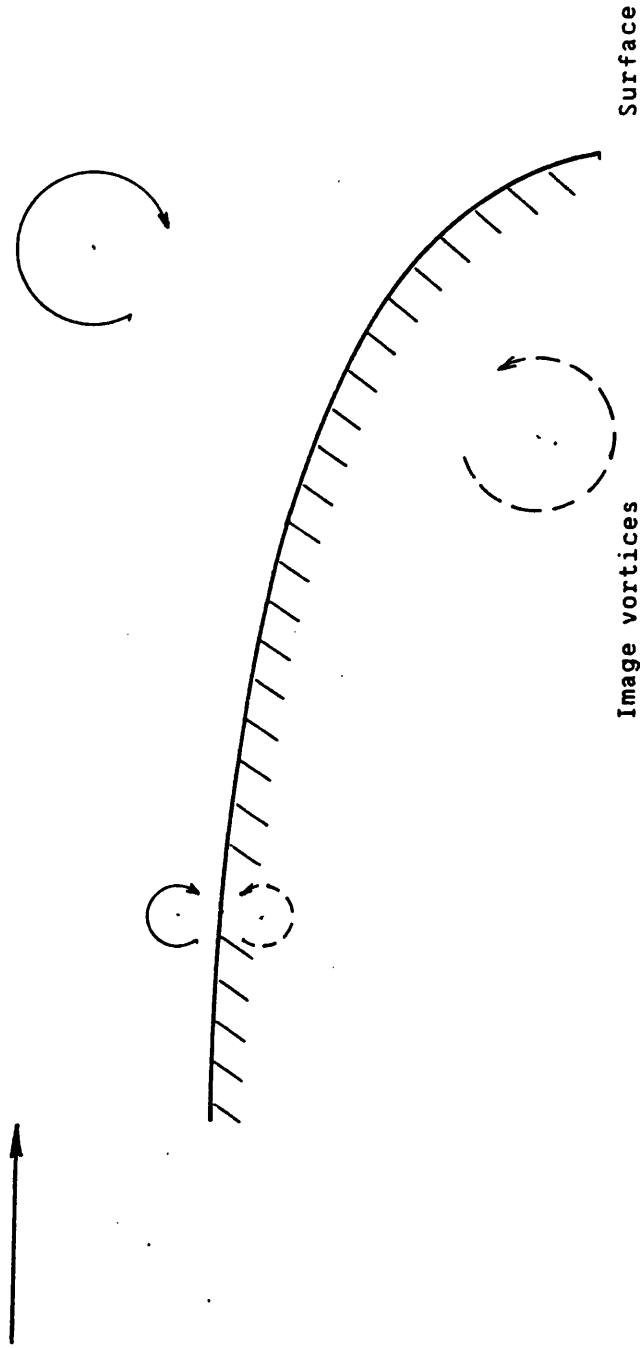
Figure 2.1 Vortices in the main stream and image vortices.
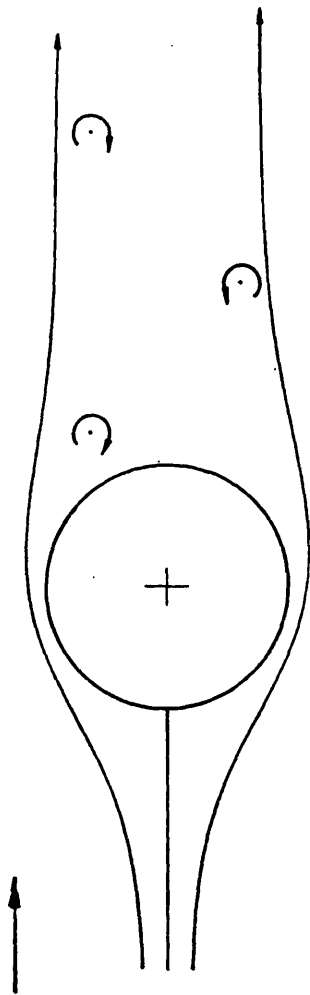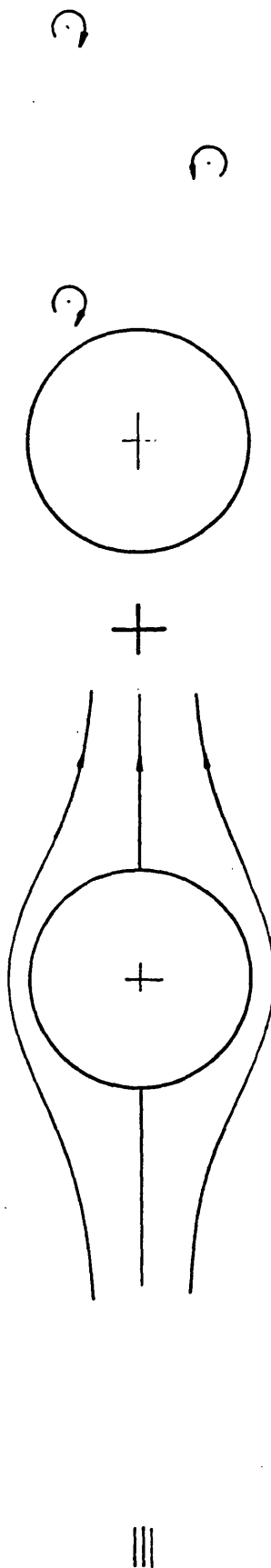
Figure 2.2 Separated flow past a circular cylinder modelled by superpositioning the ideal flow field and the vortex street.
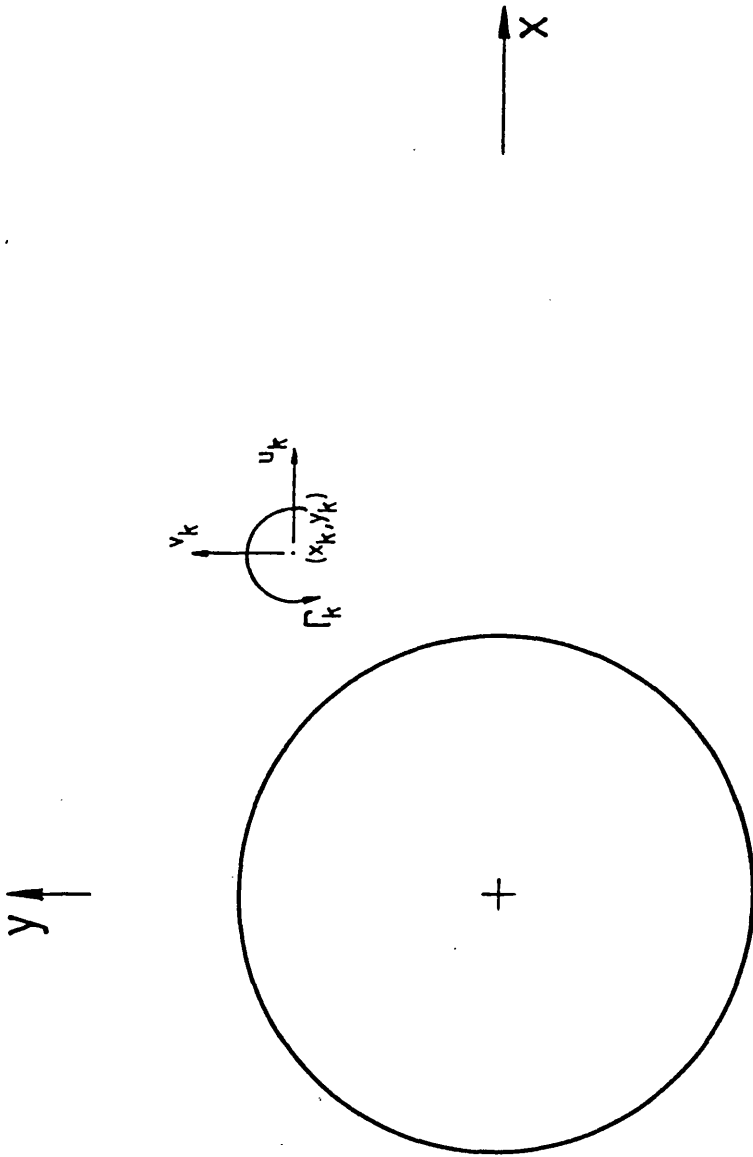
$$u_k = \frac{dx_k}{dt}$$

$$v_k = \frac{dy_k}{dt}$$

Figure 2.3 Illustration of a single vortex on the flow field past a circular cylinder. The position and the velocity of the core of the vortex are with respect to the axes fixed at the centre of the cylinder.

CHAPTER THREE

DEVELOPMENT OF A MODEL RELATIONSHIP FOR
PREDICTING FORCES ON BLUFF BODIES IN UNSTEADY MOTION

DEVELOPMENT OF A MODEL RELATIONSHIP FOR
PREDICTING FORCES ON BLUFF BODIES IN UNSTEADY MOTION

3.1 INTRODUCTION

In a potential flow field with boundaries at infinity, the circulation around and the added mass of a submerged body are dependent only on the shape and the orientation of the body, and the instantaneous values of the relative velocity between the body and the free stream. When the motion of either the body or the surrounding fluid is not steady the circulation around the body changes instantaneously with any changes in the relative velocity. Therefore, the fluid dynamic forces on a body in potential flow are dependent only on the instantaneous velocities and accelerations inclusive of the shape and attitude of the body.

In real fluids, however, the fluid dynamic forces can successfully be evaluated using instantaneous velocities only when the flow is steady. Unlike potential flow, due to their viscous properties real fluids do not respond instantaneously to any changes in velocity of either the body or the surrounding fluid. Furthermore, if there is flow separation, the circulation around the downstream vortices that have been shed at previous instants has a strong influence on the fluid dynamic force on the body.

The point of separation can vary with the unsteadiness of the fluid, thus resulting in a continuously varying downstream wake characteristics. Therefore, when the motion of either the submerged body or the surrounding real fluid is unsteady, not only the instantaneous velocity and acceleration but also their history affect the unsteady force. Thus, data associated with an expression similar to Morison's equation which considers instantaneous velocities and accelerations only, can have limitations in applications because the way in which motion is imparted is not represented.

For the analysis in the following sections of this chapter, is is considered that the fluid dynamic force on a submerged body is a function of the entire history of the motion of the body: i.e. both the velocity and the acceleration. The rates at which the effects of history of motion either rises or decays with time is given by the characteristics of the 'Impulse Response Function' which is derived using experimental results.

3.2 IMPULSE RESPONSE FUNCTION (IRF) OF FLUID DYNAMIC FORCE

The fluid dynamic forces on submerged bodies in steady flow are normally non-dimensionalised by the group $0.5\rho AU^2$ where U is the relative velocity between the body and the free stream. If the motion is unsteady the group $\rho V dU/dt$ is used to non-dimensionalise the acceleration-dependent component of the total force. Since, in real fluids, the history of both the velocity as well as

the acceleration can affect the fluid dynamic force, it can be considered that the total unsteady force in a particular direction at any instant consists of two components:

1. a velocity-dependent force component, which is dependent on the term $0.5\rho AU|U|$ and its history,

2. an acceleration-dependent force component, which is a function of accelerations and the history of both the body as well as the surrounding fluid.

The time function of $0.5\rho AU|U|$ and that of $\rho VdU/dt$ can be described by two series of impulses as shown in figure C.1. By introducing the Impulse Response Function $G_1(t)$, as the elemental time function of force due to a unit impulse of $0.5\rho AU|U|$, the total velocity-dependent force at any instant can be written as the sum of the elemental force component due to each impulse in the series. This procedure is adopted assuming a linear relationship between the velocity and the acceleration and the corresponding fluid dynamic force on the body. Whether such methods can be used effectively to write a relationship for forces in real fluids will be discussed in Chapter Five of this thesis.

The convolution integral is thus used to express the velocity-dependent force at any instant t as:

$$\int_{-\infty}^{t} 1/2\ \rho\ A\ \dot{U}(\tau)|U(\tau)|\ G_1(t-\tau)\ d\tau$$

where τ is a dummy variable. The effect of the entire history of velocity is given by the shape of the function $G_1(t)$. This expression is valid, whether or not the

velocity at previous stages of flow carry any weight.

Similarly, the acceleration-dependent force can be written as:

$$\int_{-\infty}^{t} \varrho V \; \dot{U}(\tau) \; G_2 (t-\tau) \; d\tau$$

The Impulse Response Functions $G_1(t)$ and $G_2(t)$ are to be determined from experimental results. The total fluid dynamic force at any instant in time t is given by the sum of the two component forces.

$$F(t) \quad = \quad \int_{-\infty}^{t} 1/2 \; \varrho \; A \; U(\tau) |U(\tau)| \; G_1 (t-\tau) \; d\tau$$

$$+ \int_{-\infty}^{t} \varrho V \; \dot{U}(\tau) \; G_2 (t-\tau) \; d\tau \qquad (3.1)$$

3.2.1 Properties of the Convolution Integral

The initial values of the velocity and acceleration involved in the motion are given by those at the lower limit of the convolution integral. The way in which the integral is constructed is a mathematical reflection of two general properties of a physical realizable system. Firstly, 'future' values of velocities and accelerations cannot effect 'earlier' values of the fluid dynamic force. Secondly, instantaneous response in the part of F(t) is ruled out[23].

If the history effects are negligible (i.e. the two components of the fluid dynamic force on the submerged body

are dependent on the instantaneous velocity and instantaneous acceleration respectively) then for a given function of velocity and acceleration $G_1(t)$ and $G_2(t)$ can approximately be given by impulse functions, leading to the more familiar Morison's equation given by equation (1.3).

3.2.2 Derivation of Impulse Response Function

If the motion were purely sinusoidal, then the acceleration-dependent force in equation (1.3) would lead the velocity-dependent force by 90°. In such a cases the two component forces of equation (3.1) could be analysed separately by obtaining the Fourier Transformation of the total force. If the mode of motion is arbitrary, the methods used to derive the velocity-dependent component and the acceleration-dependent component of the total force, can be much more complicated. Thus, the following procedure is suggested for deriving the Impulse Response Function (IRF) relating the force to the velocity and the acceleration.

The relationship given by equation (3.1) is modified such that:

1. The velocity-dependent component and the acceleration-dependent component of the total force are combined so that a common Impulse Response Function can be used to relate the unsteady motion to the unsteady force.

2. Suitable coefficients are introduced in the two components of force to indicate the weight carried by the velocity and the acceleration. The starting values of these coefficients are based on the

steady flow coefficients of the velocity-dependent force (C_R) and the potential flow coefficient of the acceleration-dependent force (k).

Thus, the model form of the fluid dynamic force given by equation (3.1) is re-written as:

$$F(t) = \int_{-\infty}^{t} \{ C_R \ 1/2 \ \varrho \ A \ U(\tau)|U(\tau)|$$

$$+ \ k \ \varrho V \ \dot{U}(\tau) \} \ G(t-\tau) \ d\tau \qquad (3.2)$$

Equation (3.2) can also be written using notations often used in published literature[23] as:

$$F(t) = \{C_R \ 1/2 \ \varrho A U(t)|U(t)| + k\varrho V \dot{U}(t)\} \ * \ G(t)$$

$$(3.2a)$$

The coefficients C_R and k and the Impulse Response Function G(t) given in equation (3.2) and (3.2a) are derived using the procedure outlined below.

The time series of F(t) and the terms inside the '{}' brackets on the right hand side of the equation (3.2a) are obtained from experimental results. The evaluation procedure for the function G(t) is carried out by converting the time domain functions into frequency domain ones.

The experimental results, as described in the next chapter, were obtained by oscillating test models while they were being towed under water at a constant speed. All the experimental variables (e.g. the fluid dynamic force, the

velocity of the test model, its acceleration, etc.) were of a periodic nature. These data can conveniently be expressed as harmonics of the fundamental frequency of oscillation, by transforming into Fourier series[24], such that:

$$C_R \ 1/2 \ \varrho \ A \ U(t) |U(t)| \ + \ k \ \varrho \ \forall \ \dot{U}(t)$$

$$= \ A_0 + \sum_{n=1}^{\infty} A_n \cos(n\omega t + \phi_n) \qquad (3.3a)$$

and, the measured force:

$$F(t) \ = \ B_0 + \sum_{n=1}^{\infty} B_n \cos(n\omega t + \Psi_n) \qquad (3.3b)$$

where ω is the fundamental frequency of the periodic motion. The amplitude of each harmonic indicates the magnitude of the force due to the corresponding frequency of excitation.

Now consider the oscillating bluff body to be a system, the input to which is the effect of the velocity and the acceleration, given on the left hand side of equation (3.3a). The corresponding output of the system is the fluid dynamic force given on the left hand side of equation (3.3b). If the system is considered to be linear, then each term in the input series will result in an output at the same frequency. In such a case the input and the output Fourier series can be related by considering one frequency at a time. Therefore, the modulus of the Impulse Response Function at each frequency as given by Raven[30] is:

$$|G(in\omega)| \ = \ B_n /A_n \qquad (3.4a)$$

and the argument is given by

$$\underline{/G(in\omega)} \quad = \quad \Psi_n - \phi_n \qquad (3.4b)$$

The modulus (or the amplitude) of the Impulse Response Function at a frequency of $n\omega$ is given by A_n/B_n, and the argument (or the phase angle) by $(\Psi_n - \phi_n)$. From the graphs of modulus and argument plotted against the frequency of excitation an empirical relationship for the Impulse Response Function is obtained.

The Impulse Response Function thus obtained is used to relate the fluid dynamic force to the velocity and the acceleration of the test models. The uncertainty imposed by the linearity concept will be discussed in Chapter Five.

The empirical form of the IRF is then iteratively used to re-estimate the values of coefficients C_R and k, in order to obtain a better correlation with the experimental results. These new values of C_R and k, and the corresponding IRF, are then used to re-write the relationship given by equation (3.2). This iterative procedure is then repeated until the best fit is achieved on experimental results. The best fit is considered to be reached when the difference between the measured force and the reconstructed force has reached its minimum value. A flow chart illustrating this data analysis procedure is given in Appendix A.

3.3   CONCLUSIONS

The experimental values of the coefficients C_R and k and the Impulse Response Function G(t) derived from the method outlined in the previous section are used to write a relationship between the fluid dynamic force and the history of the velocity and the acceleration. Chapter Five of this thesis includes a discussion on the model thus derived, and the coefficients C_R and k based on experimental results.

CHAPTER FOUR

APPARATUS AND EXPERIMENTAL PROCEDURE

APPARATUS AND EXPERIMENTAL PROCEDURE

In an experimental programme the required time dependent motion was obtained by towing bluff body test models along the ship-tank shown in figure 4.1. Before the beginning of each test the towing speed of the carriage was pre-set to a desired value. Test models were oscillated either along the towing motion axis or at other known angles to this axis. The velocities and the accelerations were calculated based on the speed of the towing carriage and the frequency of oscillation of the test rig.

4.1 SHIP TANK

The ship tank in the Southampton College of Higher Education is 61m long, 3.7m wide and 1.8m deep. The towing carriage which runs on rails on either side along the length of the tank can be operated at speeds of up to five metres per second. Towing speeds up to 0.82 metres per second were used during the present experimental investigation. A 'trigger switch' attached to one of the wheels of the carriage generates an electrical signal for every revolution of the wheel. The translation speed of the trolley is determined by the diameter of the wheel and the frequency of these electrical signals.

4.2 OSCILLATION TEST RIG

The models are oscillated using a piston-connecting rod mechanism, shown in figure 4.2, which is run by a variable speed drive. Technical specifications of the drive are given in Table 4.1.

The principle involved in the oscillations test rig is analogous to the piston-connecting rod assembly of a reciprocating engine. A reciprocating block which is guided by two rails is made to oscillate in a manner similar to that of a piston of the reciprocating engine. The rig could be run at speeds from 10.23 rpm to 32.21 rpm. The reciprocating block has an overall amplitude of oscillation of 379 mm.

The test model is attached to the lower end of a test sting, the upper end of which is firmly fixed to the reciprocating block as shown in figures 4.3 and 4.4. The test rig assembly is firmly hung from the underside of the towing carriage. The test models can be oscillated at any angle to the towing-carriage-motion-axis (ship tank axis) simply by rotating the test rig by the appropriate angle. A 360° potentiometer, attached to the driving shaft via a 1:1 gear assembly, gives the position of the crank at any instant in time. A constant d.c. potential difference of 5.0 volts is supplied to the potentiometer. The output of the potentiometer is pre-set to read zero when the crank angle θ equals zero. During the experiments this output is given by $5.0 \sin(\theta)$ volts. The velocity and acceleration of the model are calculated using the formulae given in Appendix A.

4.3 TEST STING

The sting-test model assembly is shown in figure 4.4. Any force applied on the test model creates a bending moment on the test sting. This causes a change in resistance of strain gauges, which are firmly stuck on the surface of the sting comprising a strain gauge bridge. The input voltage to each of the three strain gauge bridges shown in figure 4.5, is 2.0 volts d.c. Before the tests each bridge is balanced for zero output. The output signals from the bridges are amplified via a set of strain gauge d.c. amplifiers (model CIL-SGA 1100) and recorded in analogue form on a chart and in digital form on a magnetic floppy disc. The sting has been tested for no interaction between strain gauge bridges[42], i.e. the strain gauge set for the axial direction for example, responds to forces in the axial direction only. The test sting is calibrated using static loads, before and after the tests. Its natural frequencies in various directions, both in air and in water, with and without models attached to its end are also determined.

4.4 EXPERIMENTAL RESULTS

The experimental results are recorded in analogue form for immediate reference and in digital form for later analysis. The readings obtained are:

1. interrupts from the 'trigger switch' attached to the wheel of the towing carriage;

2. potentiometer output, indicating the position of the crank of the oscillation rig;

3. amplified signals from the strain bridges (see figure 3.5, strain gauge assemblies) due to

   - force on the test model in the lateral (normal) direction, given by bridge 1 2 3 4

   - force in the axial direction, given by bridge 1´2´3´4´

   - moment on the test model about the axis normal to the axial and lateral directions, given by bridge 1"2"3"4".

4.4.1 Analogue Recording

The analogue form of the data were recorded using a W+W Recorder (model 360,420) multichannel chart-recorder. Figures 4.6a and 4.6b show two typical records obtained from the tests.

4.4.2 Digital Recording

The analogue form of the strain gauge output due to the fluid dynamic forces and moments, and from potentiometer were converted into digital form via an analogue/digital converter. The results were recorded on floppy discs using a RML 380Z computer, at user specified rates of data (up to one thousand sets of reading per second.) These data were later transferred to magnetic tapes for rapid and comprehensive analysis using the Leicester University main computers CDC-CYBER 73, VMS/VAX 11/785 and VMS/VAX 8600.

4.5 TEST MODELS

The details of the test models used during the experiments are given below.

4.5.1 Circular Cylinder

The circular cylinder used for experiments is made from timber and is painted with sealant to avoid penetration by water. It is 114mm in diameter and 1000mm in length. Two end plates are fitted to the cylinder to obviate three-dimensional effects. So that the cylinder is neutrally buoyant in water an iron rod is inserted through its centre-line.

The characteristic length of the cylinder is its diameter and its projected area is considered as the characteristic area. The characteristic volume is the volume of fluid which is displaced by the submerged cylinder. The mass of the test model in air is 10.775kg.

4.5.2 Rectangular Block

A neutrally-buoyant rectangular block is of size 457mm x 153mm x 152.5mm. Its characteristic length and area are 0.457mm and 0.0699 m^2 respectively, and its characteristic volume is the volume of the fluid which it displaces. The mass of the test model in air is 9.15kg.

4.5.3 Cruciform Parachute Canopy

The non-porous parachute canopy shown in figure 4.7 is made from nylon. Its arm ratio (L_1/L_2) = 4.0 where L_1 = 0.48m (see figure 4.7a).

A 9mm mild steel rod, one end of which is attached
to the end of the parachute canopy rigging lines runs
through a hole at the apex of the canopy. The other end of
the rod is threaded for mounting at the end of the sting.

The characteristic length of the cruciform canopy
model is the diameter of a hemispherical shell with a
surface area equivalent to that of the canopy fabric. The
projected area of such a hemispherical shell is taken as the
characteristic area of the test model and the characteristic
volume is given by its included volume. The length of each
of the sixteen rigging lines is 0.285 m.

i.e.

Area of the fabric $= 0.101 \text{ m}^2$

Characteristic length $= 0.253 \text{ m}$

Characteristic area $= 0.05 \text{ m}^2$

Characteristic volume $= 4.26 \times 10^{-3} \text{ m}^3$

Mass of test model in air $= 0.35 \text{ kg}$

4.5.4 Ring-Slot Parachute Canopy

Figure 4.8 shows the model in its fully developed
position.   Disregarding the slots, the surface area of the
fabric is 0.163 m^2.   The charateristic length, area and
volume of the ring-slot canopy are given by the diameter,
the projected area and the included volume, respectively of
a hemispherical shell, the surface area of which is
equivalent to that of the canopy fabric. There are eight
rigging lines, each 0.275 m long.

i.e.

Characteristic length $= 0.32 \text{ m}$

Characteristic area $= 0.0817 \ m^2$

Characteristic volume $= 8.75 \times 10^{-3} \ m^3$

Mass of test model in air $= 0.34 \ Kg$

4.6   EXPERIMENTAL PROCEDURE

The experiments were conducted for both steady motion and oscillatory motion.

4.6.1   Steady Motion Tests

The forces for steady motion were measured by towing the models along the length of the ship tank at constant speed.   In the case of the circular cylinder the experiments were conducted by towing the cylinder with its axis normal to the direction of towing. The steady flow data for the rectangular block was obtained by towing it with its 153 x 152.5 mm^2 side facing the forward direction. In the case of parachute models, they were towed at different angles of attack for each test, so that steady flow data as functions of the angle of attack can be obtained.

4.6.2   Oscillatory Modes of Motion

These modes were obtained by oscillating the test models, while they were being translated at constant speed. For measuring forces on the cylinder in oscillation, its axis was maintained normal to its motion. The direction of motion was considered to be irrelevant because of the axi-symmetry of the model. In the case of the rectangular

block and the parachute models, however, the angle of attack, and hence the force coefficients, are very dependent on the mode of motion. Thus, it was necessary to obtain data for various angles of attack. As shown in figure 4.9 the modes of motion were divided into two categories:

1. lateral oscillations and

2. in-line oscillations.

4.6.2.1 Lateral Oscillation of Model

While a model was being translated along the ship tank at constant speed, with its axis of symmetry along the towing motion axis, it was oscillated in the lateral direction.   i.e. in the case of the rectangular block and the parachute canopy models, at 90° to the axis of symmetry of the model. This experiment simulates either a lateral gust on a steadily-moving high-sided vehicle, or the lateral oscillation of a descending parachute, the vertical speed of which remains substantially constant. For this mode of motion the acceleration in the axial direction of the model is zero. Nevertheless, the force in the axial direction is not expected to be constant because of the variations in the angle of attack. The oscillatory lateral force, on the other hand, is dependent on the constantly changing velocity, acceleration and angle of attack.

4.6.2.2 In-line Oscillation of Model

As shown in figure 4.9 the test model was towed along the length of the ship tank at constant speed, while it was oscillated in the same direction as the linear

translation of the towing carriage. This experiment
simulates either a head-on gust on a high-sided vehicle or
the axial oscillation of a parachute on which forces in the
axial direction are due to the time dependent velocity as
well as the time dependent acceleration. The motion of the
rectangular block was such that the square side (153mm x
152.5mm) always faced the oncomimg flow at right angles to
the surface. Therefore the motion was always in the axial
direction. The speeds of towing, as well as the speeds of
oscillations, used in the experiments, were such that the
displacement of the test model at any time during the cycle
is in the same direction as that of the towing carriage.
This procedure was adopted in order to avoid any negative
axial force on the parachute canopy which in releasing the
tension of the rigging lines, would cause no force to be
imparted by them to the test sting. Magnitudes of
oscillatory velocities up to the speed of the towing
carriage speed were used.

The tests were repeated by setting the test model
to small angles of attack, which are maintained constant for
each test. By this means, velocity-dependent forces and
acceleration-dependent forces at constant angles of attack
can be analysed for both normal and axial directions. In
the case of parachutes the maximum angle of attack for which
these experiments are conducted was restricted to the angle
at which the fabric canopy would collapse.

4.7   REYNOLDS NUMBER OF FLOW

The range of Reynolds number for the cyclic motion, based on the Characteristic length of each test model is given in Table 4.2.

4.8   REDUCED VELOCITY AND PERIODIC PARAMETER

The range of reduced velocity U_T/nL and the range of non-dimensional periodic parameters U_N/nL and U_0/nL, based on the fundamental frequency of oscillation n, are given in tables 4.3 and 4.4. U_T is the towing carriage velocity and U_N and U_0 are the maximum velocity of the oscillatory component of the total velocity for lateral oscillation and in-line oscillation respectively.

Drive:	'Kopp' variable speed drive, by Allspeeds Limited.
input:	constant speed, three phase motor; 0.25 kW; 1350 rpm.
output:	from 10.23 to 32.21 rpm.
Crank length:	189.5 mm
connecting rod length:	285.0 mm

Table 4.1 Technical specifications of the variable speed drive of the oscillation test rig.

Test model	Reynolds number
circular cylinder:	1.0×10^4 − 7.0×10^4
rectangular block:	1.9×10^5 − 5.3×10^5
cruciform parachute:	3.0×10^4 − 1.5×10^5
ring-slot parachute:	4.0×10^4 − 2.0×10^5.

Table 4.2   Range of Reynolds number.

TESTMODEL	U_T/nL	U_N/nL
Rectangular Block	5.4-9.5	≈ 3.2
Cruciform Parachute	6.1-8.4	≈ 5.8
Ring-slot Parachute	5.5-6.8	≈ 4.6

Table 4.3 Reduced velocity and periopdic parameter for lateral oscillations.

TESTMODEL	U_T/nL	U_0/nL
Circular Cylinder	≈ 19	≈ 13
Rectangular Block	5 - 10.5	≈ 3.2
Cruciform Parachute	≈ 7.7	≈ 5.8
Ring-slot Parachute	≈ 6.2	≈ 4.6

Table 4.4 Reduced velocity and periopdic parameter for in-line oscillations.

Figure 4.1   The   ship-tank   of the Southampton
College of Higher Education.
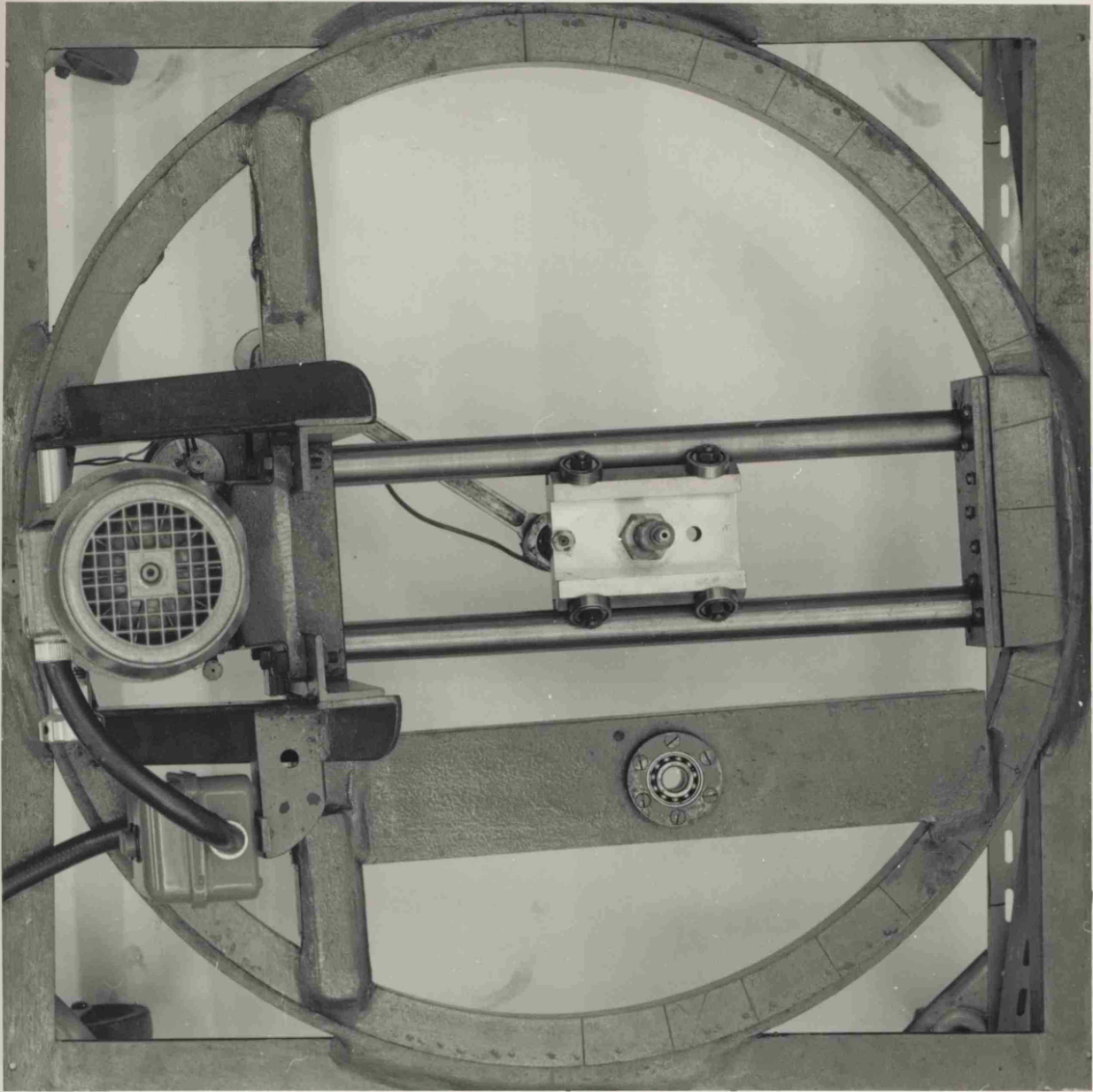
Figure 4.2   The   ´piston-connecting   rod´
mechanism   that   is   used to oscillate the test
models, at pre-set frequencies.
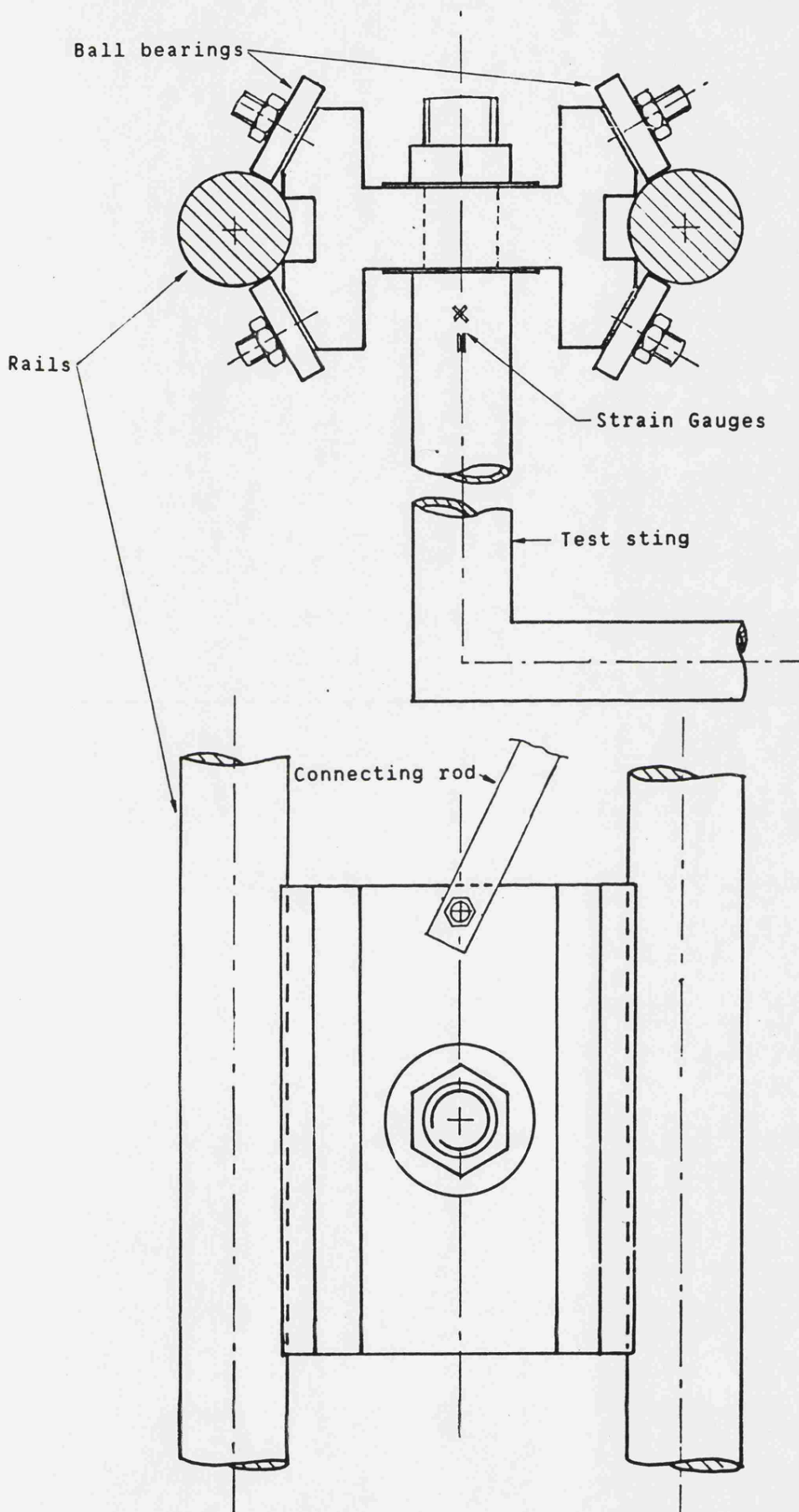
Figure 4.3 The reciprocating block of the oscillation rig, run on two rails. The upper end of the test sting is firmly attached to the reciprocating block, by a single nut.
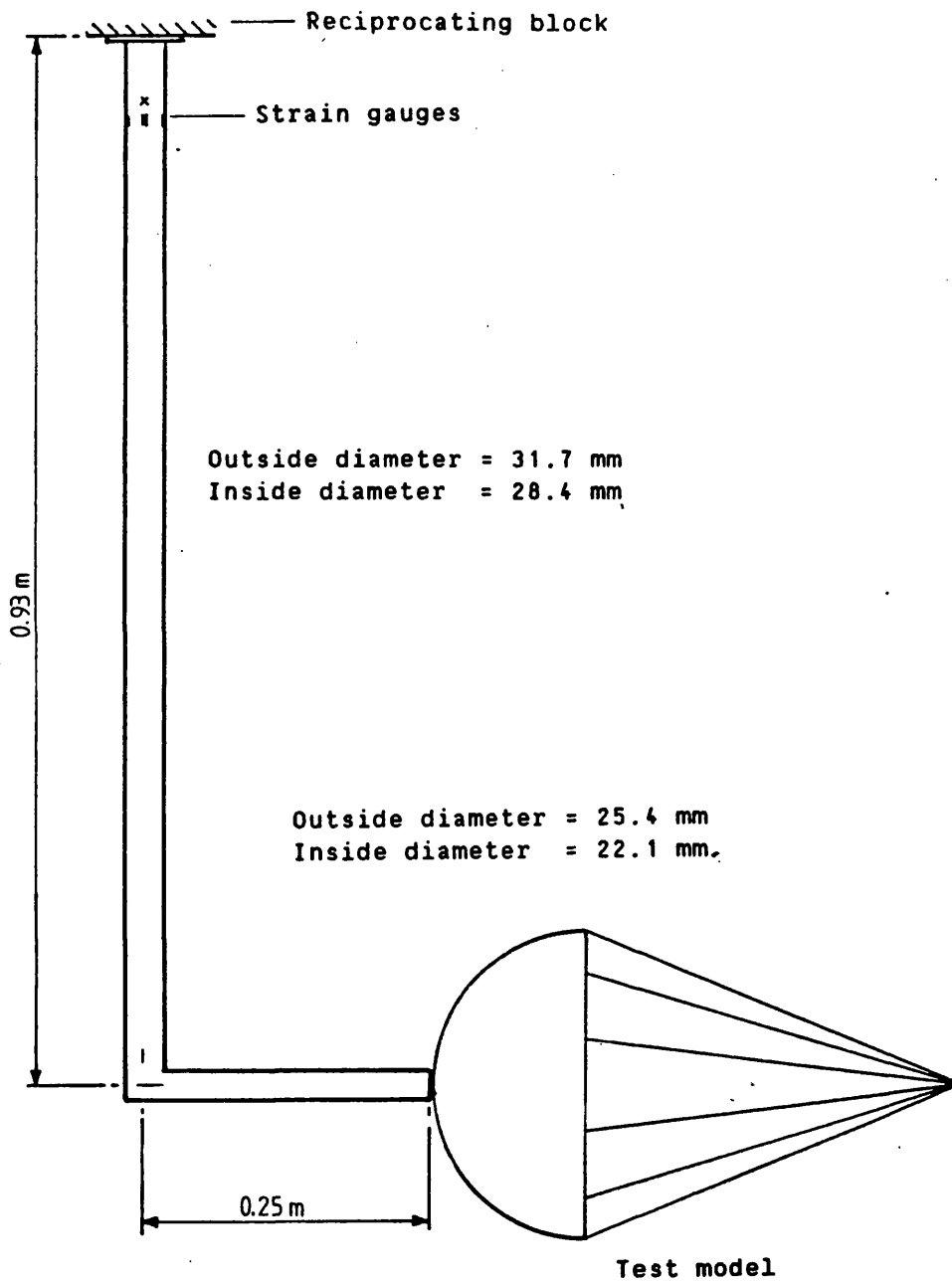
Figure 4.4   Assembly   of   test   sting and test model.
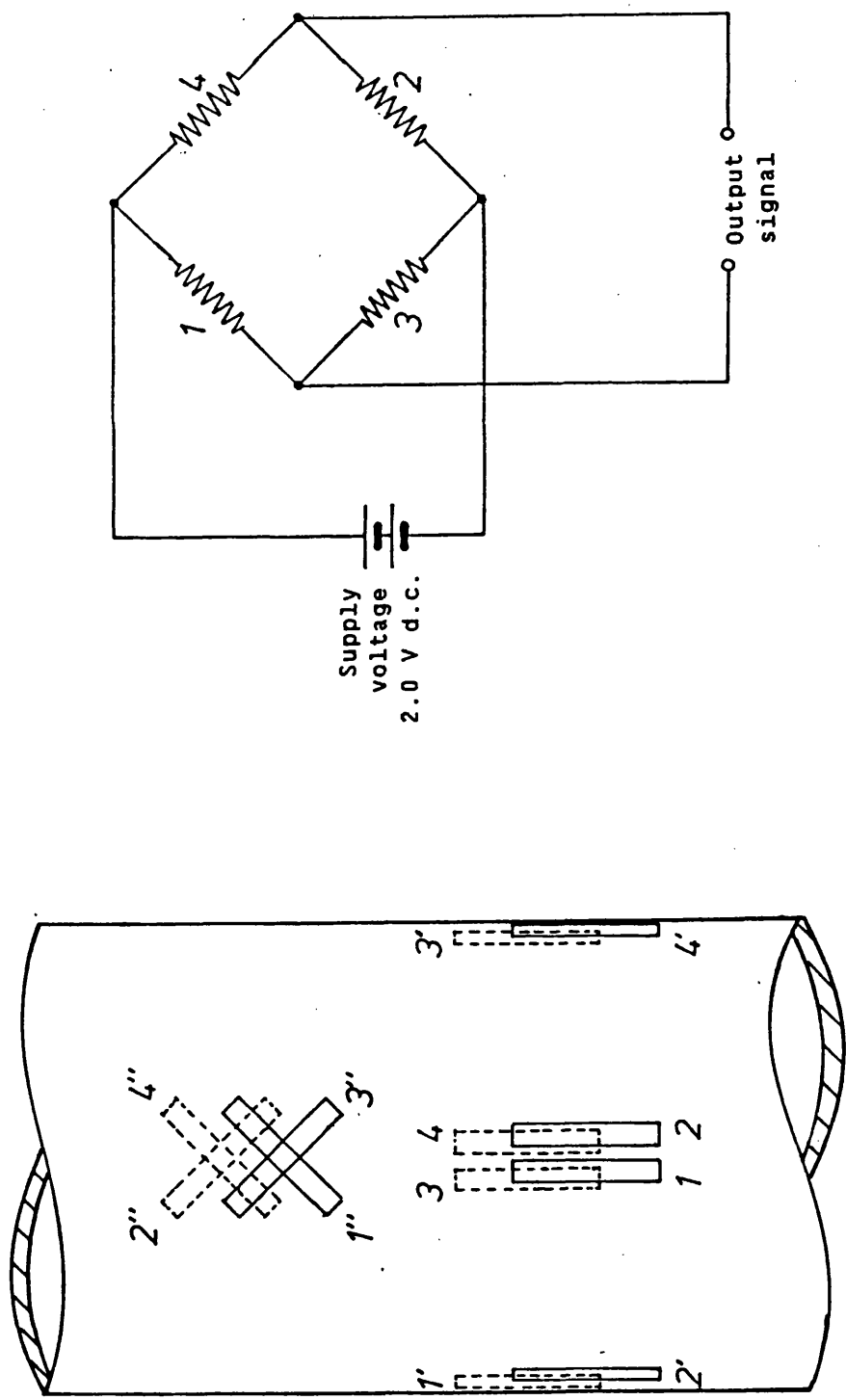
Figure 4.5 Locations of the strain gauges and
the bridge circuit for each strain gauge set.
The resistance of each strain gauge is 120 Ω.

set 1 2 3 4 indicates   force   in   normal
                           direction

set 1'2'3'4' indicates   force   in   axial
                           direction

set 1"2"3"4" indicates   moment   on   the   test
                           model
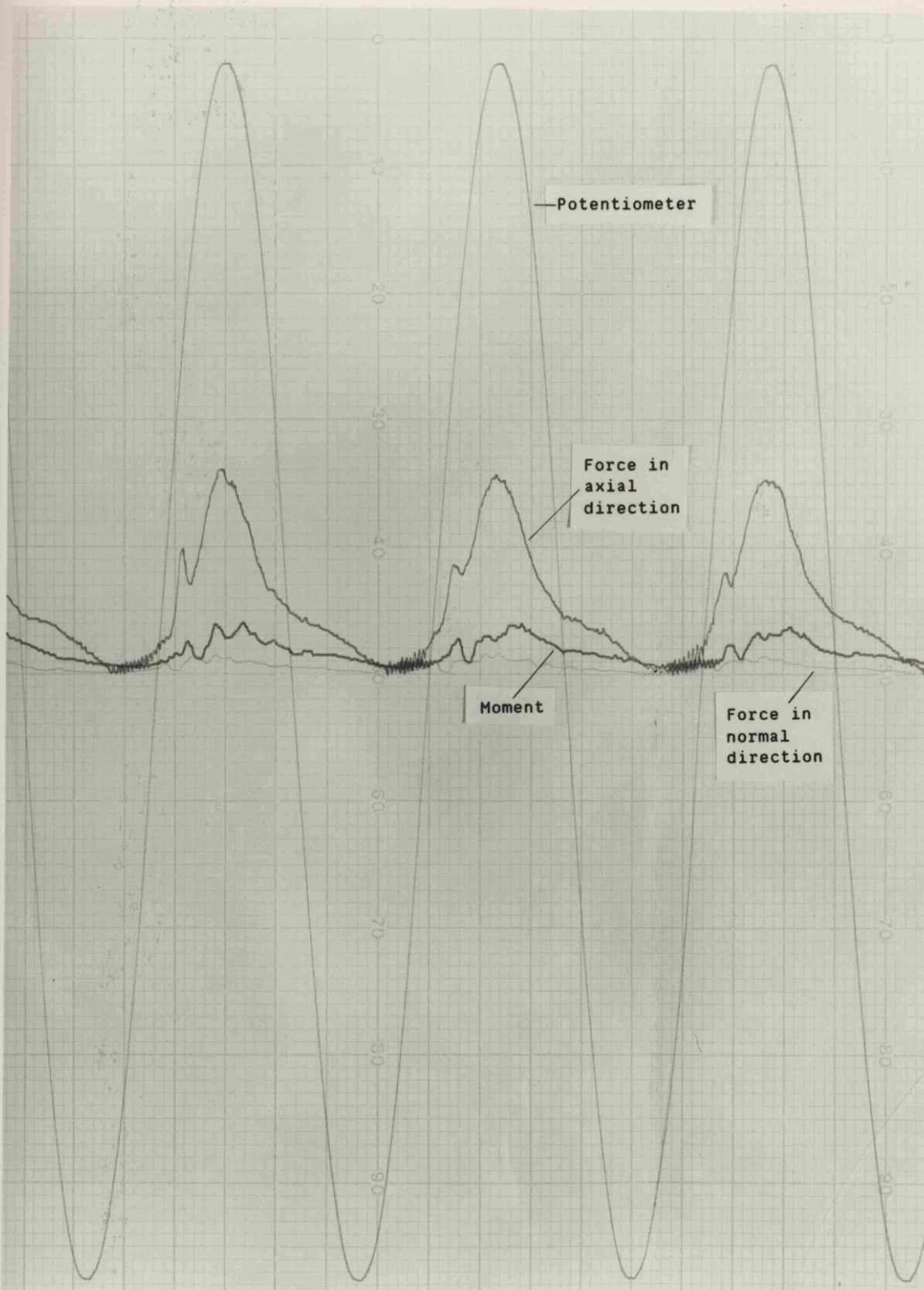
Figure 4.6a Chart recorder output for cruciform parachute model, with oscillations in-line with axial translation at costant angle of attack of 10°.
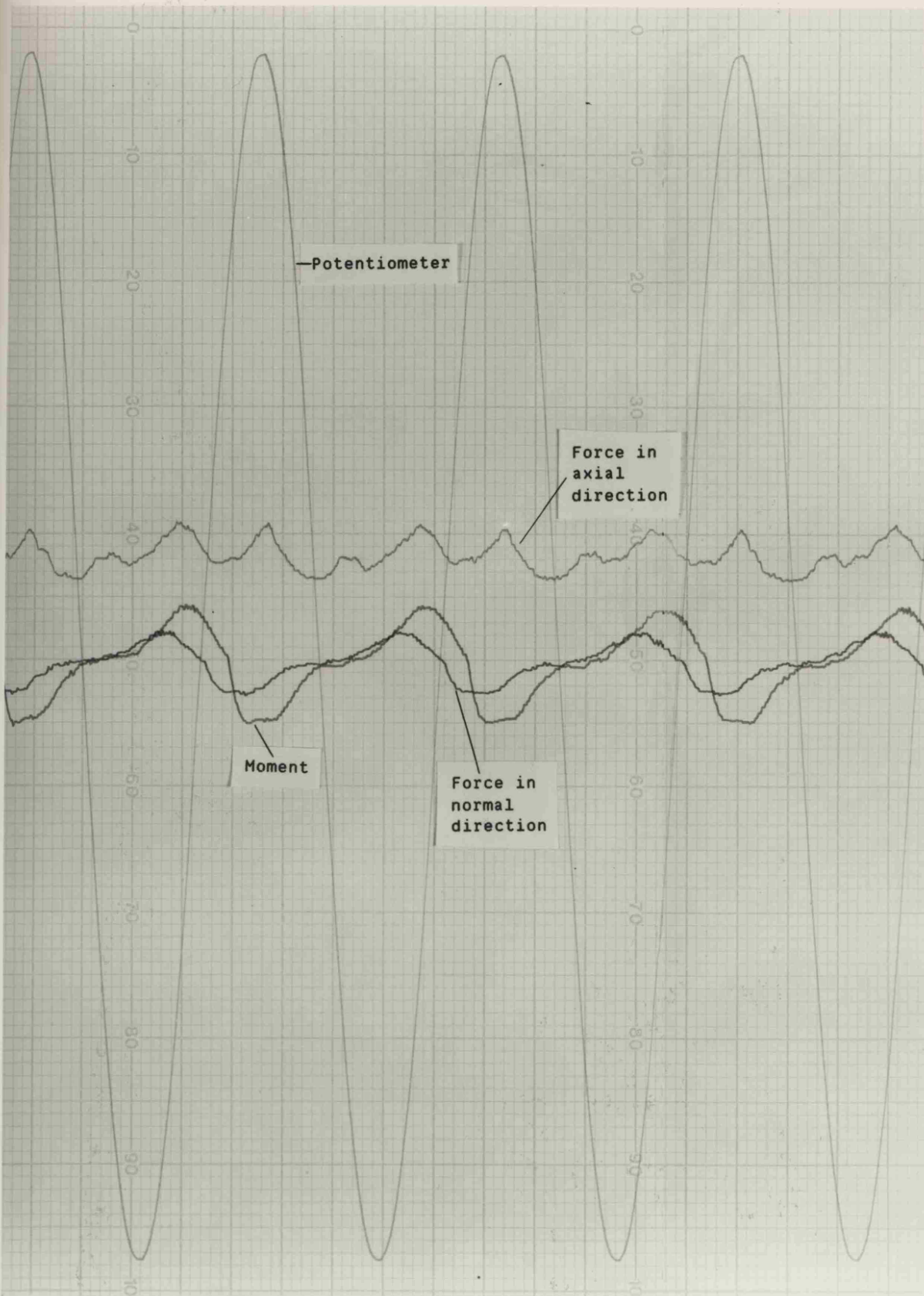
Figure 4.6b Chart recorder output for Ring-Slot parachute model in lateral oscillation, superimposed on uniform translation in axial direction.

Figure 4.7   cruciform   parachute,   with   arm
ratio of 4:1.
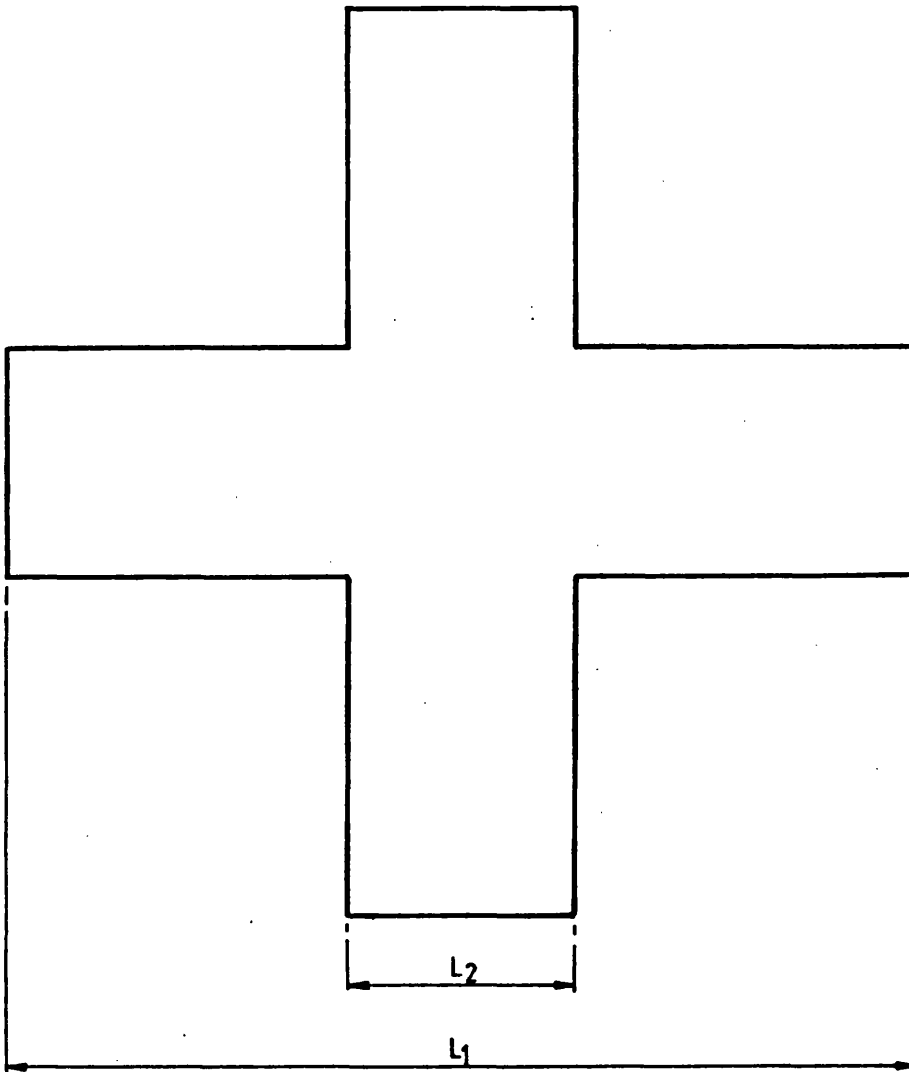
Figure 4.7a Geometric shape of a cruciform
parachute.
L_1 = 480mm; L_2 = 120mm.
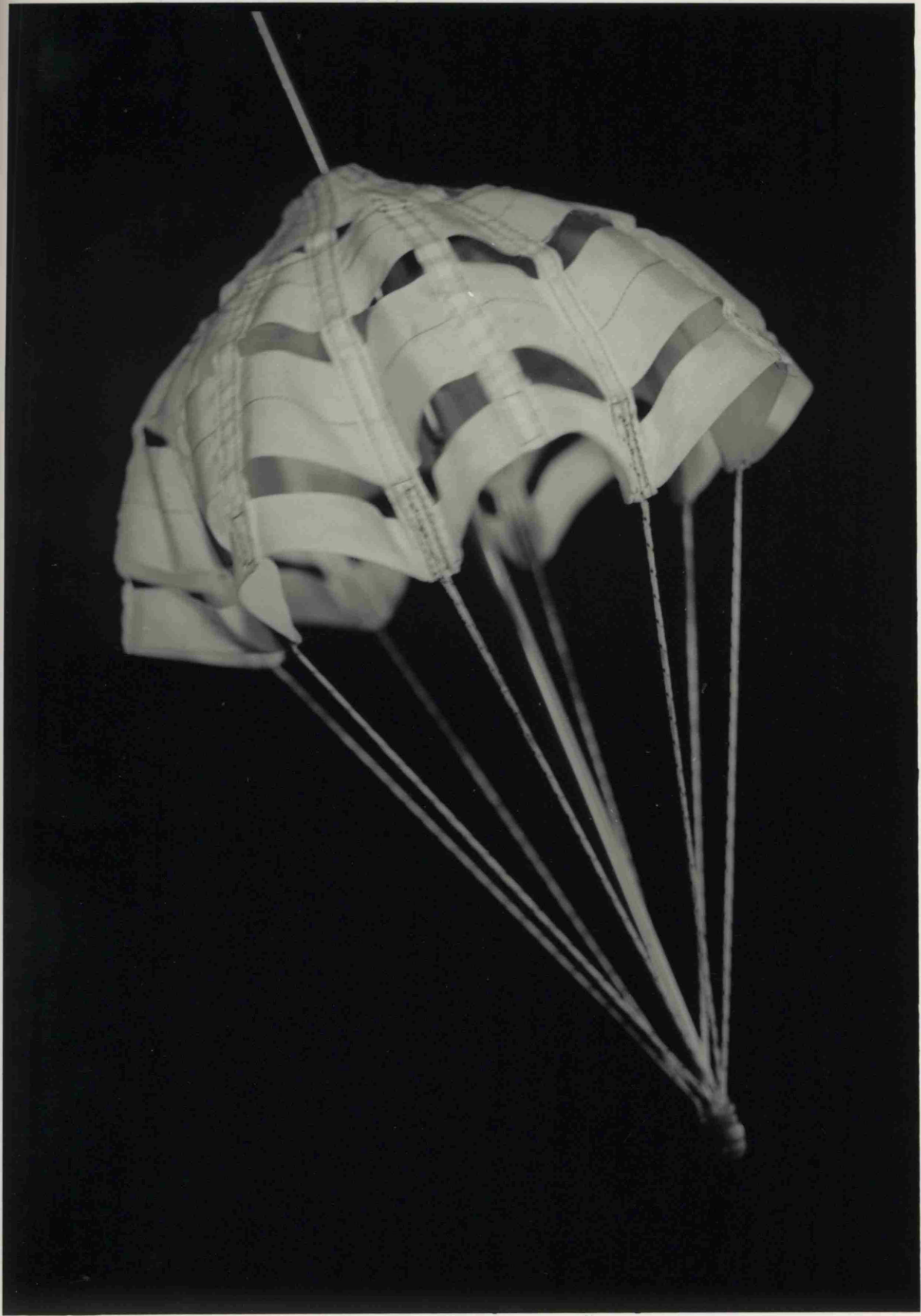
Figure 4.8   Ring-Slot parachute.
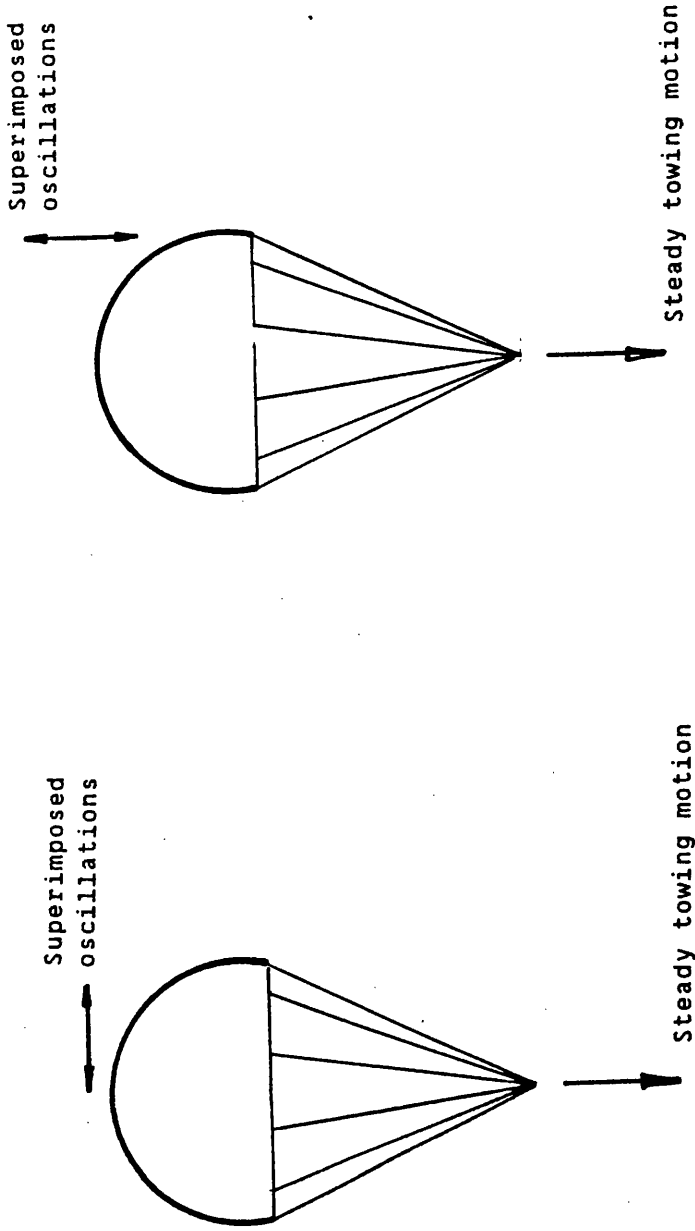
Figure 4.9   Modes of motion of the test model.

CHAPTER FIVE

ANALYTICAL PROCEDURE AND DISCUSSION OF RESULTS

ANALYTICAL PROCEDURE AND

DISCUSSION OF RESULTS

5.1 INTRODUCTION

In this chapter the discussions are divided into three sub-chapters:

(A) Analytical Procedure:

The procedure involved in deriving a relationship between the unsteady motion of a submerged body and the fluid dynamic force applied on it was discussed in Chapter Three. In this sub-chapter, which includes Sections 5.2 to 5.7 the author discusses this procedure in detail using experimental data. The process by which the Impulse Response Function of equation (3.2) is derived and used in a relationship for unsteady fluid dynamic force, is given in Sections 5.2.1 and 5.3. Also discussed are the significance of this relationship in its application, advantages, disadvantages and limitations of using this relationship to model unsteady fluid dynamic forces. Furthermore, the sub-chapter includes details of the methods used to calculate the coefficients required for the relationship.

(B) Discussion of Results:

In Section 5.8, included in this sub-chapter, the

author discusses the characteristics of the empirical coefficients associated with the relationship designed for modelling unsteady fluid dynamic forces.

(C) Comparison Between Modelled Data and Experimental Data:

In this sub-chapter, the relationship for modelling unsteady fluid dynamic forces is compared with certain relationships published by other researchers. It also includes a comparison between results modelled using the derived relationship and the experimental results.

A summary of the discussions is included in Section 5.12, at the end of the chapter.

(A)   ANALYTICAL PROCEDURE

5.2   EFFECT OF HISTORY OF VELOCITY AND ACCELERATION ON FLUID DYNAMIC FORCES

In Chapter 2, it was discussed how the actual velocity-dependent force component would continuously 'lag' behind its quasi-steady prediction (force reproduced using steady flow force coefficients in eq. 1.3), whether the acceleration is positive or negative. A typical set of velocity-dependent forces reproduced using steady flow data of C_R are shown in figures 5.1, 5.2, 5.3 and 5.4. Also shown in these figures are the acceleration-dependent forces reproduced using potential flow values of added mass. Where potential flow added mass coefficients are not available, e.g. in the case of parachute canopies, for the purpose of illustration, comparable numerical values in place of these coefficients, are used. For comparison, the experimental values of total force also are plotted on the same figures.

It is evident from these figures that the velocity-dependent component is a substantial part of the fluid dynamic force. Since the actual velocity-dependent force can 'trail' behind the predicted value based on steady flow C_R and instantaneous velocities, as discussed in Chapter Two, this lagging characteristic is expected to be vicible in the measured force, compared with the quasi-steady model. These comparisons are made in figures 5.5, 5.6, 5.7 and 5.8 in which the measured force and the

force predicted by a quasi-steady prediction model are plotted against time.

Figure 5.5: Forces on a long circular cylinder which is oscillated in the direction of its linear translation along the length of the ship tank;

Figure 5.6: Forces on the rectangular block described in Section 4.5.2 when oscillated along the axis of its linear uniform translation, with its 457mm x 153 mm side facing the front;

Figure 5.7: Lateral forces on the cruciform parachute model which is towed along the water tank in its axial direction at uniform speed. The oscillations are superimposed in the lateral (normal) direction;

Figure 5.8: Lateral forces on the ring-slot parachute model which is towed along the water tank in its axial direction at uniform speed. The oscillations are superimposed in the lateral (normal) direction.

The term quasi-steady prediction is used to represent the theoretical force in these figures because steady flow data and the instantaneous velocity are used to derive the velocity-dependent component of the force. The acceleration-dependent forces in these figures are based on the potential flow values of added mass and instantaneous values of acceleration. Thus, for the process of deriving a relationship for the unsteady fluid dynamic force, described in Chapter Three, the first approximation to the unsteady force is given by the quasi-steady force shown in these figures.

Furthermore, shown in dotted lines in the same figures are the forces modelled using published data

available to the author. The model used for this purpose has the form given by equation (1.3).

5.2.1 Considering an Expression for the Unsteady Fluid Dynamic Force

As illustrated by equation (3.2) in Chapter Three, measured fluid dynamic force can be related to the entire history of motion, using the convolution integral and the Impulse Response Function.

Using standard notation associated with the convolution integral, it can be written in the form given in equation (3.2a) as

$$F(t) \quad = \quad \{C_R \ 1/2 \ \rho A U(t)|U(t)| \ + \ k \ \rho V \dot{U}(t)\} \ * \ G(t)$$

$$(3.2a)$$

in which F(t) in the measured force as shown in figures 5.5, 5.6, 5.7 and 5.8. The theoretically predicted force, shown in these figures by solid line which is used as the first approximation, is given by the terms inside ´{}´ brackets. Thus the initial shape of the Impulse Response Function G(t) effectively represents the functional relationship between the two sets of data plotted in each of these figures.

5.3 THE IMPULSE RESPONSE FUNCTION AND ITS APPLICATION IN A PREDICTION MODEL FOR UNSTEADY MOTION

The procedure involved in the derivation of the Impulse Response Function for each test model was given in

Chapter Three. The first approximation of the prediction model is written using steady flow coefficients of the velocity-dependent force, and the potential flow values of the acceleration-dependent force. Steady flow coefficients of velocity-dependent force are obtained from experiments in which test models are towed at uniform speeds, at various attitudes. The approximate values of potential flow coefficients are based on data given in Table 1.1. The numerical values of these coefficients are irrelevant because coefficients for real fluids are re-calculated during the process of iteration described in Appendix A. However, realistic initial values minimise the need for a large number of iterative re-calculations.

The empirical form of the Impulse Response Function (IRF) is obtained from the modulus (amplitude) and the argument (phase angle) calculated using equation (3.4), for corresponding frequency of excitation.

After having found a crude first approximation to the modulus and the argument of the IRF it was possible to re-estimate the coefficient of the velocity-dependent and the acceleration-dependent force components. The procedure adopted for this purpose is explained in Section 5.4.1. The new values of coefficients were then re-used to re-estimate the modulus and the argument of the IRF. After three or four iterations the author could arrive at the properties of IRF as shown in figures 5.9, 5.10, 5.11 and 5.12.

The modulus and the argument of the IRF versus the frequency of excitation are shown in these figures, for the four types of test models.

Figure 5.9: circular cylinder,

Figure 5.10: rectangular block,

Figure 5.11: cruciform parachute and

Figure 5.12: ring-slot parachute.

All four graphs in these figures show that for both "d.c." component and first harmonic component of the IRF the modulus remain approximately equal to one. The argument, however, having being equal to zero for the "d.c." component possesses a negative value for the first harmonic frequency.

The fact that the modulus of IRF is approximately equal to one implies that the values of coefficients of velocity-dependent and acceleration-dependent forces corresponding to this IRF could be used, with instantaneous velocity and acceleration, to derive the magnitude of the unsteady fluid dynamic force. Nevertheless, the negative value of the argument of the IRF implies that there is a lag in the part of the actual force, compared to the force derived using instantaneous velocity and acceleration. Since the argument of the IRF is zero at zero frequency, and negative for non-zero frequency, the phase lag appear to be frequency dependent.

At this stage it was becoming apparent that the characteristics of the IRF cannot clearly be defined using the fundamental frequencies of oscillations without data over a wider range of frequencies. However, the range of frequencies over which experiments could be conducted was limited by the lowest frequency of oscillation of the test rig, and the frequencies at which the test models would yield to produce reliable results, due to vibration,

parachute collapsing etc. Thus it was decided to consider the higher harmonics of the IRF using equations (3.4a) and (3.4b). It can be seen in figures 5.13, 5.14, 5.15 and 5.16 that the moduli of the IRF for the second, and sometimes even the third harmonic frequency, is approximately equal to that for the "d.c." component and the fundamental frequency. The arguments, however, are decreased for the higher harmonic frequencies. Since the lower frequencies dominate the fluid dynamic force as shown in Table 5.1, the characteristics of the IRF are decided predominantly by data at lower frequencies.

Thus, it can be considered that the modulus of the IRF is approximately equal to one and that the argument is proportional to the frequency. These characteristics are summed up in Table 5.2.

Test model	Modulus (approx)	Argument	
		deg/rad/sec	sec(approx)
Circular cylinder	1.0	-12	-0.22
Rectangular block	1.0	-13	-0.23
Cruciform parachute	1.0	-20	-0.35
Ring-slot parachute	1.0	-17	-0.29

Table 5.2 Modulus and argument of the Impulse Response Function.

Such characteristics can be expressed by a 'delayed impulse function' as[11],

$$IRF \quad = \quad G(t) \quad = \quad 1.0^{-i\omega\tau}$$

$$= \quad \delta(t-\tau)$$

where $-\tau$ refers to the negative gradient of the graph of argument versus frequency.

Now, by substituting in equation (3.2) one gets,

$$F(t) \quad = \quad \int_{-\infty}^{t} C_R \, 1/2 \, \rho AU|U| \, \delta(t-\tau) \, d\tau$$

$$+ \quad \int_{-\infty}^{t} k \, \rho V \dot{U} \, \delta(t-\tau) \, d\tau$$

Thus it is more appropriate to consider this 'lag' as a time-lag rather than a phase-lag because unlike the argument of the IRF, the gradient of the argument versus frequency appears to be approximately constant.

Hence the magnitude of the fluid dynamic force can be written in the conventional form as

$$C_R \, 1/2\rho AU|U| \quad + \quad k \, \rho V \dot{U}$$

The time-lag can be incorporated into this expression as:

$$F(t) \quad = \quad C_R \, 1/2 \, \rho A \, U(t-\tau)|U(t-\tau)| \quad + \quad k\rho V \dot{U}(t-\tau)$$

$$(5.1)$$

where, τ is estimated from the graphs of argument of the Impulse Response Function versus frequency of excitation. In other words, the fluid dynamic force at any instant in time can be expressed by a relationship similar to Morison's equation in which the force coefficients are constants, and by assuming that the effect of the velocity and the acceleration is delayed by a period of time τ. All the test models used during the experiments are bluff bodies, and the characteristic time-delay is found to be a common phenomenon. Nevertheless, the magnitude of this time-delay appear to depend on the shape of the submerged body.

5.3.1 Dependence of τ on the Frequency

From the figures 5.9, 5,10, 5.11 and 5.12 it appears that the range of frequencies over which experiments were conducted is inadequate to establish the dependence of τ on the frequency of oscillation of the body. Nevertheless, by considering harmonic frequencies as shown in figures 5.13, 5.14, 5.15 and 5.16, it is evident that the argument for the "d.c." component of the total force, as expected, is zero. As the frequency increases, so does the magnitude of the argument also. In the absence of an accurate functional relationship, for the purpose of current investigation it is assumed that the argument in figures 5.13, 5.14, 5.15 and 5.16 is proportional to the frequency of each harmonic component. Since the gradient of a linear relationship between the argument and the frequency (ω) is given by $\omega\tau$, the time-lag τ itself can be regarded as independent of the frequency.

5.3.2 History Effects on Acceleration-Dependent Force

In the procedure adopted in this thesis the author considered a common Impulse Response Function to govern the effects of both the velocity and acceleration. This procedure was adopted, instead of employing independent IRF's in each component of force, so that equations (3.2) to (3.4) would not include more unknowns than the maximum permissible for obtaining their solutions. Nevertheless, it is hard to justify that the history effect (which determines the shape of the IRF) on the velocity-dependent component is identical to that on the acceleration-dependent component.

Thus, the author at this point strongly recommends that further experimental investigation should be carried out with emphasis paid on the behaviour of the two components of the force separately.

5.3.3 Limitations in Application of the Prediction Model Given by Equation (5.1)

The application of the prediction model given by equation (5.1) for deriving unsteady fluid dynamic forces on submerged bodies is limited mainly by two constraints: (a) the nature of the motion of the submerged body. e.g. linear, oscillatory or other arbitrary modes, and (b) the frequencies of oscillations imparted on the submerged body.

5.3.3.1 Limitations due to Modes of Motion

The empirical relationship between the fluid dynamic force and the velocities and the accelerations of the submerged body, given by equation (5.1), is obtained

from experimental results for which oscillations are superimposed at various attitudes, on linear translation of the body. Thus the application of this relationship is limited to such cases. A further restriction of the model given by equation (5.1) arises from the fact that the modes of motion of test models during the experiments were such that the mean velocities of the test models were non-zero. The mean velocities were sufficiently large that at no time the test models were moving back into their own wakes.

Several examples of the applications of the prediction model are:

1. Estimating forces on cylindrical sections of offshore structures that are towed at uniform speeds. The unsteady forces arise due to the sea waves superimposed on the towing motion.

2. Analysing forces on high-sided vehicles which are driven at uniform speed. The unsteady forces are due to superimposed ´lateral´ and ´head-on´ gusts.

3. Analysing forces on parachute canopy systems. Fully deployed descending parachutes oscillate both in the vertical direction as well as in the lateral direction. The descending speed of the parachute depends on the vertical fluid dynamic force applied on the canopy. The stability of the canopy system, and its frequencies and amplitudes of oscillation depend on the lateral (normal) fluid dynamic force.

It is not yet known whether this model can be applied for non-periodic unsteady fluid dynamics.

5.3.3.2 Limitations due to Frequencies of Oscillations

As can be seen in figures 5.13, 5.14, 5.15 and 5.16 the Impulse Response Function of the analysed systems, behaves as a 'delayed impulse' for frequencies only up to 3 rad/sec. Both moduli and arguments of the IRF at higher frequencies appear to be quite arbitrary. The model given by equation (5.1) is based on the linear relationship for the frequencies in the range 0 to 3 rad/sec, thereby discarding the effects of high frequency components of the fluid dynamic force. Thus, the application of the prediction model is restricted to motions of either unsteadily moving bodies or unsteadily moving fluids involving frequencies less than 3 rad/sec. As shown in Table D.1 the components of the fluid dynamic forces, as predicted by equation (5.1), at frequencies less than 3 rad/sec. normally amounts to more than 90% of the total force. Thus the fluid dynamic forces predicted by this model can possess an error margin of about ten per cent. Also shown in Table D.1 are the percentages of the components of the measured force which have frequencies above 3 rad/sec.

It should be noted that forces at frequencies higher than 3 rad/sec are more likely to be due to vortex shedding, natural frequencies of vibrations, system noise, etc. (See Appendix B for an analysis of the natural frequencies of vibration and the vortex shedding frequencies.) Therefore, discarding higher harmonic signals becomes an effective method of filtering the experimental results because this method isolates high frequency signals,

without distorting the fluid dynamic force near the more dominating lower frequencies.

The prediction model given by equation (5.1), therefore, is applicable for frequencies below 3 rad/sec. only. As a direct result the model does not predict oscillatory force components due to vortex shedding which normally occur at higher frequencies. The lowest vortex shedding frequency of about 0.5 Hz was observed for the circular cylinder. The order of magnitude of forces due to vortex shedding are analysed in Section 5.10 of this chapter.

5.3.4 Validity of Linear Theory Used to Derive the Impulse Response Function

The derivation of the model given by equation (5.1) is based on the assumption that linear theory can be used to establish the relationship for the unsteady fluid dynamic force (see Section 3.2.1 of Chapter Three). As discussed in Section 5.3.3, the Impulse Response Function derived using this assumption was reliable only for low frequencies of excitation. Thus the model is applicable only for slow unsteady motion where the effects of high frequencies are insignificant.

5.4 ACQUISITION OF COEFFICIENTS OF FORCE COMPONENTS, AND BUILDING THE PREDICTION MODEL

The procedure involved in deriving the coefficients C_R and k and the Impulse Response Function was outlined in

Chapter Three. It is conceivable at this stage that the IRF can be expressed by a delayed-impulse provided that the harmonics of motion for frequencies above 3 rad/sec have negligible effects on the fluid dynamic force. Since the 'delayed-unit-impulse' can be given by a single variable τ, provided that the attitude of the submerged body is unchanged, the model given by equation (5.1) can effectively be used with only three experimentally determined parameters. They are:

1. the coefficient of velocity-dependent component of the total force -- C_R

2. the coefficient of acceleration-dependent component of the total force -- k

3. the time constant involved in the Impulse Response Function -- τ.

The first approximation of τ is obtained using steady flow data of C_R and values of k that are based on potential flow, for bodies with similar geometries.

5.4.1 Evaluation of Coefficients of Velocity-Dependent Force and Acceleration-Dependent Force

Both sides of the equation (5.1) are divided by $1/2\rho AU(t-\tau)|U(t-\tau)|$, and it is re-written as

$$\frac{F(t)}{1/2\rho AU(t-\tau)|U(t-\tau)|} = C_R + k\frac{\rho V\dot{U}(t-\tau)}{1/2\rho AU(t-\tau)|U(t-\tau)|}$$

$$(5.1a)$$

Using the first approximation of τ, the graph of

$$\frac{F(t)}{1/2\varrho AU(t-\tau)|U(t-\tau)|} \quad Vs \quad \frac{\varrho \forall \dot{U}(t-\tau)}{1/2\varrho AU(t-\tau)|U(t-\tau)|}$$

is plotted. These parameters are chosen so that, in a straight line relationship, the intercept on the vertical axis and the gradient of the graph give the coefficient of the velocity-dependent force and the coefficient of the acceleration-dependent force respectively.

The graphs plotted using $\tau=0$, shown by the figures 5.17a, 5.18a, 5.19a and 5.20a, do not represent relationships that can be interpreted by straight lines. These results have been obtained from unsteady movements of test models at uniform attitude - i.e. constant angle of attack. This is clearly evident in the figures 5.19a and 5.20a, which are drawn using test results of parachute models. Corresponding graphs using the calculated values of τ, are shown in figures 5.17b, 5.18b, 5.19b and 5.20b. The straight line relationship in these graphs indicate that in a prediction model similar to equation (5.1) the force coefficients C_R and k can be regarded as constants, whereas, in a relationship similar to Morison's equation, the force coefficients are functions of further independent parameters.

Although success has been claimed by numerous authors[15] in correlating experimental results and results modelled using expressions such as equation (1.3) with two constant cocefficients (C_R & k), the introduction of a third

parameter τ, which represents the history of motion, appeared to have improved this correlation.

5.5 USEFUL CHARACTERISTICS OF THE PREDICTION MODEL INCLUDING 'TIME-DELAY'

The fact that the entire history of motion of the test models can be represented by a 'time-delay' leads to a prediction model that has several advantages over other methods.

Around a body moving unsteadily in a real fluid the flow field continuously changes from one instant to another. Thus, in an expression similar to equation (1.3) the coefficients of the two force components should be regarded as variables since both coefficients depend very much on the shape of the flow field. Expressing these coefficients as functions of further independent parameters brings further complications into the analyses. If both C_R and k are variables the number of possible values of these coefficients that could satisfy a certain set of data can be as much as infinity. The difficulty of evaluating the force coefficients is overcome if either one or both coefficients are constants. The model given by equation (5.1) is rather useful because the experimentally determined parameters in it, namely C_R, k and τ, are found to be independent of the accelerations imparted on the body. i.e. these parameters could be determined from a limited number of experiments.

In order to avoid the requirement to define the force coefficients as functions of further independent

parameters many researchers use quasi-steady expressions (see Section 1.5.2) in which the steady flow data are used to identify the component of the total force which is dependent on the velocity. Hence the remainder of the force is assumed to be acceleration-dependent. In doing so one almost certainly assumes that, either a part of the total fluid dynamic force that is velocity-dependent to be acceleration-dependent, or vice versa. Although it is possible to reach a numerical answer by adopting this method the derived coefficients of acceleration-dependent force can possess very unrealistic values: either too high or too low, or even negative!. Frazer and Simmons[12] provide evidence for such results. Furthermore, Yavuz[42], Jorgensen[18] and Cockrell et al[8] obtained very high coefficients of acceleration-dependent force for low acceleration numbers. This inconvenient situation arises because the component of the total fluid dynamic force that is velocity-dependent and that which is acceleration-dependent, are not identified properly.

Keulegan and Carpenter[22] successfully separated the two components of the total fluid dynamic force using Fourier series by assuming the coefficients of two component forces to be constants. This process was made possible because in their experiments the motion was purely sinusoidal. In such case the acceleration always leads the velocity by 90°. This method cannot be used to analyse the two components of the total force if the motion is non-sinusoidal. The author was able to overcome this difficulty during the present investigation by using the

'time-delay' in equation (5.1), which arises from the effect of the history of motion. The straight-line relationship obtained in figures 5.17 to 5.20 imply that the coefficients of the velocity-dependent force and those of the acceleration-dependent force are independent of time. Despite the scattered results, figures 5.21 to 5.28 support the fact that the coefficients C_R and k are independent of acceleration number, and thus of time. An important significance of the model given by equation (5.1) is that the coefficients in this model reflect the forces due to the entire history of both velocity and acceleration of motion rather than those due to the instantaneous velocity and the instantaneous acceleration.

Once the coefficients C_R and k are known to be constants (with respect to time) they can be derived, as explained in Section 5.4.1, from the graphs in figures 5.17 to 5.20 of which the gradients are equal to the values of k and the intercepts on the vertical axes are equal to the coefficients of C_R. This procedure effectively separates the two components of the total force that are dependent on velocity and on the acceleration. Thus, it gives the fluid dynamicist the opportunity to study the two components of the force separately. Furthermore, it enables him to draw a direct comparison between the forces in steady flow and in potential flow, and the respective components of the unsteady real fluid force. These comparisons are illustrated in Tables 5.3 and 5.4.

Decades of experimental research have shown that real fluid dynamic forces on submerged bodies are dependent

not only on the instantaneous velocity and acceleration but their history also. Although models similar to that given by equation (1.5) include a term expressing the history of motion, little success has been achieved in accumulating relevant data because the dependence on acceleration of the coefficients involved in each force component has not been established. Equation (5.1) has the advantage because the entire history of motion also has been taken into account during the analysis. The data for C_R, k and thus calculated found to have negligible dependence on the acceleration number.

5.5.1 Significance of Time-Independent Force Coefficients

Application of either equation (1.3) of its derivations fundementally implies that the acceleration-dependent force is given by the rate of change of momentum of the fluid surrounding a submerged body, inclusive of the pressure gradient due to the free stream acceleration. In the case where the free stream is at rest, the momentum of the fluid is given by $k\rho V U(t)$ where $U(t)$ is the velocity of the submerged body. Thus, the rate of change of momentum, and hence the acceleration-dependent force, is given as:

Acceleration-dependent force $= d/dt(k\rho VU)$

$$= k\rho V\, dU/dt\ +\ \rho VU\, dk/dt$$

If k is not independent of time, then equation (1.3) would include a further term involving the rate of change of the added mass. Thus, methods used by numerous authors [e.g. 8,12,17,19,43] in which the acceleration-dependent force coefficient (k) is defined as a function of the acceleration number, (hence a function of time) fundamentally misuse the underlying interpretation of equation (1.3) in which k should be regarded as independent of time.

Nevertheless, it hard to conceive that in a constantly changing flow field, the coefficients of two component forces would remain independent of time.

Thus, the author considers that it is significantly important that the modified form of equation (1.3), given by equation (5.1) gives rise to coefficients C_R and k which are effectively independent of time, hence overcoming the above mentioned difficulty.

5.5.2 Use of τ to Rectify the Delay in Measured Force

It can be argued whether it is necessary to use a further function (IRF), or a further parameter (τ), in addition to equation (1.3) in its form, to represent the unsteady fluid dynamic force. For example, the phase-lag of the measured force seen in figures 5.1 to 5.8 can be rectified to a certain extent by selecting suitable relative magnitudes of C_R and k. By doing so one may be able to make the maximum of the modelled force coincide with the maximum of the measured force, even for τ=0. But nevertheless, it may not be possible to obtain an overall fit to the experimental results this way. Figures 5.17 to 5.20 show

that in this method, the use of constant coefficients cannot be justified, if the attitude of the body remains the same. The introduction of the parameter τ has improved the overall fit to the experimental results while maintaining constant values of C_R and k.

The process of optimising C_R and k, with $\tau=0$, shown in Appendix E, indicates that the extent to which the forces modelled using equation (1.3) can be matched with the experimental forces is limited. The forces modelled by equation (1.3) where $\tau=0$, are compared in Appendix E, with those modelled using equation (5.1) where $\tau\neq0$.

5.6   REYNOLDS NUMBER AND ACCELERATION NUMBER EFFECTS

From steady flow experimental results using similar parachute test models and methods Yavuz[42] and Jorgensen[18] reported that the effect of the Reynolds number in the respective region is insignificant. Steady flow data given by Hoerner[13] suggest that the range of Reynolds number used for the circular cylinder and the rectangular block has negligible effects on the force coefficients.   Keulegan and Carpenter[22] noted the non-existence of Reynolds number dependence on their unsteady force coefficients. Thus the author regards that the Reynolds number effects on the forces coefficients in the present investigation are insignificant. Furthermore, figures 5.13 to 5.20 show that the coefficients C_R and k derived by the method outlined by this thesis are independent of the acceleration number.

5.7   NON-DIMENSIONAL FORM OF τ

In order that the model given by equation (5.1) may be applied to bodies of different scales the experimental data for τ should be expressed in a non-dimensional form. Because of the lack of data for test models of different sizes studies on scaling effects are regarded as an extended part of the present research programme.   However, the possibilities indicated below are available for future consideration.

Considering   the   independent   parameters   in incompressible and infinite unsteady fluid flow, namely the geometry and the attitude of the submerged body, ρ, L, υ and U(t) in a dimensional analysis it can be shown that the group U(t)τ/L is a possible non-dimensional form of τ. The reference velocity U(t) for this purpose can be either the mean velocity of the body or the maximum velocity of the oscillatory component of the unsteady motion.   The dependence of (Uτ/L) on parameters such as Reynolds number should be determined experimentally.

The author is unaware of any other research programme in which similar techniques have been adopted.

(B)   DISCUSSION OF RESULTS

5.8   COEFFICIENTS OF FORCE COMPONENTS

Having found negligible dependence on the acceleration number, the force coefficients for each test model are expressed as functions of its attitude of motion (i.e. the angle of attack) in figures 5.29 to 5.39. These coefficients are to be used on a prediction model given in the form of equation (5.1).

5.8.1   Coefficients of Velocity-Dependent force

In Sections 5.8.1.1, 5.8.1.2, 5.8.1.3 and 5.8.1.4 the coefficients of velocity-dependent force derived from unsteady flow experiments for each test model are compared with the appropriate steady flow results. The unsteady force coefficients are derived from tests in which the oscillations are superimposed on the steady motion either in the same direction (in-line oscillations) or in the lateral (normal) direction. Experiments with in-line oscillations are conducted for varied angles of attack by setting the test model to the required angle before the beginning of each test. Some of these coefficients are compared in Table 5.3 with steady flow data published by other researchers.

5.8.1.1   Circular Cylinder

The coefficients of velocity-dependent and acceleration-dependent components of the total fluid dynamic force on the circular cylinder are derived from the graph in

figure 5.9b. The coefficient of velocity-dependent force (C_R) given by the intercept on the vertical axis is approximately equal to 1.25. This value of C_R is very similar to the steady flow force coefficient for corresponding Reynolds number range, given by Hoerner[13] (see table 5.3). It should be noted that the unsteady forces on the cylinder were obtained from experiments in which the oscillations are superimposed in-line with the linear translation of the cylinder normal to its axis. Since the displacement of the cylinder is always in the same direction, the flow field around the cylinder would have developed to an extent for which it is not unlike that from the flow field in steady motion. Thus the coefficients of C_R in such unsteady flow are approximately equal to that in steady flow. The experimental results of Verley and Moe[41] which were obtained by superimposing sinusoidal motion and steady motion agree well ($C_R \approx 1.2$ from reference [41]) with those in the present study. The coefficients of velocity-dependent force obtained by Keulegan and Carpenter[22], however, were more than 2.0. The author considers that this disagreement is mainly due to the fact that in the experiments of Keulegan and Carpenter the mean velocity of the fluid was zero.

5.8.1.2 Rectangular Block

Figures 5.29 and 5.30 illustrate the coefficients of the velocity-dependent force on the rectangular block against its attitude of motion. The forces in the lateral (normal) direction were measured by oscillating the test

model in the lateral direction while it was being towed in the axial direction at constant speed. The coefficient of velocity-dependent lateral force shown in figure 5.29 is almost proportional to the angle of attack.

The coefficients of velocity-dependent force in the axial direction, for the same experiments are shown in figure 5.30. The unsteady force coefficient in the axial direction remains substantially constant for small and moderate angles of attack. It gradually falls for $\alpha > 20^{\circ}$. Also given in the figure 5.30 are the coefficients of velocity-dependent force for the same direction when in-line oscillations are superimposed on the linear translation. The force coefficients for in-line oscillations, are similar in magnitude to those in steady flow. (see also Table 5.3) This similarity can be expected because for in-line oscillations the test model always moves in the same direction. Thus there is very little variation in the flow field around the body. Lateral oscillations superimposed on uniform axial translation, however, increase the axial force by about 30 per cent.

5.8.1.3 Cruciform Parachute

The coefficients of velocity-dependent force components, for the lateral (normal) direction and for the axial direction are illustrated in figures 5.31 and 5.32. The force coefficients in the lateral direction for unsteady flow are as much as 100% greater than those in steady flow. Yavuz[43,42] and Jorgenson[19,18] reported values of C_N in steady flow that are about 20 per cent less than the

unsteady flow coefficients given in figure 5.31. The magnitude of the coefficient C_N given in figure 5.31 is positive for all positive values of α. The gradient of C_N Vs. α graph also is positive for all α.

Figure 5.32 shows the variation of the coefficient of velocity-dependent force in the axial direction on the descending cruciform parachute. The steady flow results shown here agree well with those given by Yavuz[43,42] and Jorgenson[19,18]. In-line oscillations on the vertical descent does not appear to have a significant effect on the velocity-dependent force. Lateral oscillations on the canopy during its vertical descent however, increase the force in the axial direction by about 25 per cent.

The coefficients for unsteady flow are compared with the steady and unsteady flow values obtained by other researchers in Table 5.3.

5.8.1.4 Ring-Slot Parachute

The coefficients of velocity-dependent force components in the normal and axial directions of the ring slot parachute are shown in figures 5.33 and 5.34. Steady flow test results show that the forces in the lateral direction for small angles of attack are almost zero. In-line oscillations superimposed on descent at small angles of attack appear to have very little effect on the magnitude on the force either in the lateral direction or in the axial direction. Superimposed lateral oscillations however, substantially increase the velocity-dependent force in both the lateral and the axial directions. This increase in the

axial force is found to be as much as 40 per cent. The magnitude of the velocity-dependent force in the lateral direction is positive for positive angles of attack, and vice versa. The gradient of C_N Vs. α graph is positive for all α.

5.8.1.5 Remarks on Velocity-Dependent Force

From unsteady flow experimental results it is apparent that the changes in the coefficient of the velocity-dependent force due to the oscillations of the test model are not appreciable if the motion persists in the same direction. In such case the flow field would not change substantially to cause a significant change in the force coefficient. By contrast, any fluctuations in the lateral direction generally increases the velocity-dependent force in the direction of the towing motion, even though the velocity in this direction is uniform. This implies for example, that a lateral gust on a high-sided vehicle moving at constant speed increases the drag on it even though the head-on velocity of air is constant. Furthermore, lateral oscillations of a fully inflated parachute increase its drag even when its axial speed of descent is constant. i.e. the lowest value of velocity-dependent component of force on a parachute is achieved when the descent is vertical and uniform.

It is evident from these results that any lateral oscillations imparted on a steadily moving submerged body substantially increases the fluid dynamic force on it. However, effects of in-line oscillations on the coefficients

of velocity-dependent force are not so significant. These characteristics are not surprising considering that lateral oscillations give rise to wider wakes than in-line oscillations. Wider wakes are associated with higher values of fluid drag, hence the increase in the fluid dynamic force is to be expected.

The data obtained from unsteady experimental results raise considerable doubts in the design criteria adopted for industrial purposes. In parachute design it is customary to use steady flow results to estimate their effective drag forces. This procedure underestimates the capacity of parachutes by as much as 30 - 40 per cent. Although this 'error' falls on the 'safer' side as far as the drag forces on the parachutes are concerned, it substantially misinterprets the dynamic characteristics of the parachute canopy systems. Furthermore, the author wonders whether the design engineers take into consideration that lateral gusts on high sided road vehicles increase the force of resistance in the forward motion.

Since lateral oscillations superimposed on linear translation increase the force along the axis of linear translation, it is necessary to establish this dependence using appropriate parameters. Considering that the force in the direction of linear translation $F_T(t)$, depends on the steady velocity in the axial direction as well as the frequency and amplitude of the lateral oscillations, one can write:

$$F_T(t) = f(\varrho, \upsilon, L, U_T, U_N, T) \qquad (5.2)$$

where,

> U_T - the uniform translational velocity,
>
> U_N - the amplitude of oscillatory velocity in the
>
> lateral direction,
>
> T - the period of oscillations and
>
> L - the characteristic length of the body.

From dimensional analysis one gets

$$F_T(t)/0.5\rho AU^2 = f(Re, U_N/U_T) \qquad (5.3)$$

Where U is the total velocity of the body.

Since $U_N/U_T = \tan(\alpha_{max})$

$$C_T = f(Re, \alpha_{max}) \qquad (5.4)$$

The effect of α_{max} is observed by relating C_T to its steady flow value for which α_{max} is zero.

Disregarding the effects of Re on the coefficients of the velocity-dependent forces[18], the increase in C_T is related to α_{max} in figure 5.44. It should be noted that the experiments in the present investigation were not designed for the purpose of establishing this relationship. Thus the range of α_{max} available for which C_T can be correlated is limited. Figure 5.40 show that the coefficient of velocity-dependent force increases steadily with the maximum angle of attack imparted by the lateral oscillations. More experimental data are required in order to obtain an

empirical relationship between the increase in C_T and α_{max}.

5.8.2   Coefficients of Acceleration-Dependent Force

Due to the boundary layer, and the consequent wake associated with separated flow, it is generally regarded that the acceleration-dependent forces in real fluids are greater than those in potential flow.   This fact is supported by the experimental results obtained within the course of the present research. The experimental values of k are compared in Table 5.4 with those obtained by other researchers.   Certain potential flow values also are included in this table for comparison.

5.8.2.1   Circular Cylinder

The coefficient of the acceleration-dependent force on the circular cylinder, in the direction normal to axis, is derived from the graph(b) of figure 5.17.   The coefficient given by the gradient of this graph is approximately 2.4, compared to the potential flow value of 1.0.   The coefficient of acceleration-dependent force in this case is 140 per cent in excess of its potential value. For values of the 'amplitude/diameter' ratio similar to that in present study, Keulegan and Carpenter[22] obtained coefficients of acceleration-dependent force which were negative.   These values are vastly different from those in the present investigation because in the experiments of Keulegan and Carpenter the mean velocity of the unsteady flow is zero. Coefficients of Acceleration-dependent force obtained by Verley and Moe[41] were approximately equal to 0.6.

5.8.2.2 Rectangular Block

Experimental results shown in figure 5.35, for the three-dimensional rectangular block with fineness ratio of 3:1 indicate a coefficient of acceleration-dependent force (k_{33}) of about 1.9 for its axial direction. (Compare this value with a two-dimensional rectangular section with fineness ratio of 2:1 having a potential flow coefficient of acceleration-dependent force of 0.61 - see Table 1.1. Therefore, the rectangular block used for the present experiments is expected to possess a force coefficient less than 0.61.) Experimental results in figure 5.35 show that the coefficient of acceleration-dependent force (k_{11}) for the lateral direction is about 2.4. (Compare with a two-dimensional square section which has a potential flow value of 1.19 - see table 1.1) i.e. for both lateral and axial directions the acceleration-dependent force is well in excess of their potential flow values.

Figure 5.35 shows that k_{11} slightly increases with α. Sufficient data are not available to observe the variation of k_{33} with α.

5.8.2.3 Cruciform Parachute

Figures 5.36 and 5.37 show the coefficients of acceleration-dependent force for lateral (normal) direction and axial direction respectively. The coefficient for the lateral direction k_{11}, shown in figure 5.36 increases with the angle of attack (α), and has a minimum value of about 0.7 at α=0°.

The coefficient of the acceleration-dependent force in the axial direction, k_{33} is plotted against the angle of attack in figure 5.37. This coefficient has a maximum of about 4.0 at $\alpha=0^{\circ}$, and decreases gradually with increasing α.

The values of k_{33} obtained by Yavuz[42] and Jorgensen[18] are shown in Table 5.4 for comparison. They, however, used a quasi-steady model (see Section 1.5.2) to derive the acceleration-dependent component of the total force. Thus the force coefficients were found to be dependent on the acceleration number. The potential values of k_{33} for a hemispherical shell, the shape of which is comparable with that of a parachute, is also given in Table 5.4. The experimental values from the present investigation and those of Yavuz show that in real fluids the acceleration-dependent forces on bluff bodies are much higher than the potential flow values known to the author.

5.8.2.4 Ring-Slot Parachute

The coefficient of acceleration-dependent force in the lateral (normal) direction, k_{11} given in figure 5.38 shows a gradual variation with the angle of attack. A minimum value of about 0.6 occurs at $\alpha=0^{\circ}$. The coefficient for the axial direction, k_{33}, shown in figure 5.39, is approximately equal to 3.0. It remains substantially constant for the given range of angle of attack.

As seen in Table 5.4, the experimental values of k_{33} are greater than potential flow values of bodies with comparable geometric shapes.

5.8.2.5 Remarks on Acceleration-Dependent Force

The correlations between the coefficients of the acceleration-dependent force and the angle of attack α, (or the attitude of motion) for each test model was established using results of repeated tests. The coefficients of acceleration-dependent lateral force which were derived for angles of attack up to 40° were found to be independent of acceleration number, but dependent on the angle of attack.

In the case of parachutes the coefficients for the axial direction (k_{33}) have been derived only for low angles of attack because for in-line oscillations the canopies collapsed earlier than for lateral oscillations.

The experimental results show that the acceleration-dependent forces in a real fluid are substantially greater than those in potential flow. The experimental results of the present investigation dispute those of Yavuz because the coefficients of acceleration-dependent force did not reach their potential flow values for large acceleration numbers. The nature in which the test models were moved during the experiments was such that at no time the body was moving into its own wake. Thus the flow fields around the test models can be regarded to have developed to such an extent that the acceleration-dependent force coefficients cannot be expected to be equal to those in potential flow.

(C)   COMPARISON BETWEEN MODELLED DATA AND EXPERIMENTAL DATA

5.9   VALIDITY OF THE MODEL

The model given by equation (5.1) can be applied to estimate unsteady fluid dynamic forces on bluff bodies only if the components of the total force at frequencies above 3 rad/sec. are negligible.   However, the data analysed during the present investigation were influenced to a certain extent by force components at high frequencies.

5.9.1   Effects of High-Frequency Signals in the Measured Force

The motion imparted on the test models were such that when the unsteady fluid dynamic forces on these bodies are analysed using equation (5.1), the components of forces that have frequencies above 3 rad/sec. are found to be between 4% and 14% of the total force.   Given in Table D.1 are the effects of these high frequency components on equation (5.1), for different modes of motion.   Also given in Table D.1 are the components of the measured force at frequencies above 3 rad/sec.   These high frequency components occur due to oscillations imposed by vortex shedding, natural frequencies of vibration and 'noise' associated with the apparatus used.   It can be seen in Table D.1 that the components of the measured force at frequencies above 3 rad/sec. are between 3% and 40% higher than those predicted by equation (5.1).   In the case of oscillations at small angles of attack the forces in the lateral direction

are small and the 'noise' level compared to the lateral force is relatively high.

5.9.2 Deviation of the Forces Modelled by Equation (5.1) from the Measured Forces

Whether equation (5.1) can be effectively used to model forces on submerged bodies in unsteady motion is verified by reproducing the unsteady forces using above equation and comparing them with the measured forces. The deviation of the modelled force from the measured force, for each test model, is given in Table D.1.

The deviation of the modelled force on the cylinder is about 17% of the measured force. For the rectangular block it varies from 11% to 13% depending on the nature of motion imparted on the body. Higher levels of deviation, which ranged from 14% to 24% can be observed for the parachute models.

The application of equation (5.1) to model forces on the parachute canopies has been relatively less effective because of the relatively high level of high frequency oscillatory components in the lateral force at low angles of attack. For other modes of motion the deviation of the force modelled by equation (5.1) is of the order of the percentage of the forces at frequencies above 3 rad/sec. Thus the method specified in Sections 5.3 and 5.4, by which the model given by equation (5.1) is derived can be regarded as effective only in the range of frequencies less than 3 rad/sec.

For the circular cylinder and the rectangular block, the deviations of the modelled force are of the same order as the experimental uncertainty given in Table D.2. For the parachute models, the deviations of the forces modelled by equation (5.1) are more than the experimental uncertainty shown in Table D.2

Examples of forces reproduced using equation (5.1) are shown in figures 5.40 to 5.43. These forces are compared in these figures with their corresponding experimental values.

The deviation of the forces modelled by equation (5.1), and those modelled using other methods are shown in Table 5.6. The other methods considered are:

1. Using steady flow data and instantaneous velocities to calculate the fluid dynamic force, ignoring the the effects of the acceleration-dependent force;

2. Using published data available to the author, either from steady flow tests or from unsteady tests, in equation (1.3).

Forces reproduced using these two methods also appear in figures 5.5 to 5.8. A comparison can be drawn between these figures and figures 5.40 to 5.43, which have been produced using equation (5.1). The improvements made by equation (5.1) can be observed in Table 5.6.

5.10 LATERAL OSCILLATORY FORCES DUE TO VORTEX SHEDDING

No attempt has been made during the present investigation to analyse lateral oscillatory forces on

symmetrical submerged bodies, that occur due to vortex shedding. As shown in Table D.1 these lateral forces on two-dimensional bodies can be as much as 50% of the in-line force. In steady flow, as shown in figure 5.45a, these force are regular and to a certain extent predictable (see Appendix B for vortex shedding from circular cylinders). In unsteady motion however, the lateral oscillatory forces are very irregular, both in their magnitudes and their frequencies (see figure 5.45b).

For three-dimensional bodies the lateral force components at zero angle of attack are relatively small. As shown in Figures 5.46, 5.47 and 5.48 these forces are not as regular as for two-dimensional bodies. This irregularity appears to increase when the motion of the submerged body is unsteady. The frequencies at which these oscillatory components occur can be as low as 0.6Hz and they are much less than the natural frequencies of vibration for each test model given in Table 5.5. Such oscillatory forces are likely to be due to vortex shedding. The author is unaware of any procedure by which vortex shedding by three-dimensional bodies can be analysed. However, since these oscillatory forces occur at or above 3 rad/sec, they are not included in the process of deriving coefficients for the application of equation (5.1).

5.11 BLOCKAGE EFFECT AND FREE-SURFACE EFFECTS

The data given in Section D.5 and Table D.3 of Appendix D show that the maximum blockage effect is of the

order of about one per cent. Using analogous formulae given for spheres by Robertson[33] it can be shown that the maximum effect on the unsteady forces coefficients due to nearby solid boundaries of the ship tank is less than one per cent.

Studying the surface effects on submerged spheres, Srokosz[39] showed that for a/h = 1/3 the maximum effect of the free surface waves on the added mass was less than five per cent. Since the analogous L/2h for present experiments are much less than 1/3 (see Table D.3) the surface effects are ignored.

5.12 SUMMARY

The fluid dynamic force in unsteady flow is often incorrectly represented in terms of the instantaneous velocities and accelerations of the submerged body and the surrounding fluid: incorrect because for real fluids the history of motion plays an important role. This method can successfully be applied only if the component of the total force that is dependent on acceleration, can effectively be separated from the velocity-dependent component. Adopting steady flow data in order to extract the forces that are acceleration-dependent leads to answers that are acceleration number dependent. The coefficients of acceleration-dependent force thus calculated can have very unrealistic numerical values especially for low acceleration numbers. Thus the unsteady forces calculated using these very high coefficients of acceleration-dependent force and

very low acceleration numbers can lead to large ranges of uncertainty.

By considering that the unsteady fluid dynamic force is dependent not only on the instantaneous velocity and the acceleration, but their respective history also, the author has derived the coefficients of the two force components which are virtually independent of the acceleration number. Using experimental results obtained by oscillating test models it was possible to show that the effect of the history of motion was such that the velocity and acceleration at a certain time τ prior to the instant is more dominating than those at other times that the total force can be regarded as being 'delayed' by this period of time.

By using this characteristic in an empirical model in the form given by equation (5.1), it is possible to separate the components of the total fluid dynamic force that are dependent on the velocity and acceleration. This enables the fluid dynamicist to study the effect of velocity and acceleration separately.

Examples of forces forces reproduced using equation (5.1) compared with experimental values are shown in figures 5.40 to 5.43. These figures, inclusive of figures 5.5 to 5.9, and Table 5.6 give a fair indication to improvements made by equation (5.1) in modelling unsteady fluid dynamic forces on submerged bluff bodies.

Although it was possible to derive the 'time-delay' associated with each test model sufficient data is not available to non-dimensionalise these values. Using

Buckingham's π theorem it can be shown that the group (Uτ/L) is a possible non-dimensional form of τ where, L is the characteristic length of the body and U the reference velocity.

Test Model	Mode of Motion	Up to 1st Harmonic Frequency	Up to 2nd Harmonic Frequency	Up to 3rd Harmonic Frequency
Circular Cylinder	in-line osc.	77%	91%	96%
Rectangular Block	lateral osc.	65%	86%	90%
	in-line osc.	69%	88%	95%
Cruciform Parachute	lateral osc.	69%	85%	90%
	in-line osc.	71%	88%	93%
Ring-slot Parachute	lateral osc.	71%	89%	92%
	in-line osc.	74%	89%	94%

Table 5.1   Weight of harmonic frequencies on the fluid dynamic force.

Test model	Steady flow C_N & C_T	Unsteady flow C_N & C_T	Published data
Circular cylinder	≈ 1.2	≈ 1.25	(steady) ≈ 1.2[13] (unsteady) ≈ 1.2[41]
Rectangular block C_T (α=0deg)	≈ 0.35	0.33-0.48	≈ 0.34[13]
Cruciform parachute C_N (α=10deg) C_T (α=0deg)	≈ 0.32 ≈ 1.15	≈ 0.32 1.15-1.5	≈0.28[42] 0.2-0.32[18] ≈1.0[42] 1.0-1.24[18]
Ring-slot parachute C_N (α=10deg) C_T (α=0deg)	≈ 0.05 ≈ 1.0	≈ 0.2 1.1-1.5	

Table 5.3 Coefficients of velocity-dependent force for steady motion and unsteady motion.

Test model	Experi-mental	Published data	Potential flow
Circular	≈ 2.4	≈ 0.6[41]	1.0
Rectangular block k_{11} (α=Odeg) k_{33} (α=Odeg)	≈ 2.4 ≈ 1.9	·	(for 2-D) 1.19[38]
Cruciform parachute k_{11} (α=Odeg) k_{33} (α=Odeg)	≈ 0.53 ≈ 4.3	3-4[42] 2-3[18]	(Hemispher. shell) 2.1[16]
Ring-slot parachute k_{11} (α=Odeg) k_{33} (α=Odeg)	≈ 0.52 ≈ 3.0		Hemispher. shell) 2.1[16]

Table 5.4   Coefficients of acceleration-dependent force in real fluids and in potential flow.

Test model	Estimation (Hz) (disregarding natural frequencies)	Measured (Hz)
Circular cylinder	≈ 3	≈ 2.5
Rectangular block	≈ 3.2	≈ 3
Cruciform parachute	≈ 4.2	≈ 3
Ring-slot parachute	≈ 3.5	≈ 3

Table 5.5   Lowest natural frequencies of vibration compared with estimations based on experimental values of added mass.

Test Model	Mode of Motion	Using vel-dep force only	Using published data of vel-dep & acc-dep forces in eq(1.3)	Using eq(5.1)
Circular Cylinder	in-line osc.	18.1%	17.8%	17.1%
Rectangular Block	lateral osc.	27%	21%	11%
	in-line osc.	14.5%	14.8%	13.2%
Cruciform Parachute	lateral osc.	30%	28%	14%
	in-line osc.	24%	24%	22%
Ring-slot Parachute	lateral osc.	34%	29%	19%
	in-line osc.	27.5%	27%	24%

Table 5.6   Deviation from the measured force of various modelled forces
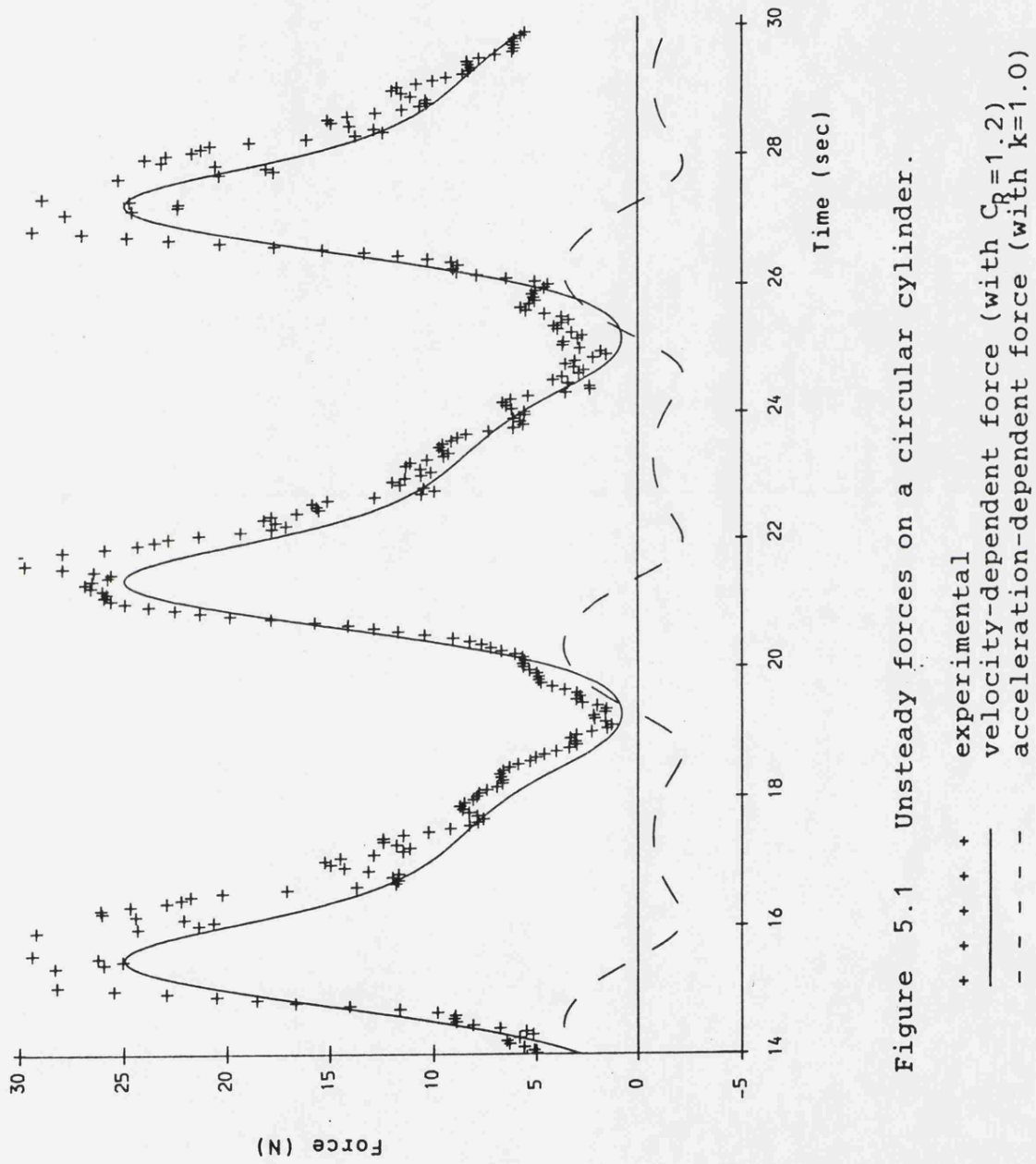
Figure 5.1 Unsteady forces on a circular cylinder.

+ + + + +   experimental
————————   velocity-dependent force (with C_R=1.2)
– – – –   acceleration-dependent force (with k=1.0)
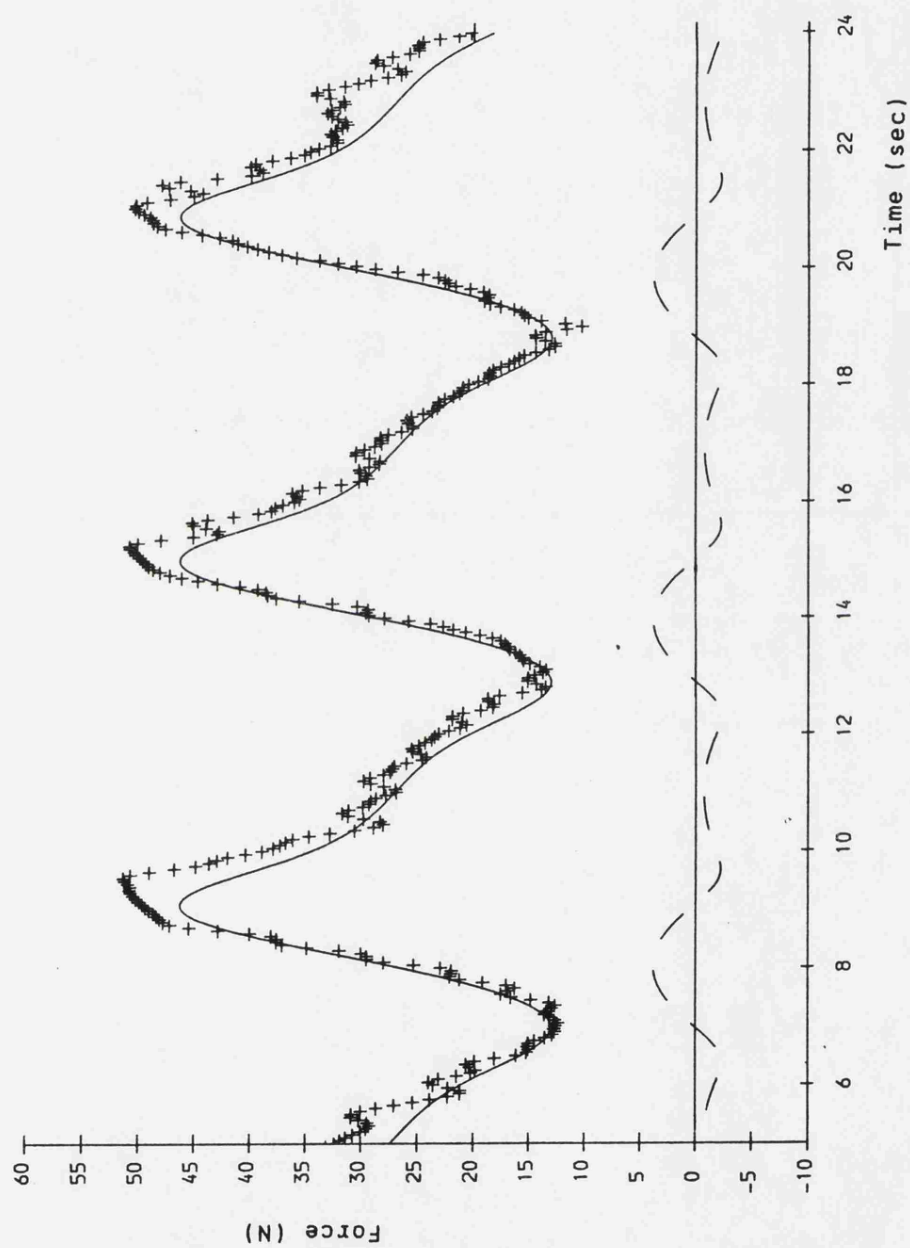
Figure 5.2   Unsteady forces on a rectangular block.

+ + + +   experimental
          velocity-dependent force (with $C_R=1.2$)
- - - -   acceleration-dependent force (with $k=1.19$)
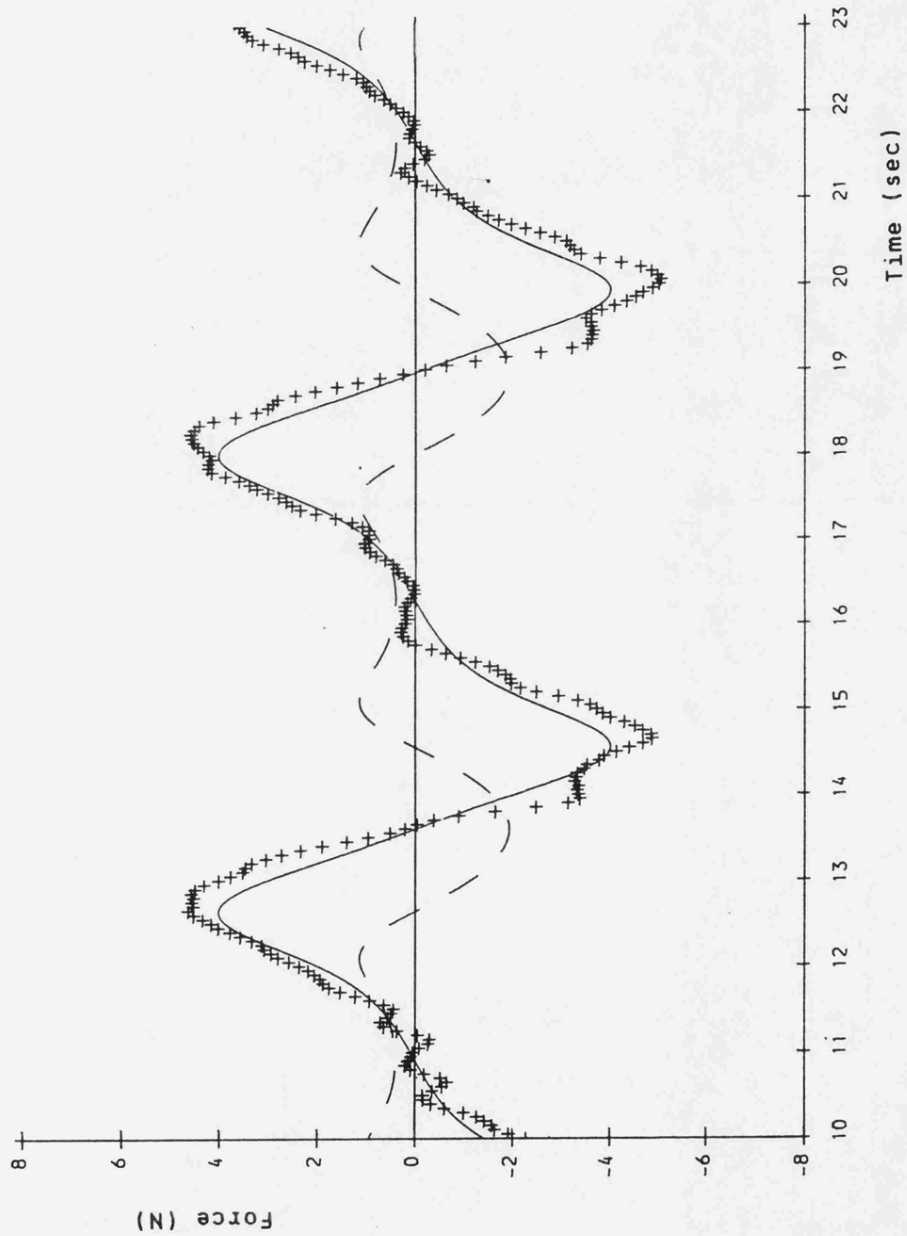
Figure 5.3 Unsteady forces on a cruciform parachute.

+ + + +   experimental

————   velocity-dependent force (with $C_\tau = 1.2\alpha$)

- - - -   acceleration-dependent force (with $k_\tau = 1.05$)
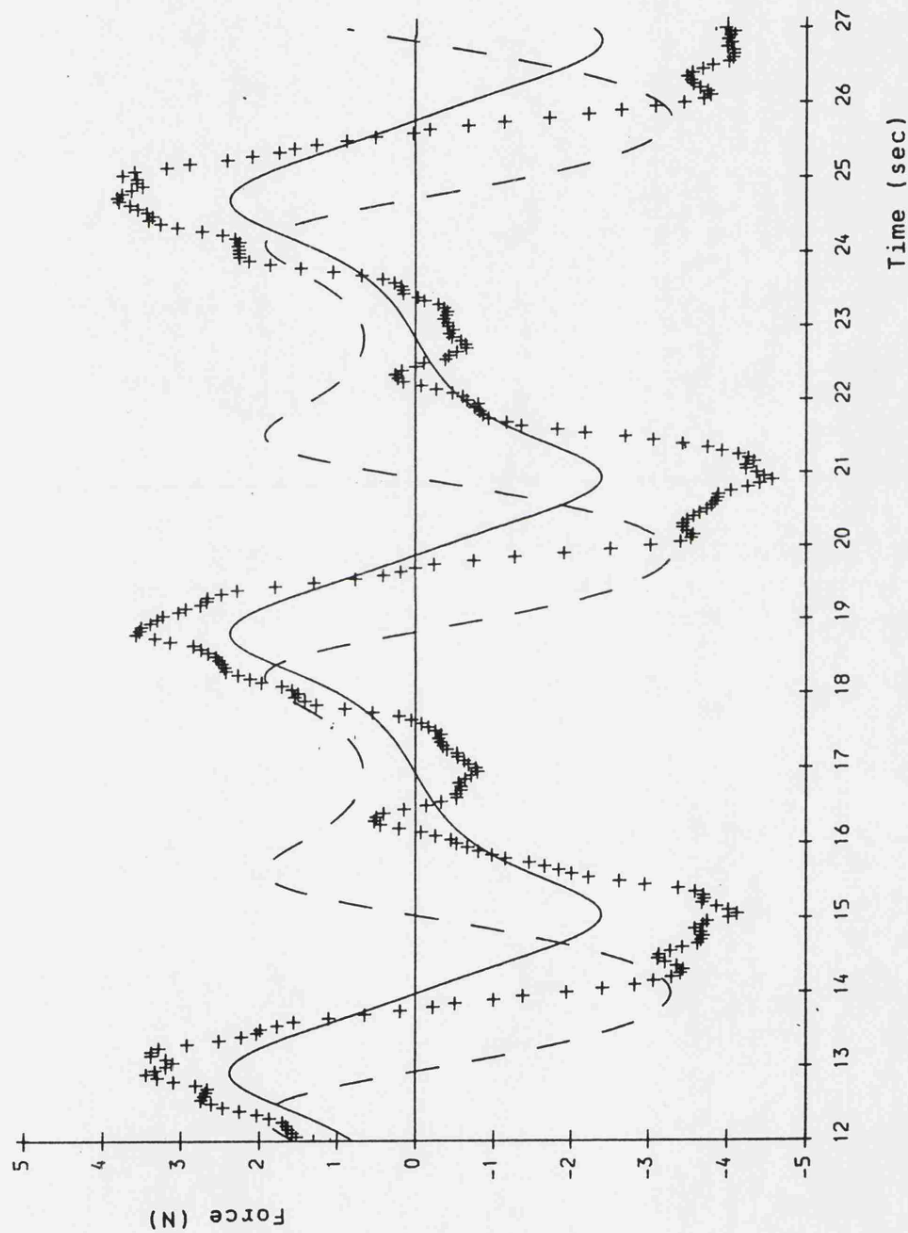
Figure 5.4 Unsteady forces on a ring-slot parachute.

+ + + + + experimental

————— velocity-dependent force (with $C=0.5\alpha$)

— — — acceleration-dependent force (with $k_a=1.05$)
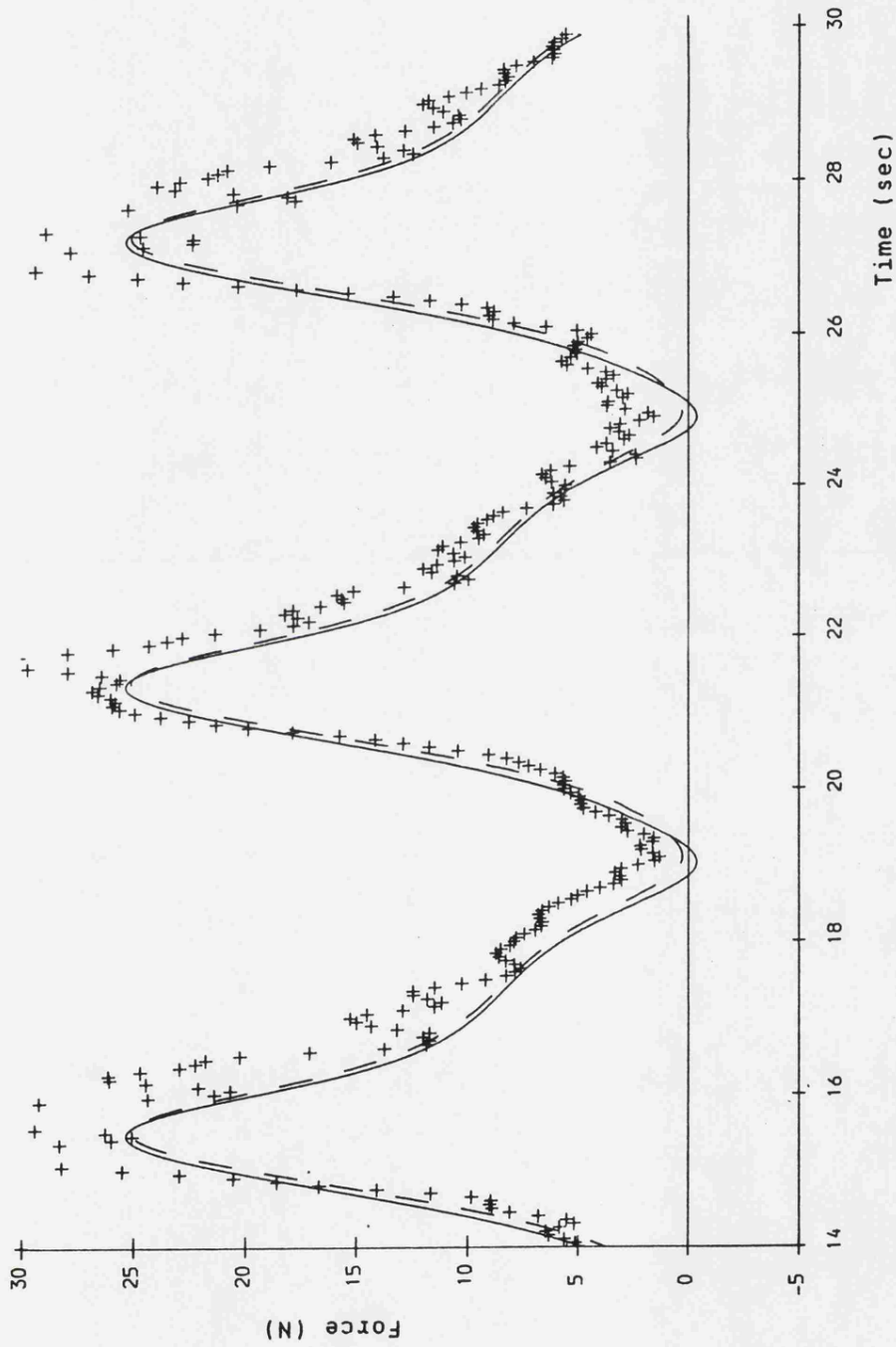
Figure 5.5 Unsteady forces on circular cylinder.

+ + + + +   experimental
————————   quasi-steady model (with C_R=1.2 & k=1.0)
– – – – –   quasi-steady model (with C_R=1.2 & k=0.6)
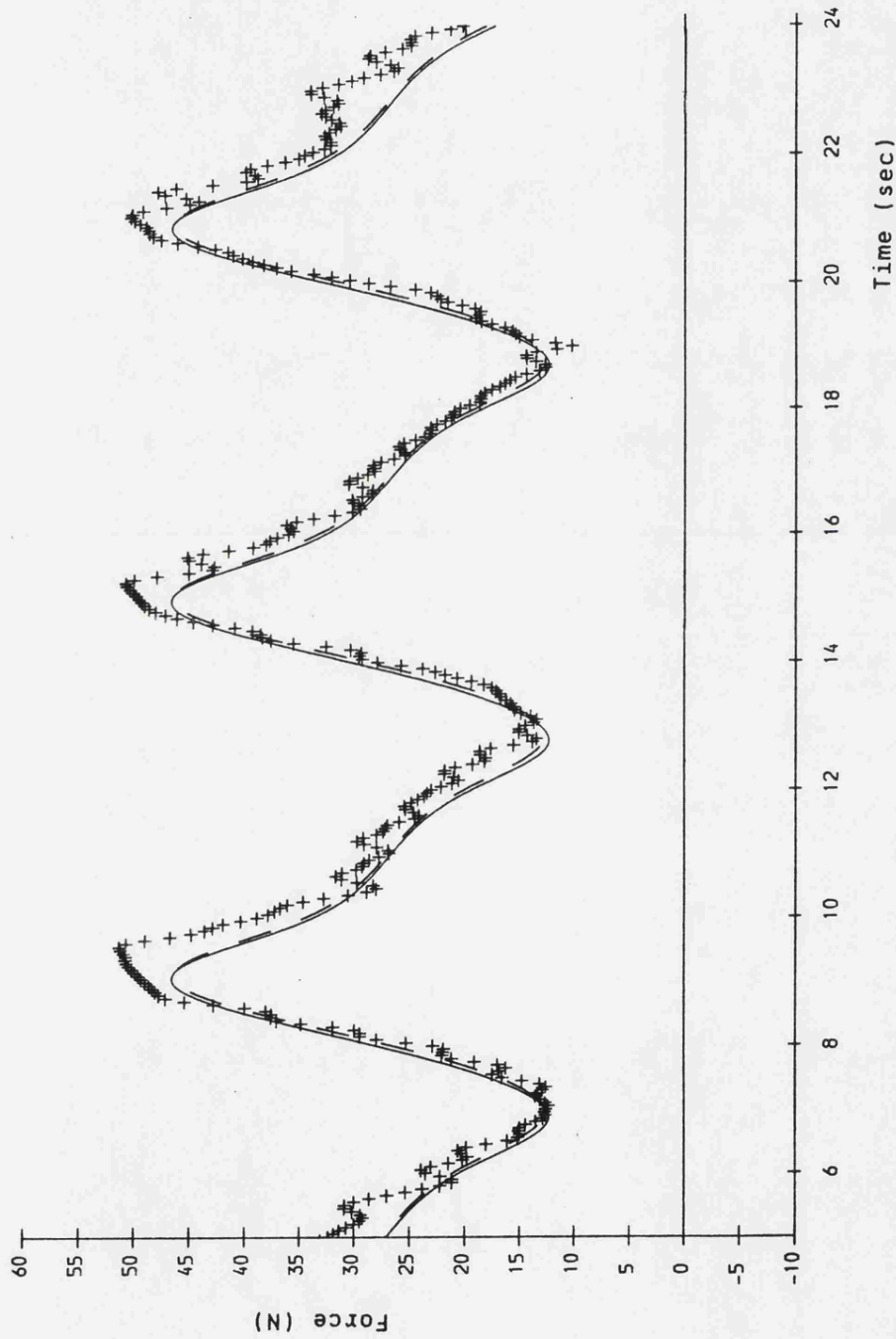
Figure 5.6   Unsteady forces on rectangular block.

+ + + +   experimental

———————   quasi-steady model (with $C_R = 1.2$ & $k = 1.19$)

– – – –   quasi-steady model (with $C_R = 1.2$ & $k = 1.85$)
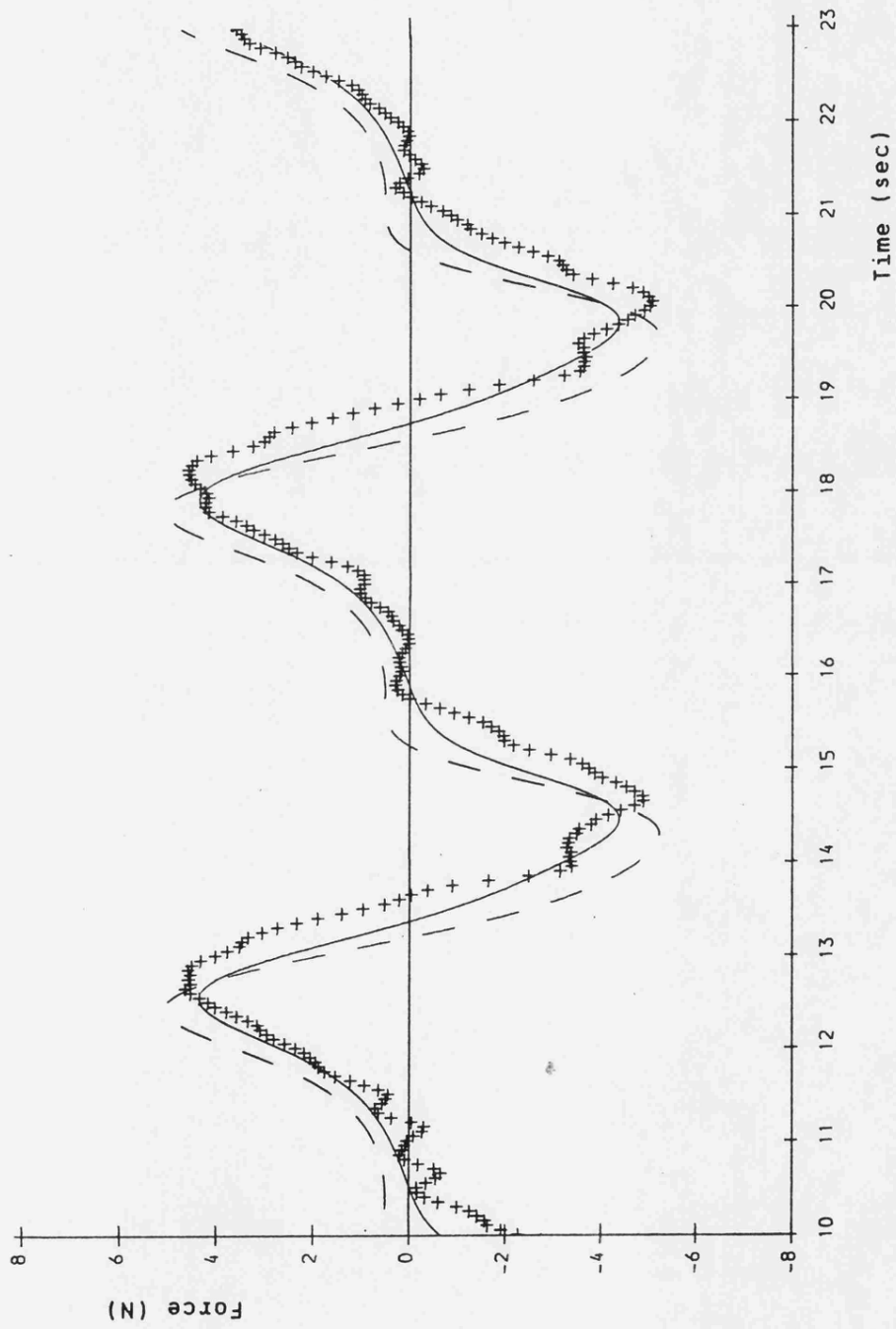
Figure 5.7   Unsteady forces on cruciform parachute.

+ + + +   experimental

—————   quasi-steady model (with $C_N = 1.2\alpha$ & $k_{ii} = 1.05$)

– – –   quasi-steady model (with $C_N^N = 1.2\alpha$ & $k_{ii} = 2.0$)
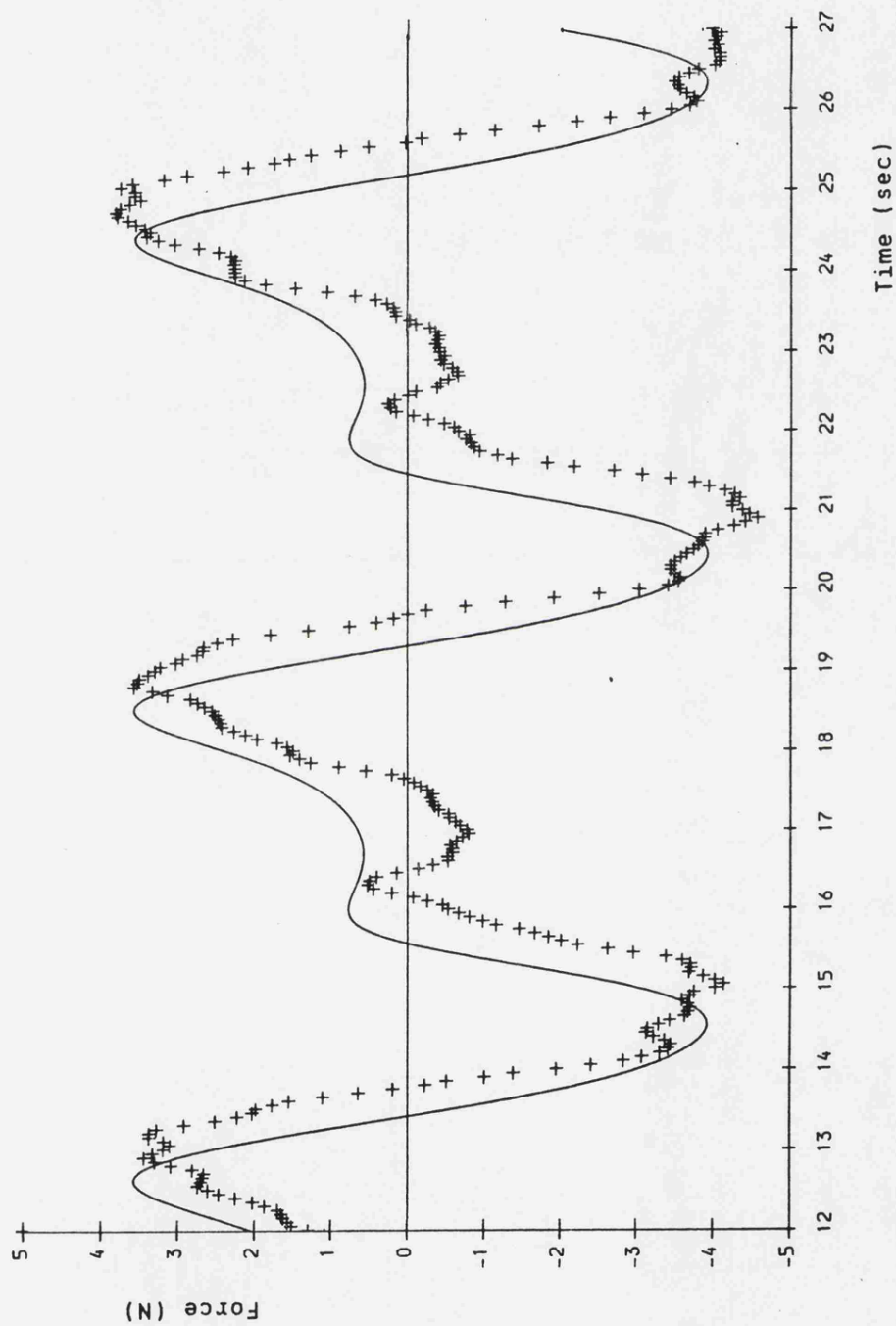
Figure 5.8   Unsteady forces on ring-slot parachute.

+ + + +   experimental

———————   quasi-steady model (with $C_N = 0.5\alpha$ & $k_i = 1.05$)
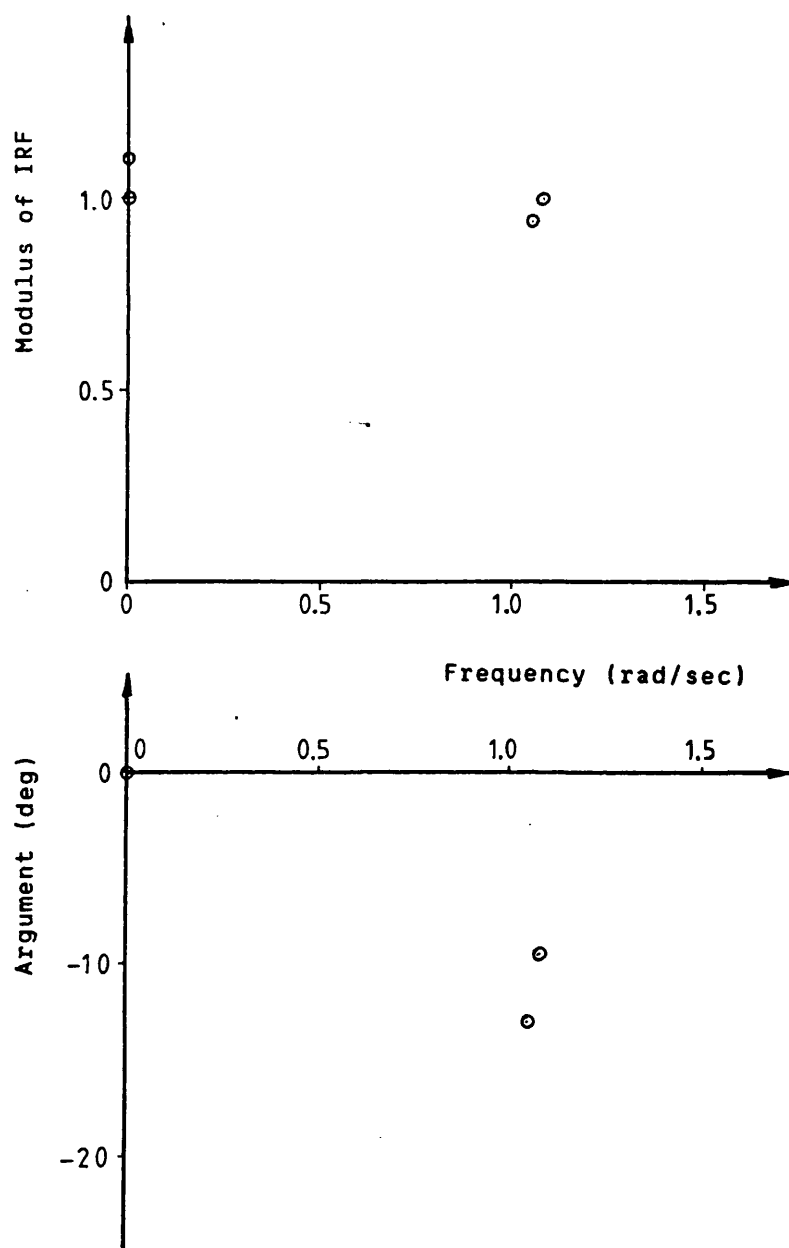
Figure 5.9 Modulus and argument of Impulse Response Function.
Test model: Circular cylinder (diameter = 0.114m; length = 1.0)
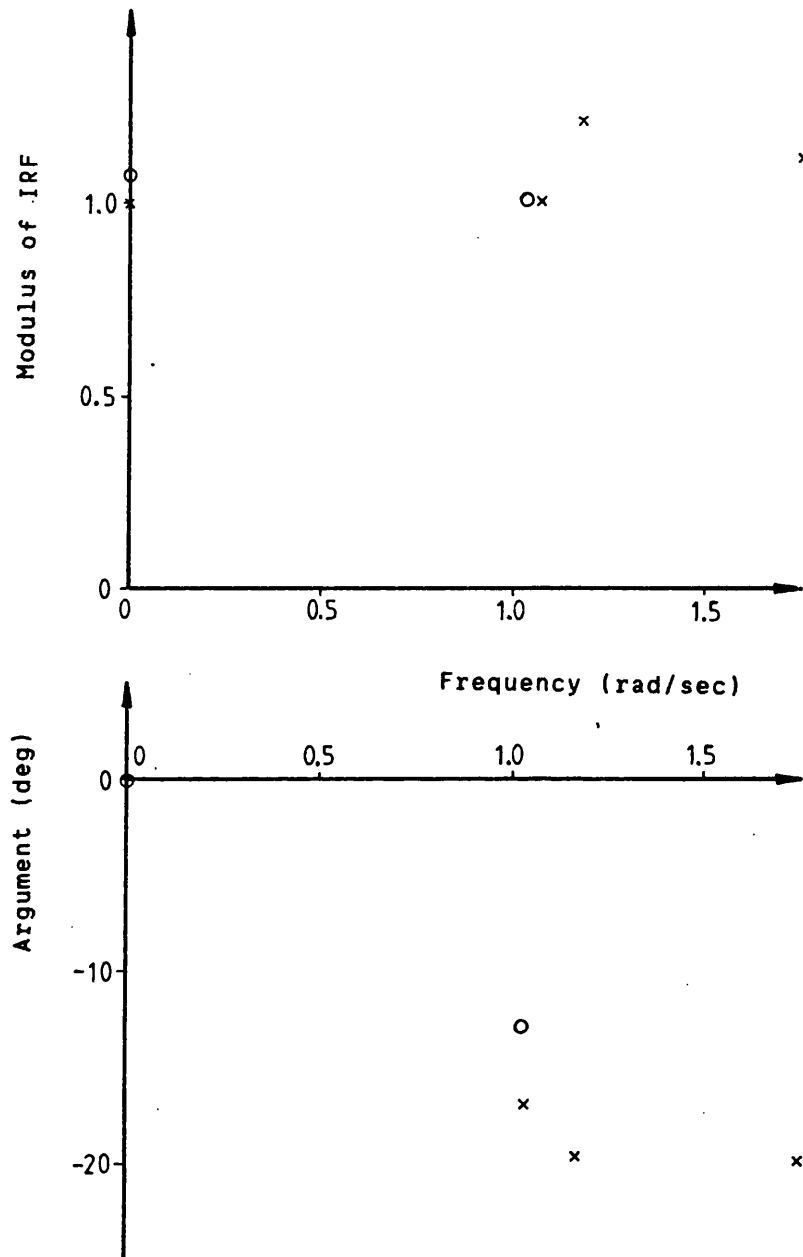
Figure 5.10 Modulus and argument of Impulse Response Function.
Test model: Rectangular block (of size:
              457mm x 153mm x 152·.5)

      o o o o o   for lateral direction
      x x x x x   for axial direction
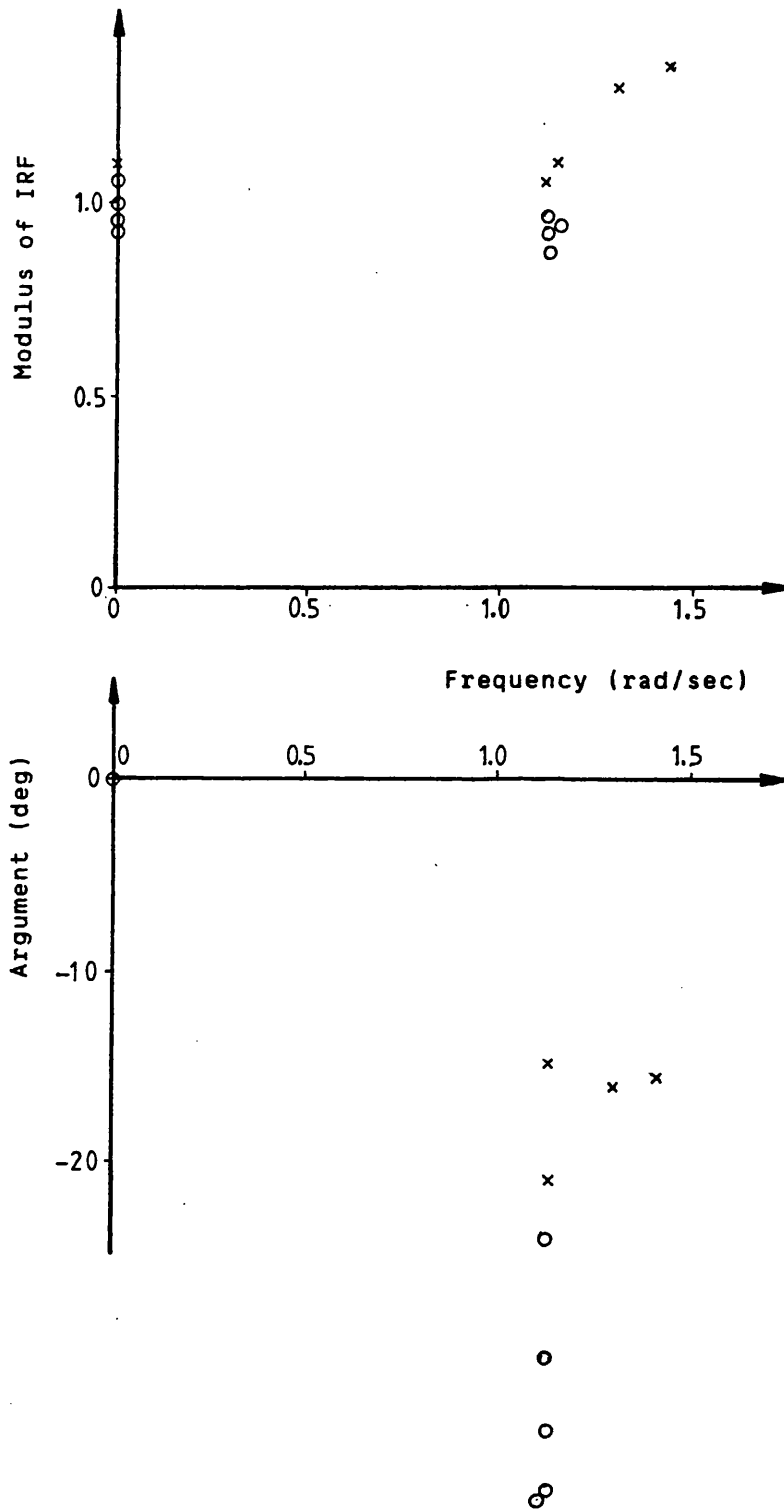
Figure 5.11 Modulus and argument of Impulse Response Function.
Test model: Cruciform parachute (arm ratio = 4:1)

o o o o o   for lateral direction
x x x x x   for axial direction
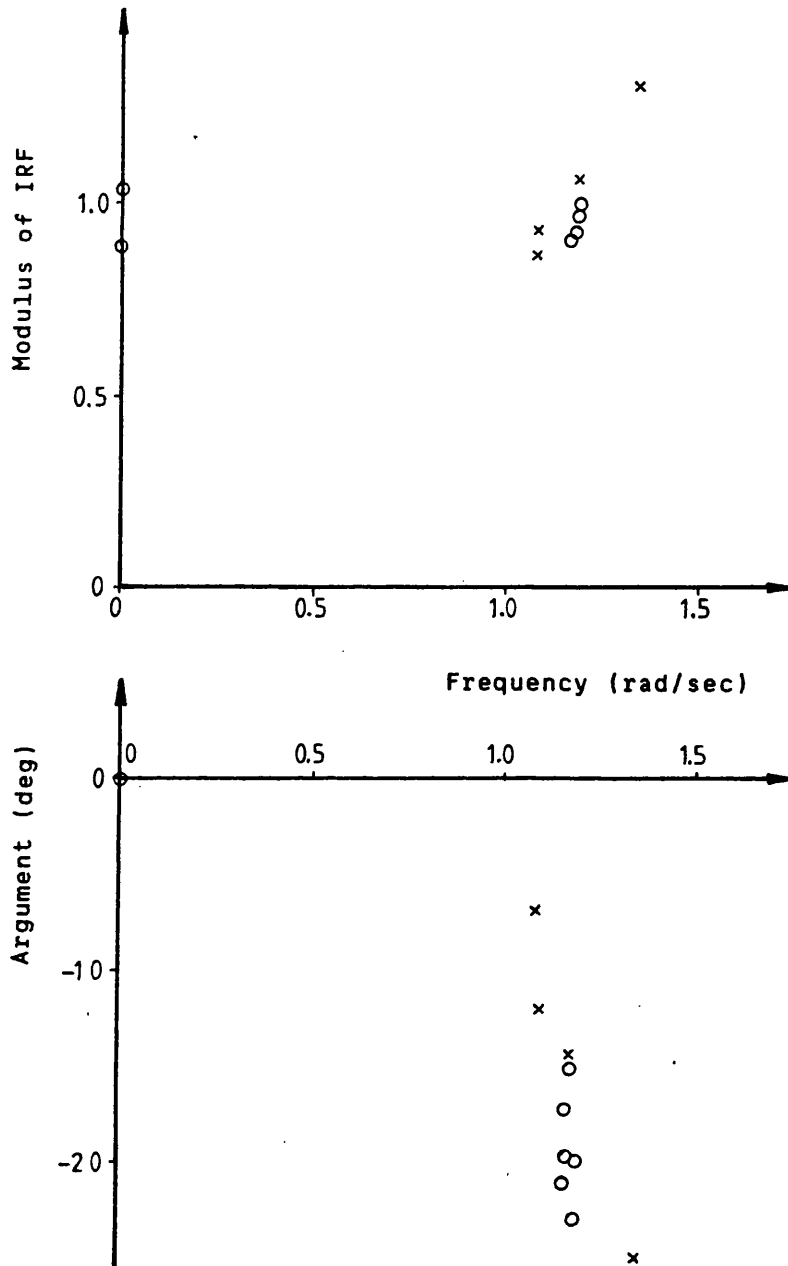
Figure 5.12 Modulus and argument of Impulse
Response Function.
Test model: Ring-slot parachute.

o o o o o   for lateral direction
x x x x x   for axial direction
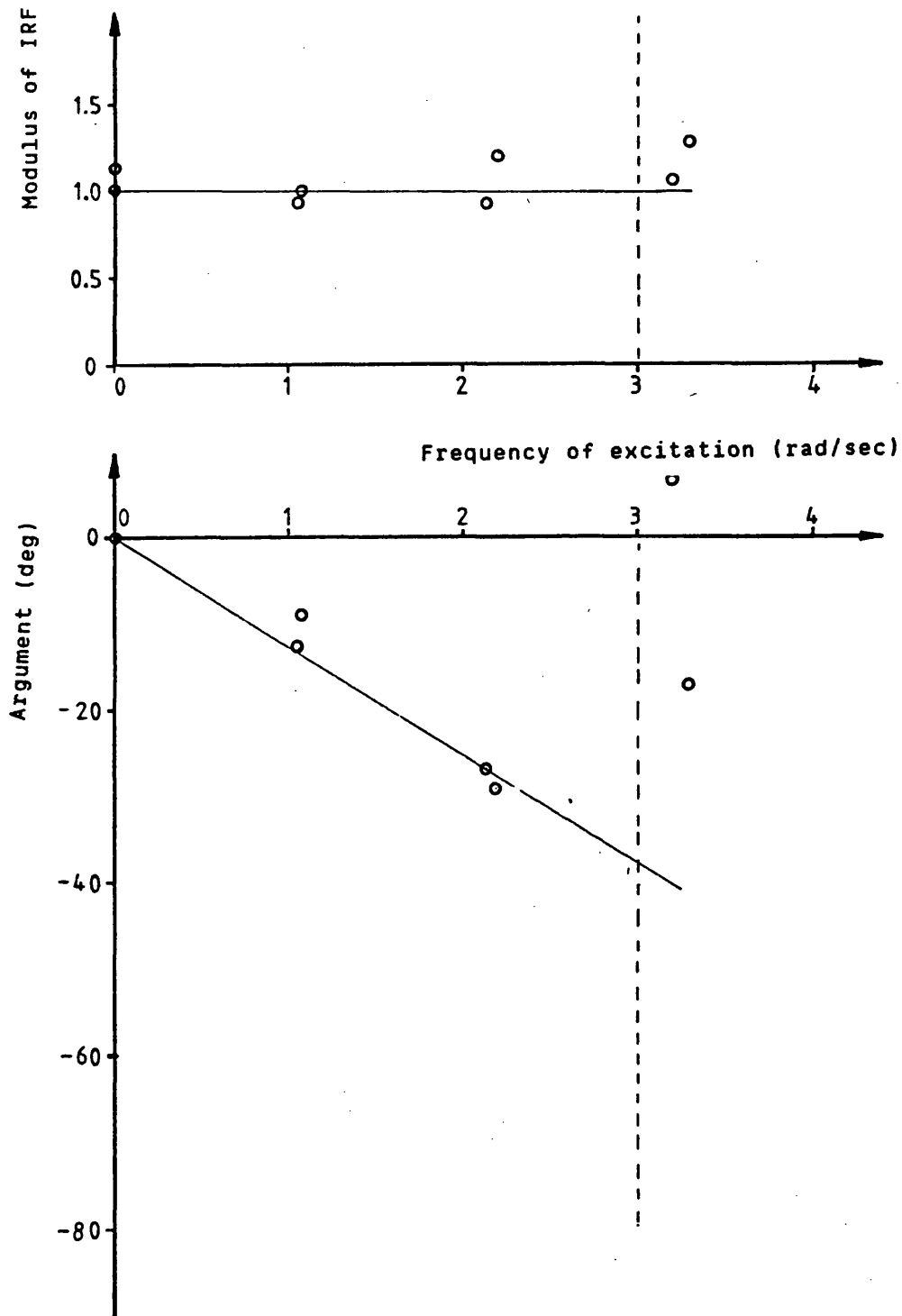
Figure 5.13 Graphs of modulus and argument of the Impulse Response Function versus the frequency of excitation.
Test model: Circular cylinder (diameter = 0.114m; length = 1.0m)
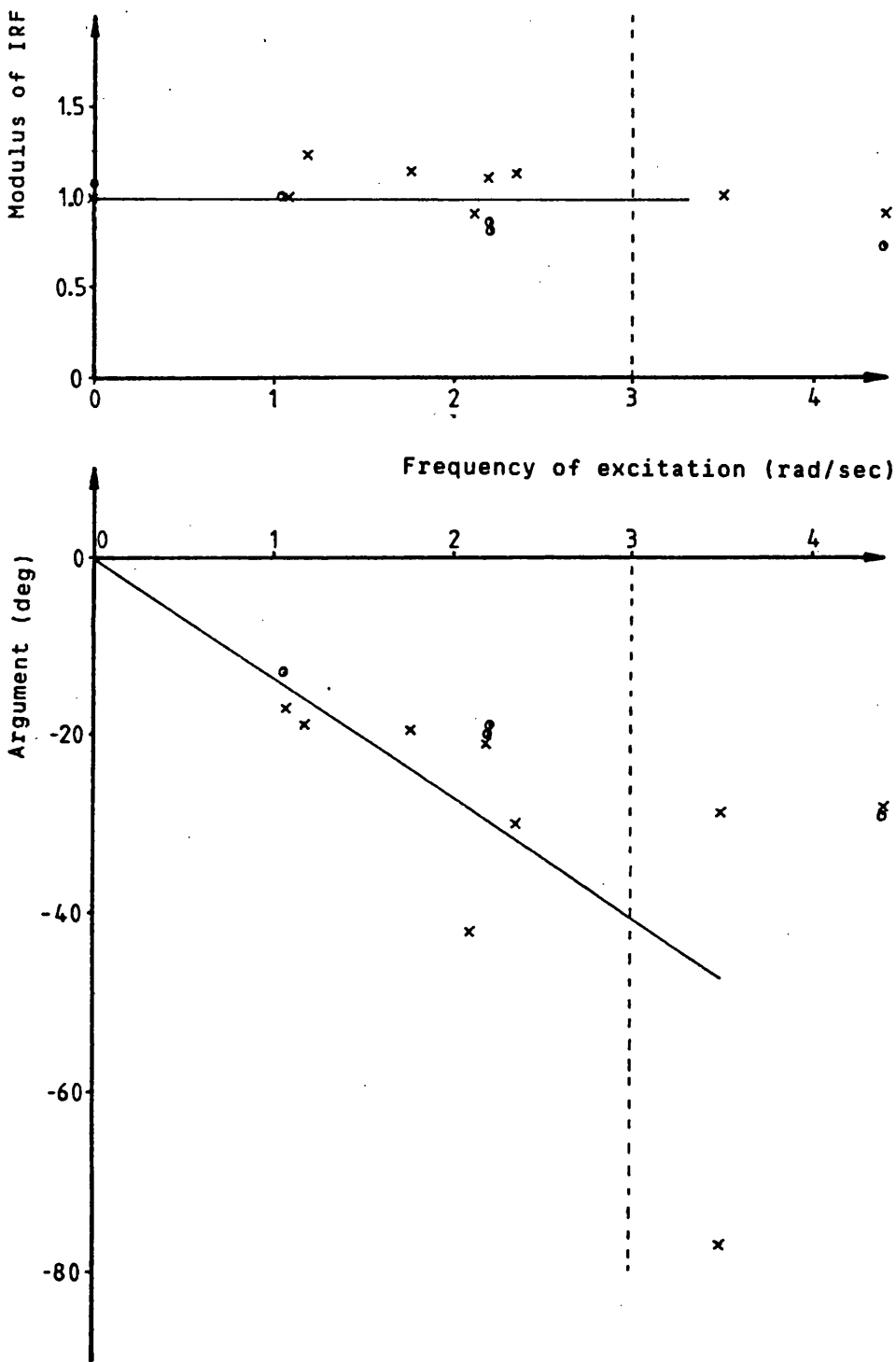
Figure 5.14 Graph of modulus and argument of the Impulse Response Function versus the frequency of excitation.
Test model: Rectangular block (of size: 457mm x 153mm x 152.5mm)

o o o o o   for lateral direction
x x x x x   for axial direction
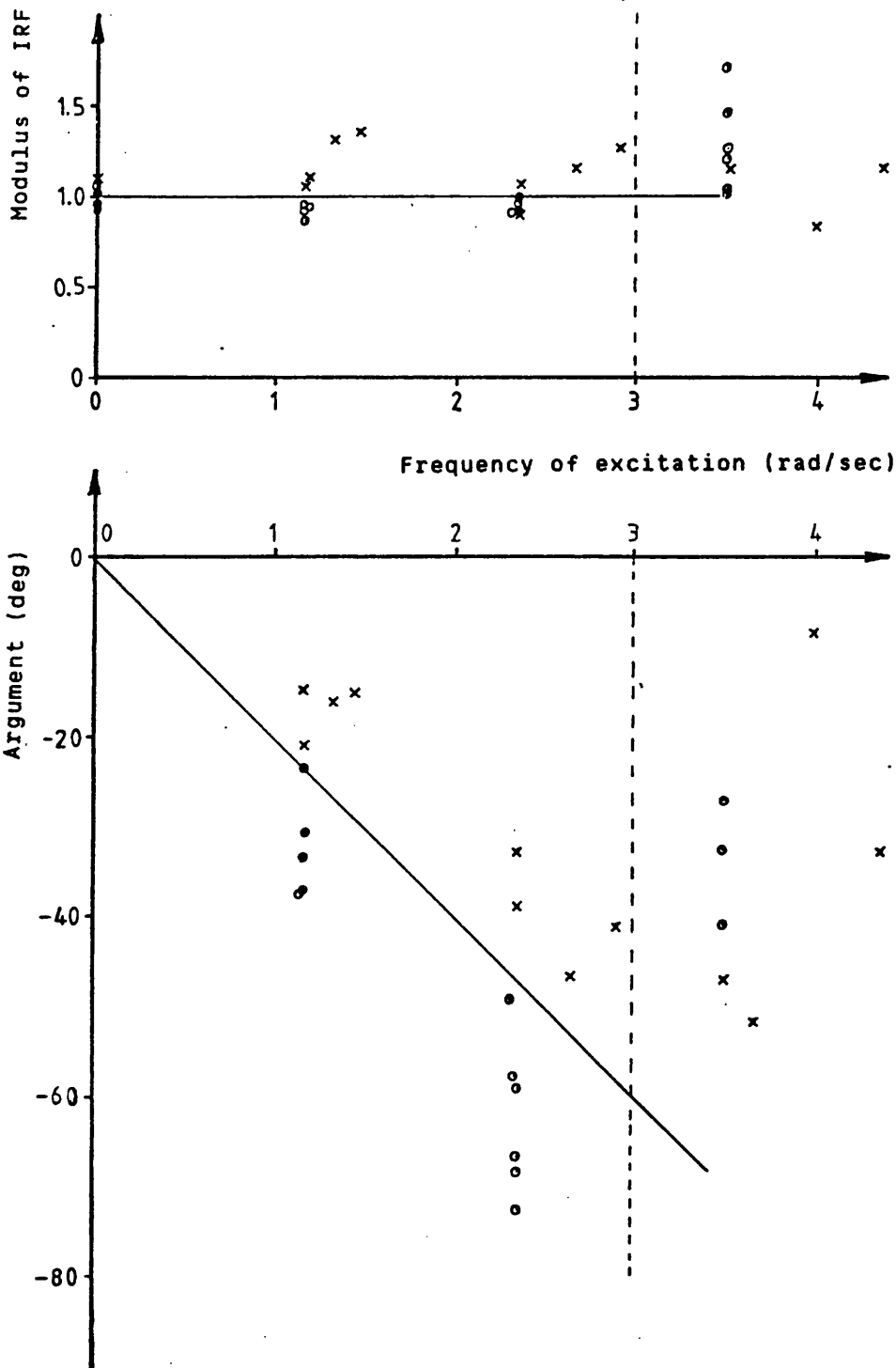
Figure 5.15 Graph of modulus and argument of the Impulse Response Function versus the frequency of excitation.

Test model: Cruciform parachute (arm ratio = 4:1)

o o o o o   for lateral direction
x x x x x   for axial direction
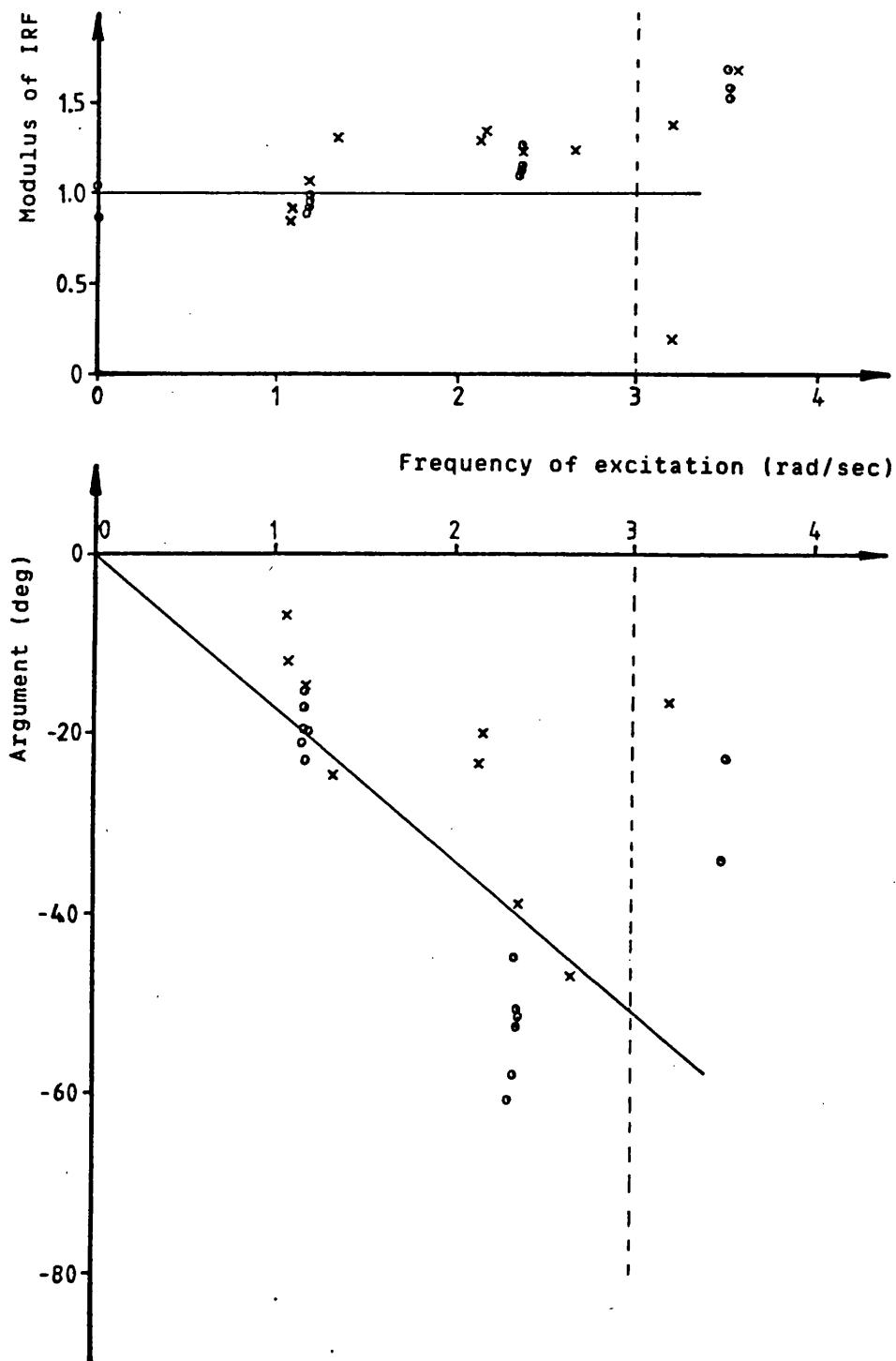
Figure 5.16 Graph of modulus and argument of the
Impulse Response Function versus the frequency of
excitation.
Test model: Ring-slot parachute

    o o o o o   for lateral direction
    x x x x x   for axial direction

$$\frac{F(t)}{1/2\varrho AU(t)|U(t)|}$$

$$\varrho V\dot{U}(t)$$

$$\frac{1}{1/2\varrho AU(t)|U(t)|}$$

(a)

$$\frac{F(t)}{1/2\varrho AU(t-\tau)|U(t-\tau)|}$$

$$\varrho V\dot{U}(t-\tau)$$

$$\frac{1}{1/2\varrho AU(t-\tau)|U(t-\tau)|}$$

(b)
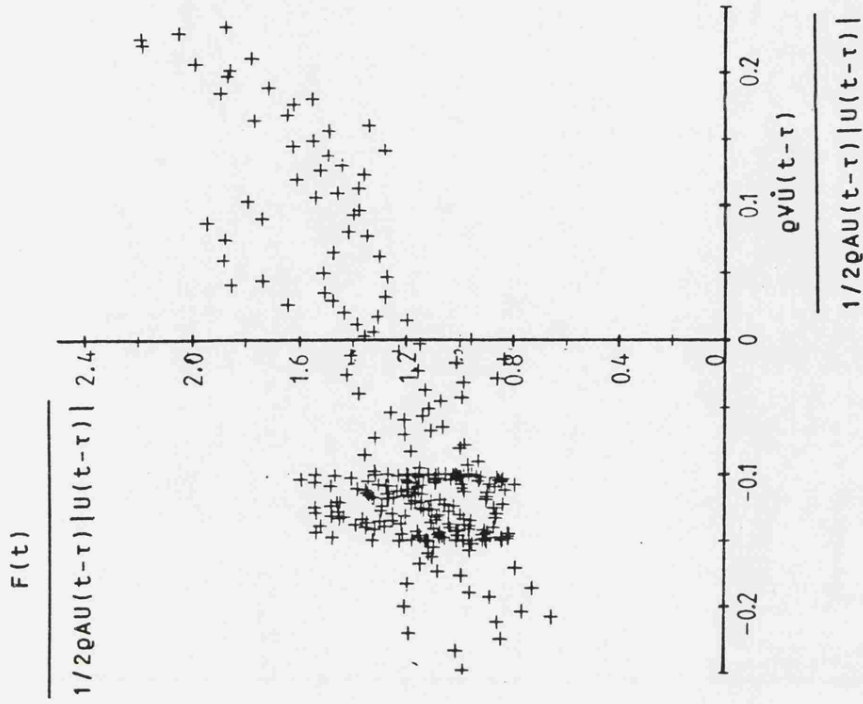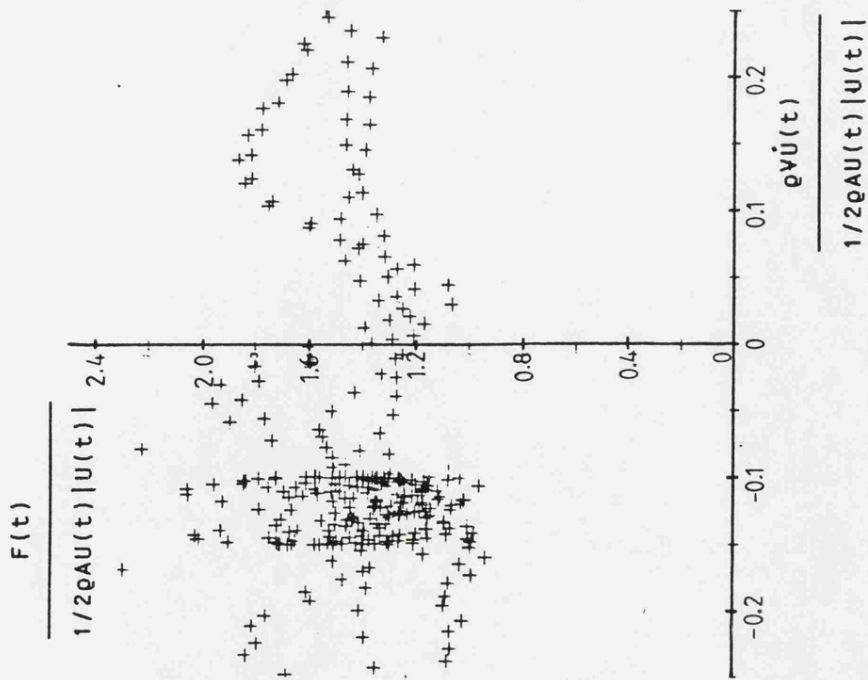
Circular cylinder

Figure 5.17

Rectangular block

Figure 5.18

$$\frac{F(t)}{1/2\rho AU(t)|u(t)|}$$

$$\frac{\varrho V \dot u(t)}{1/2\varrho AU(t)|u(t)|}$$

(a)

$$\frac{F(t)}{1/2\varrho AU(t-\tau)|u(t-\tau)|}$$

$$\frac{\varrho V \dot u(t-\tau)}{1/2\varrho AU(t-\tau)|u(t-\tau)|}$$

(b)
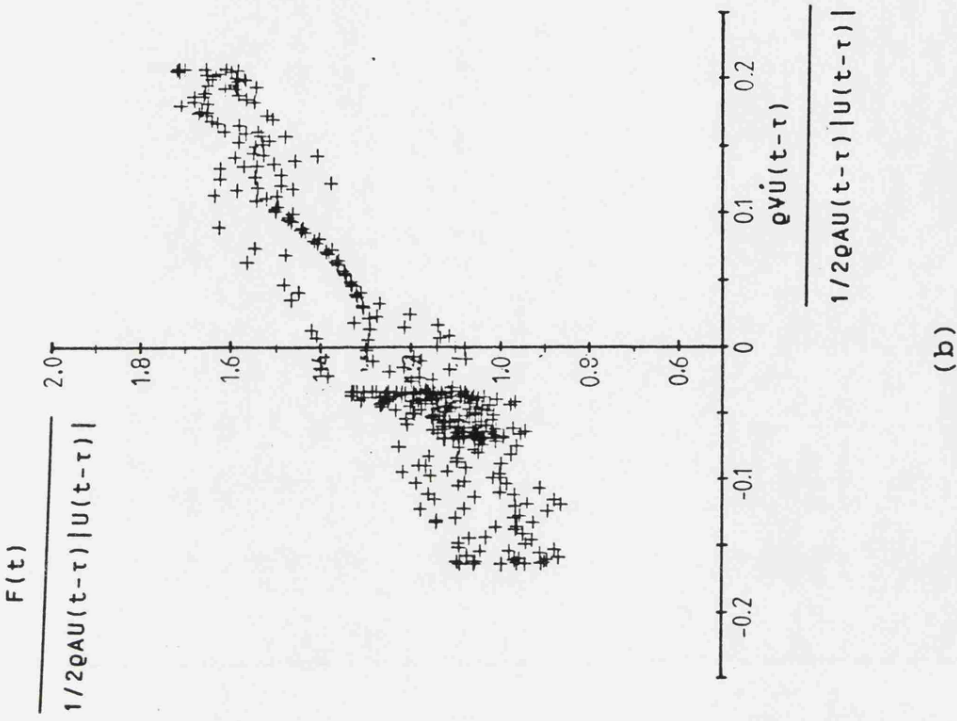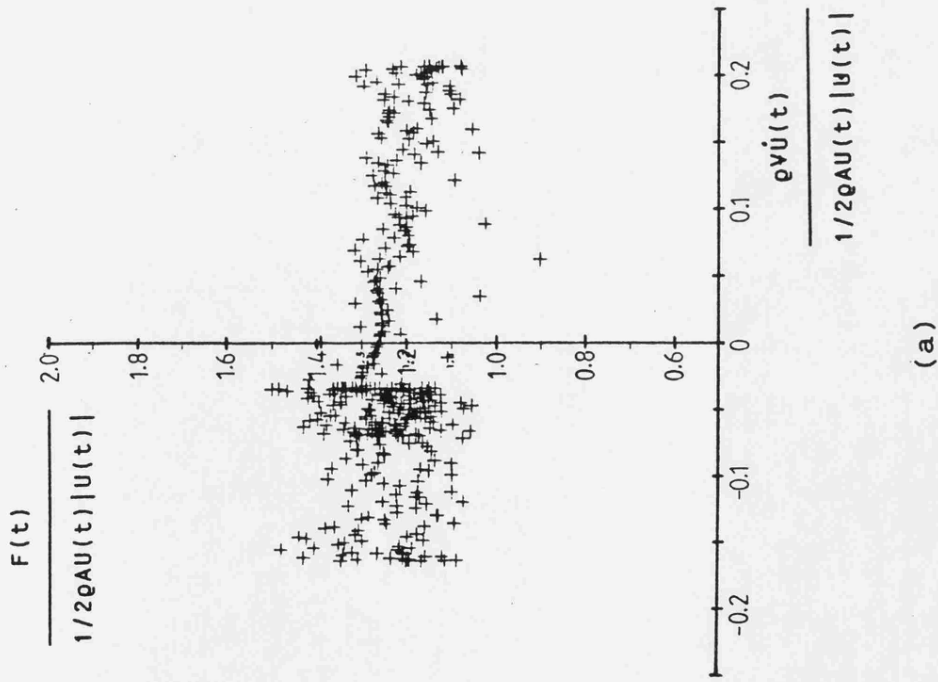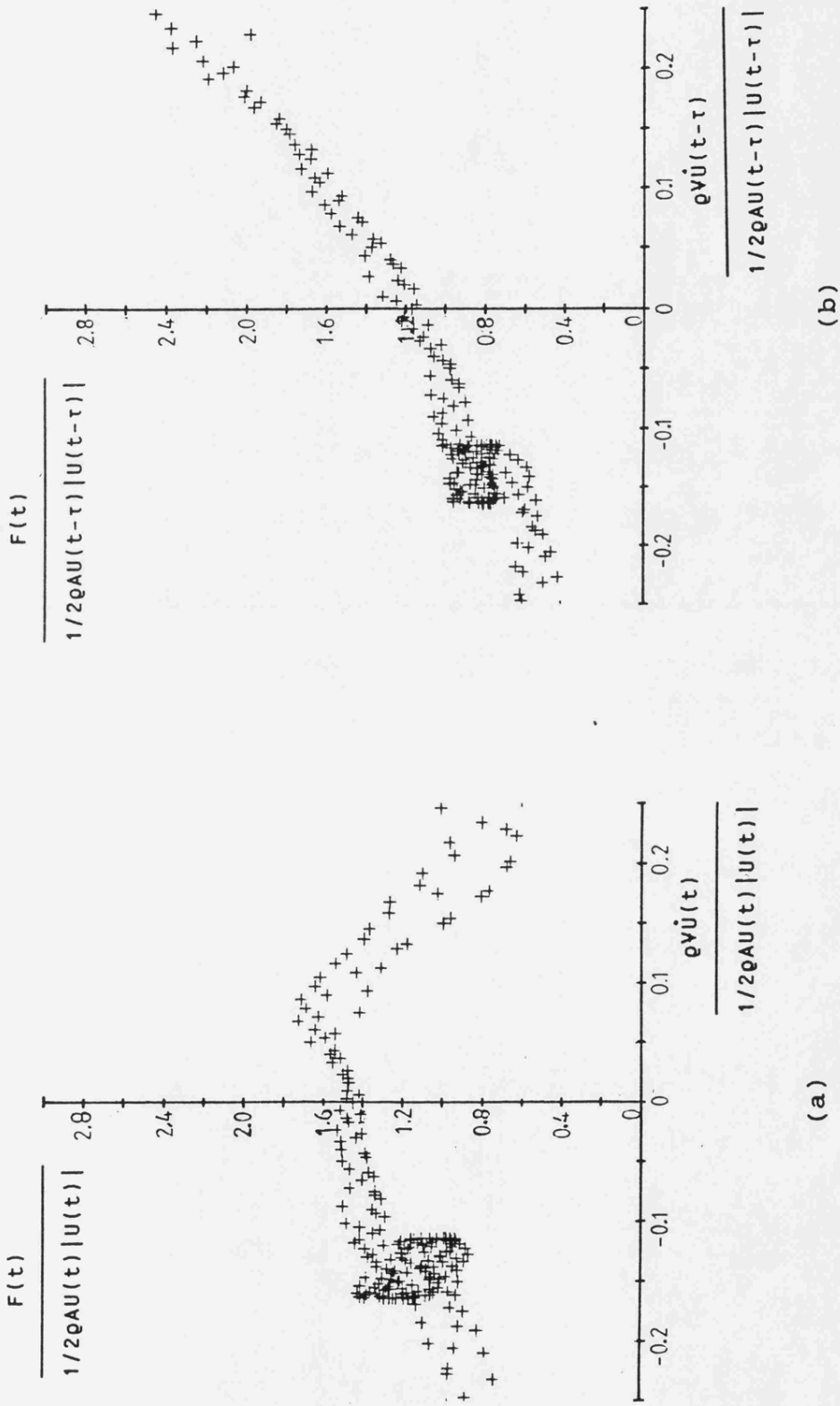
Cruciform parachute

Figure 5.19

153
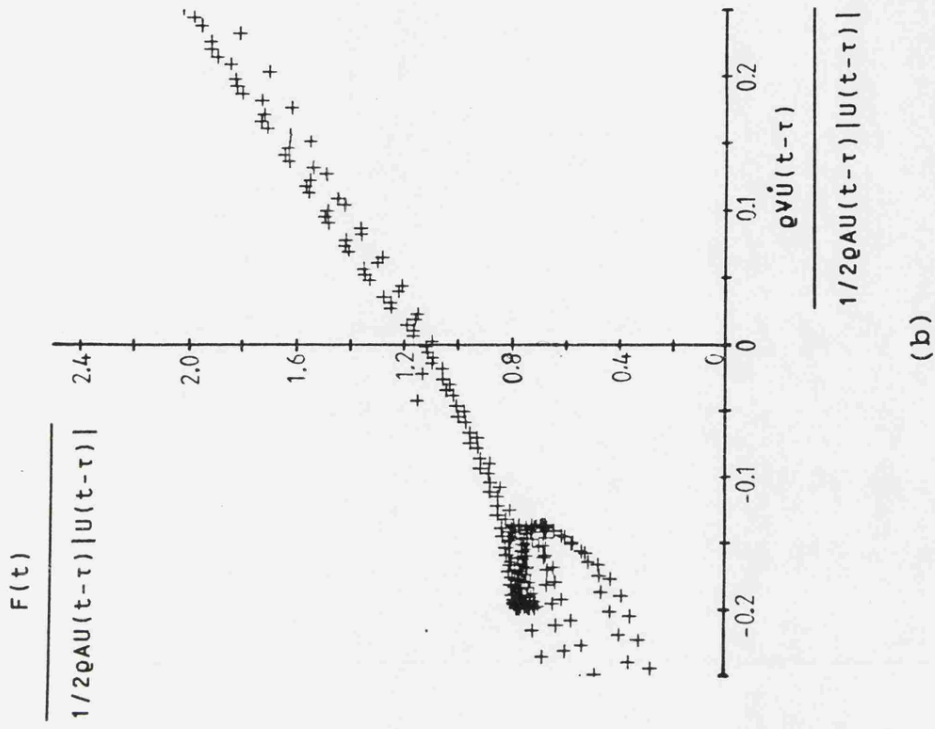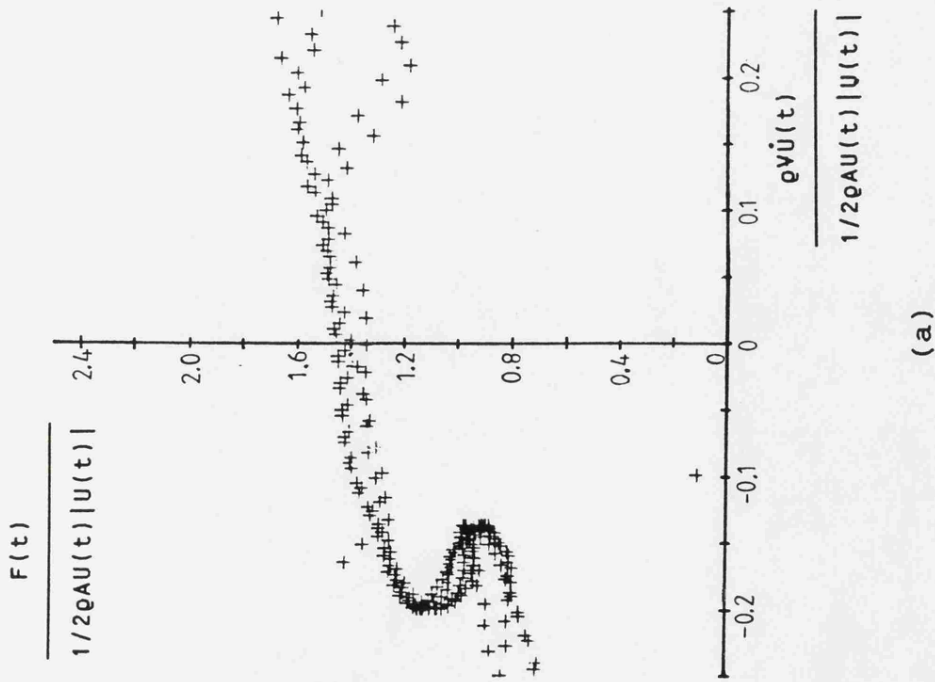
Ring-slot parachute
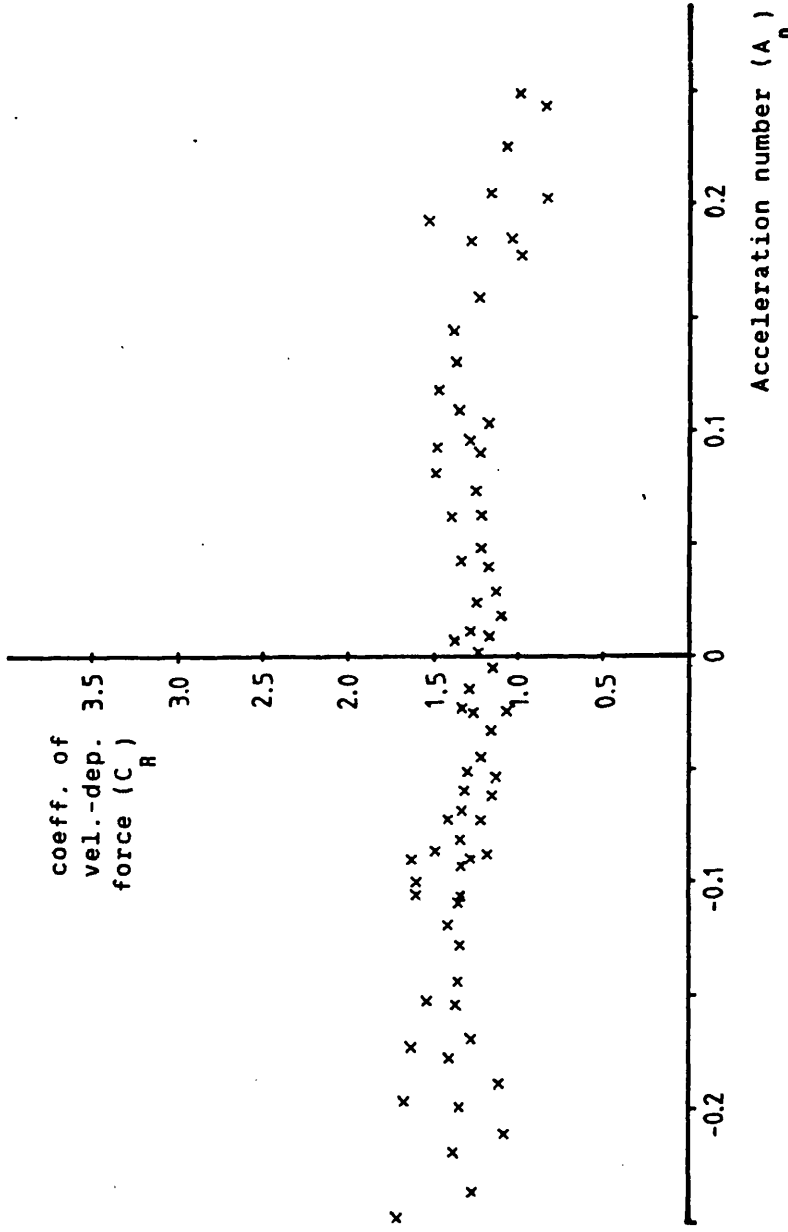
Figure 5.20

Figure 5.21 Graph of C_R Vs. A_n for circular cylinder.
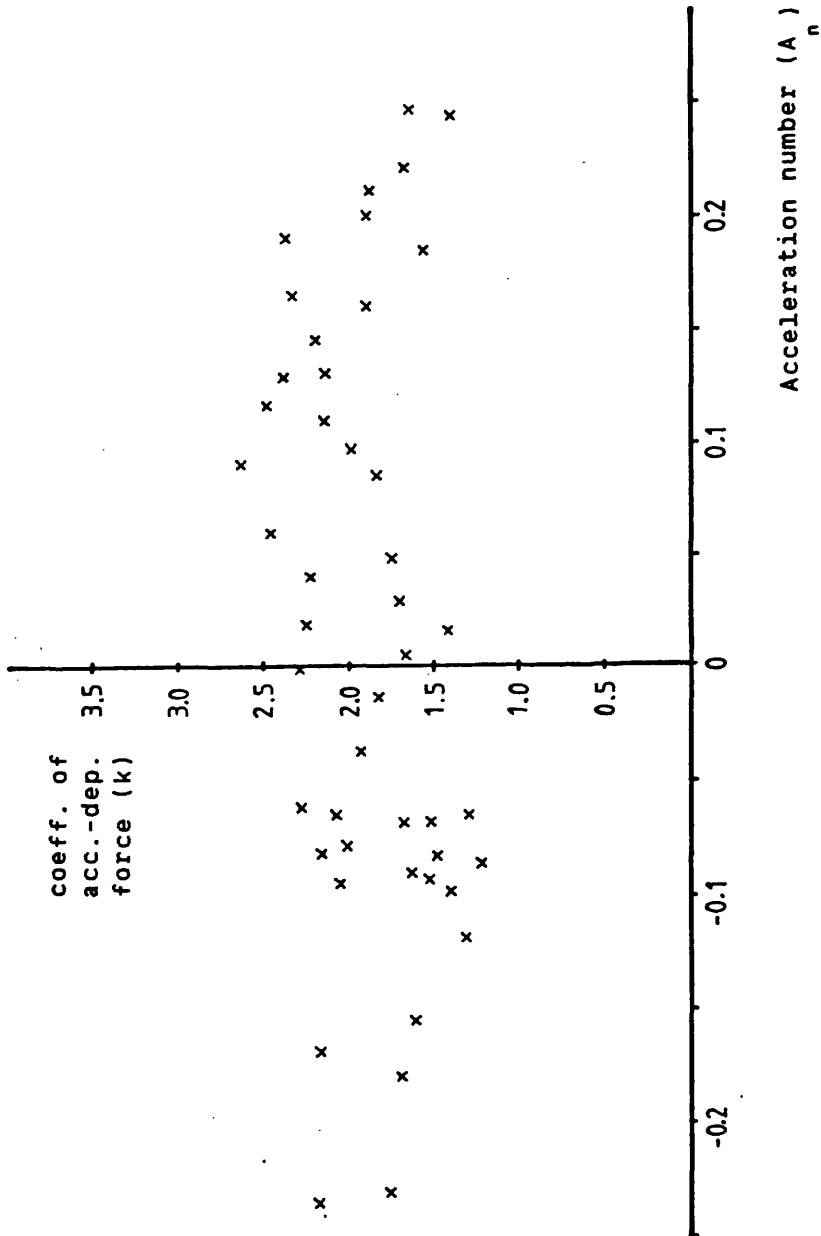
Figure 5.22 Graph of k Vs. A_n for circular cylinder.
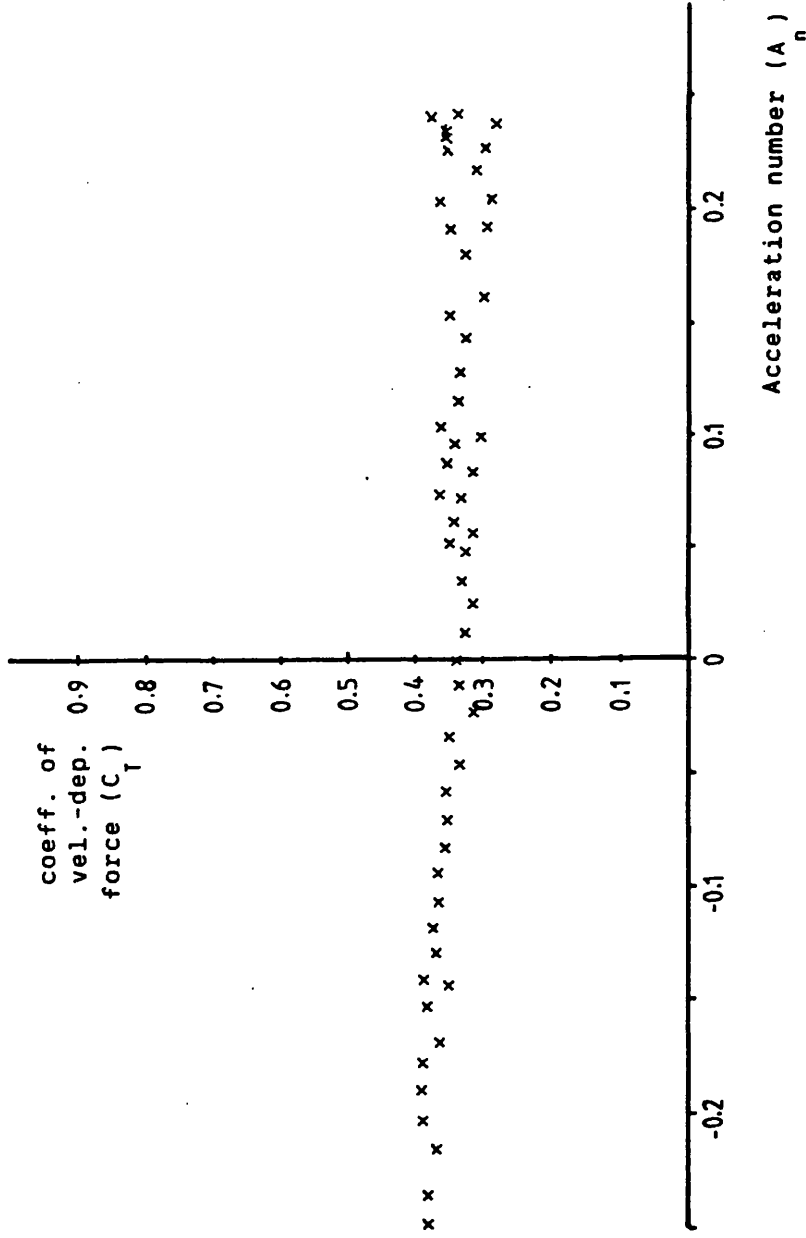
Figure 5.23 Graph of C_T Vs. A_n in the axial direction for rectangular block.
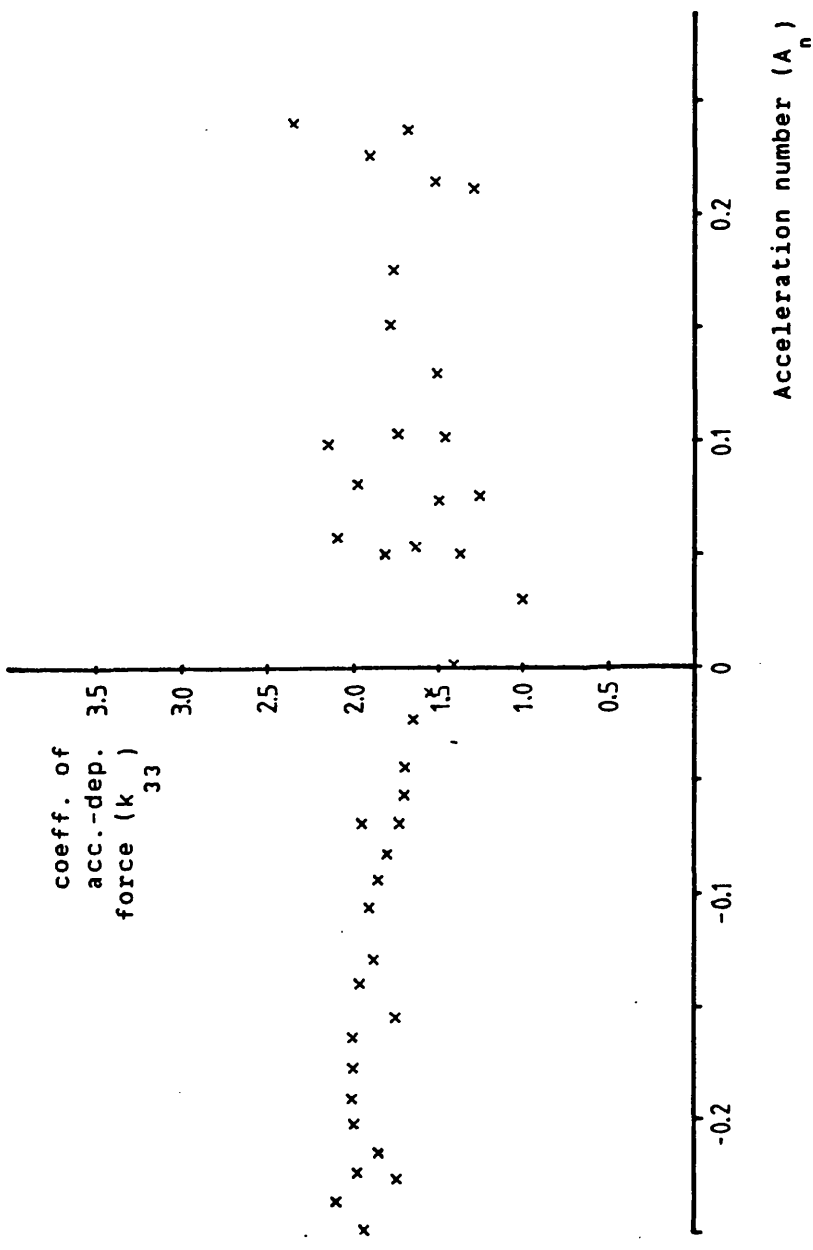
Figure 5.24 Graph of k_{33} Vs. A_n in the axial direction for rectangular block.
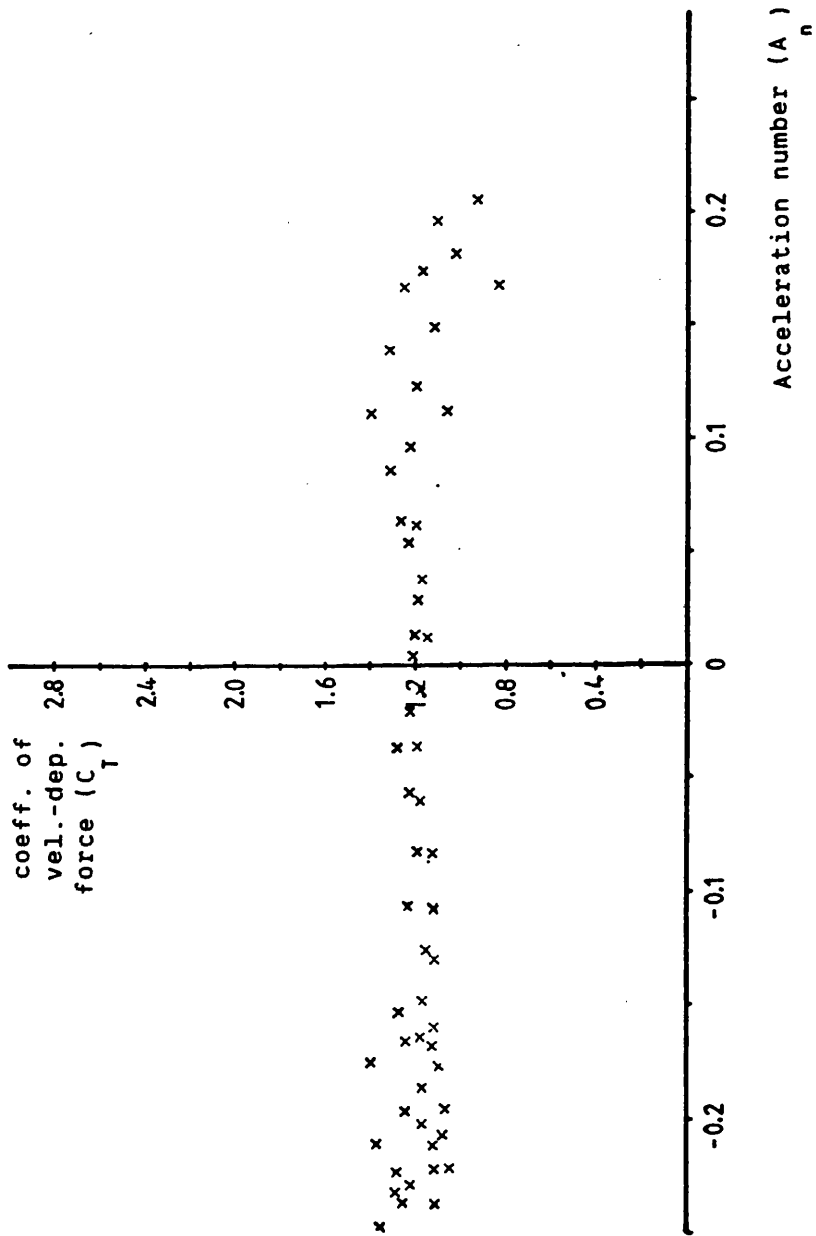
Figure 5.25 Graph of C_T Vs. A_n for cruciform parachute.
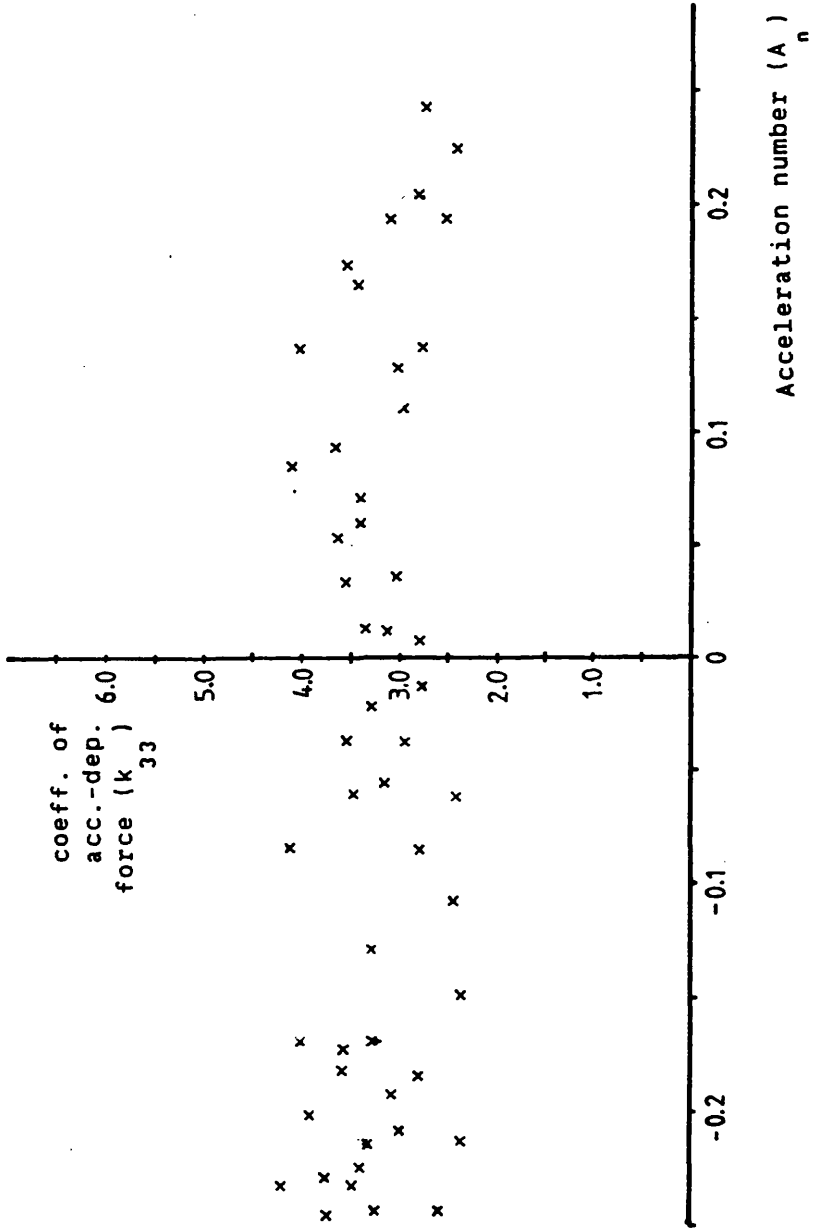
Figure 5.26 Graph of k_{33} Vs. A_n for cruciform parachute.
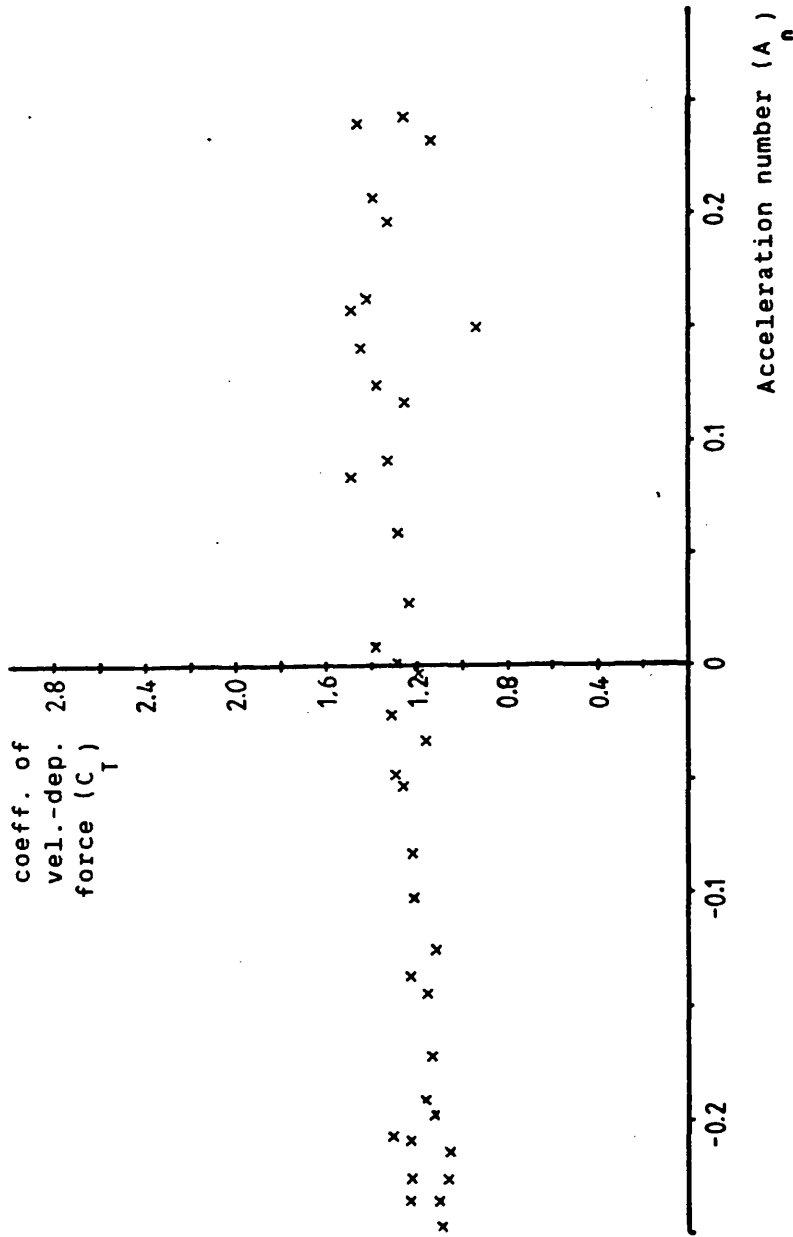
Figure 5.27 Graph of C_T Vs. A_n for ring-slot
parachute.
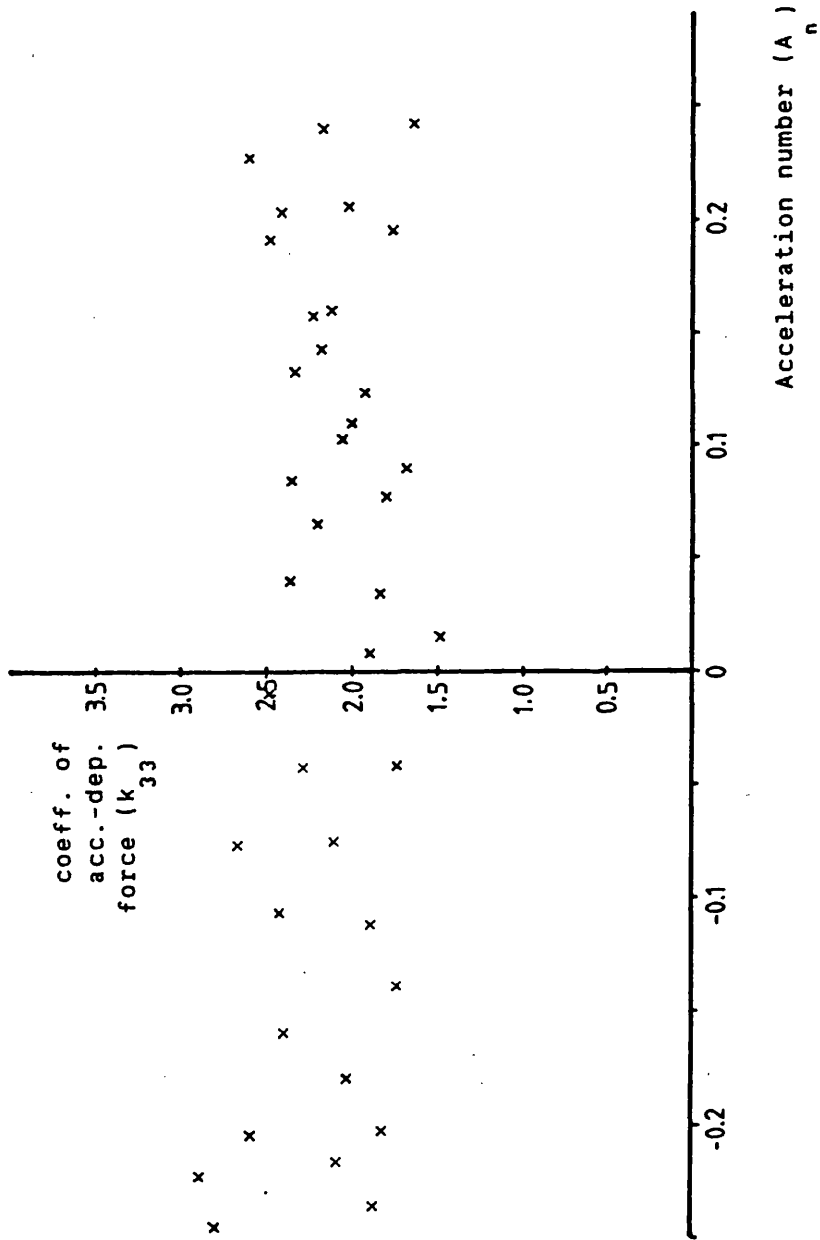
Figure 5.28 Graph of k_{33} vs. A_n for ring-slot parachute.
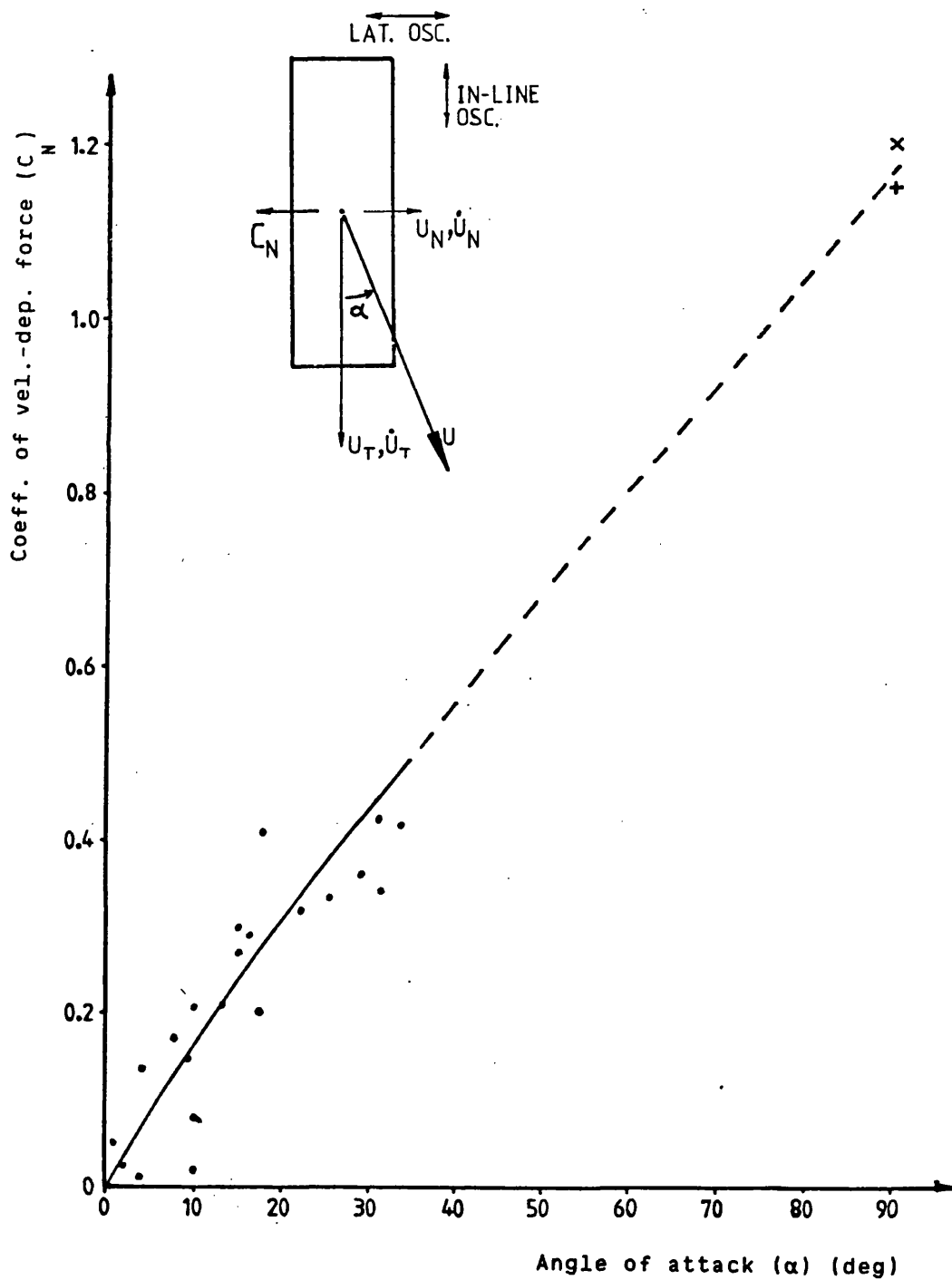
FIgure 5.29 Coefficient of velocity-dependent force in the lateral direction (C_N) versus angle of attack (α).

x —— Steady motion
+ —— Oscillations in the direction of motion
• —— Oscillations in the lateral direction

Test model: Rectangular block of size
457 x 153 x 152.5 mm³
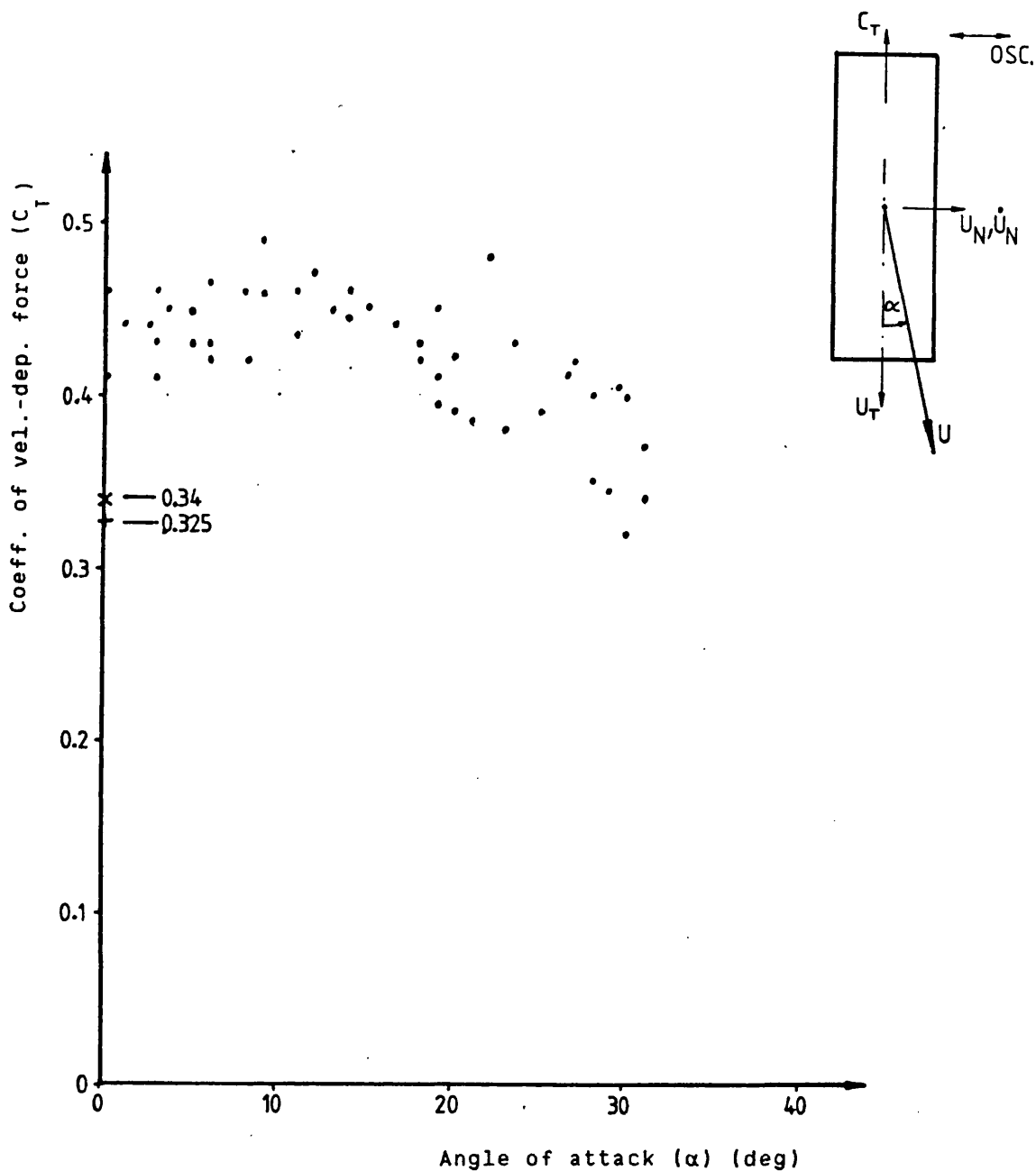
Figure 5.30 Coefficient of velocity-dependent force in axial (forward) direction (C_T) versus angle of attack (α).

    x —— Steady motion
    + —— Oscillations in the direction of
         motion
    • —— Oscillations in the lateral
         direction

Test model: Rectangular block of size
          457 x 153 x 152.5 mm^3
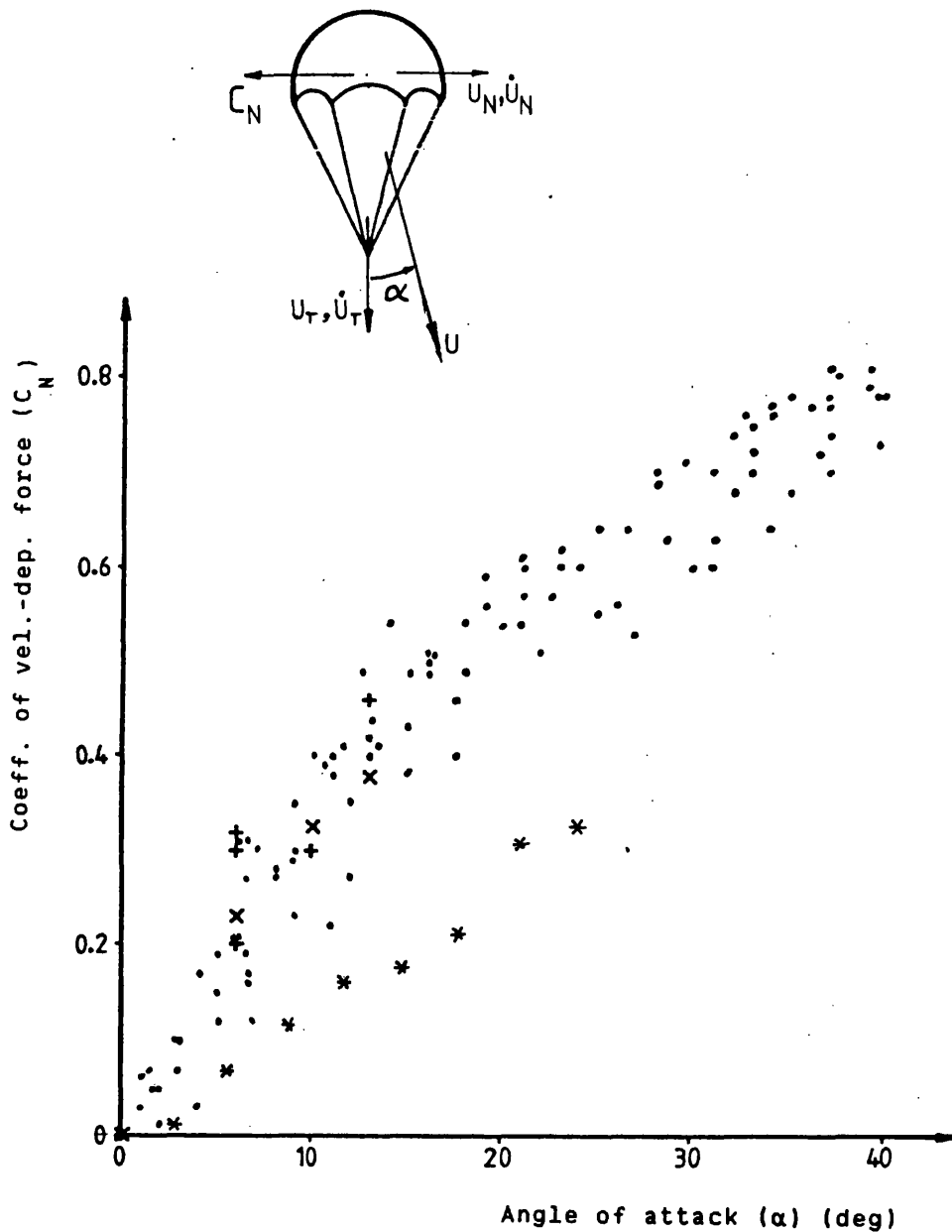
Figure 5.31 Coefficient of velocity-dependent force in the lateral (normal) direction (C_N) versus angle of attack (α).

x —— steady motion (* - from wind tunnel tests)
+ —— oscillations in the direction of motion
• —— oscillations in the lateral direction
Test model: Cruciform parachute with arm ratio of 4:1.
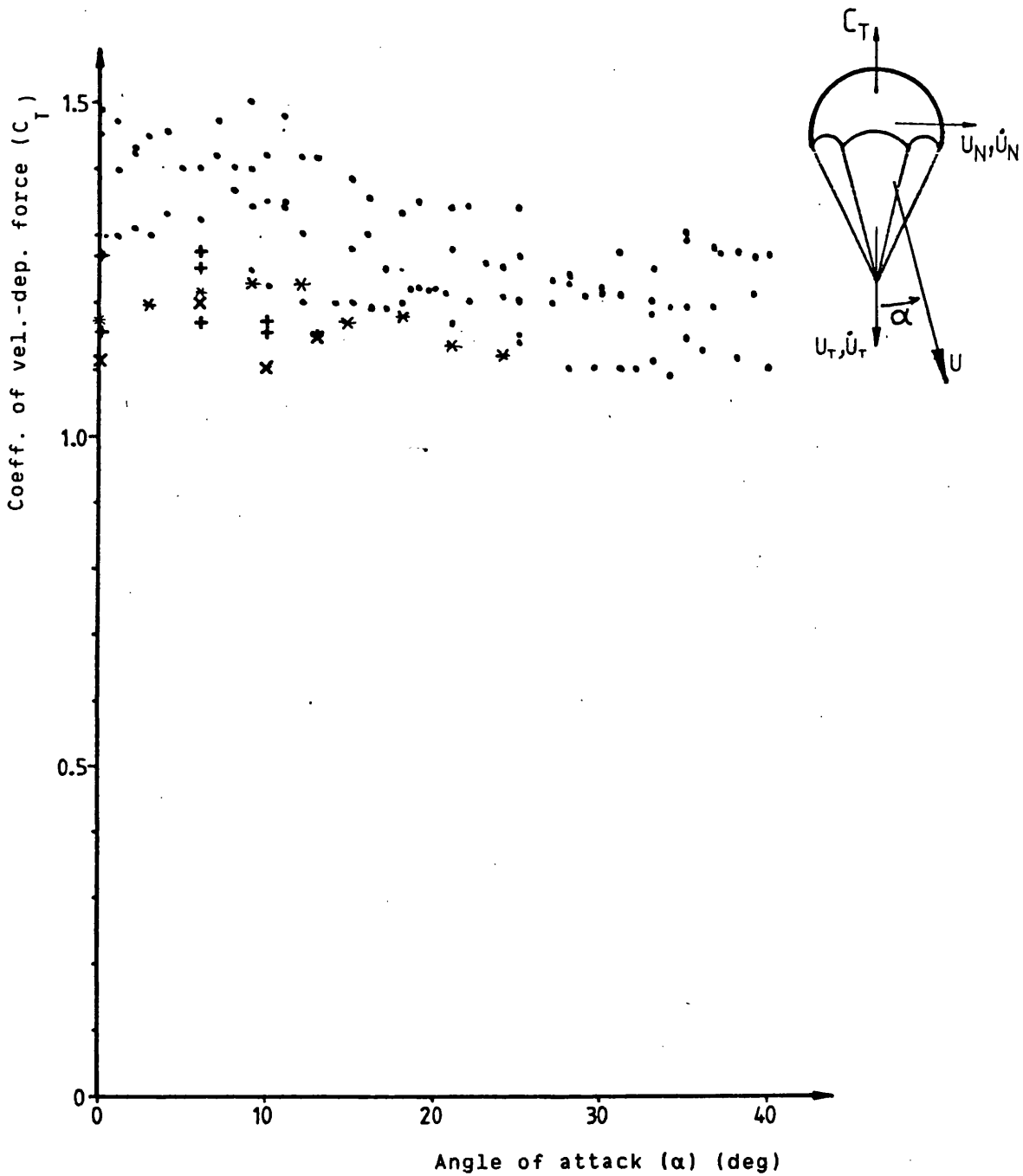
Figure 5.32 Coefficient of velocity-dependent force in the axial direction (C_T) versus angle of attack (α).

x —— steady motion (* - from wind tunnel tests)

+ —— oscillations in the direction of motion

• —— oscillations in the lateral direction

Test model: Cruciform parachute with arm ratio of 4:1.
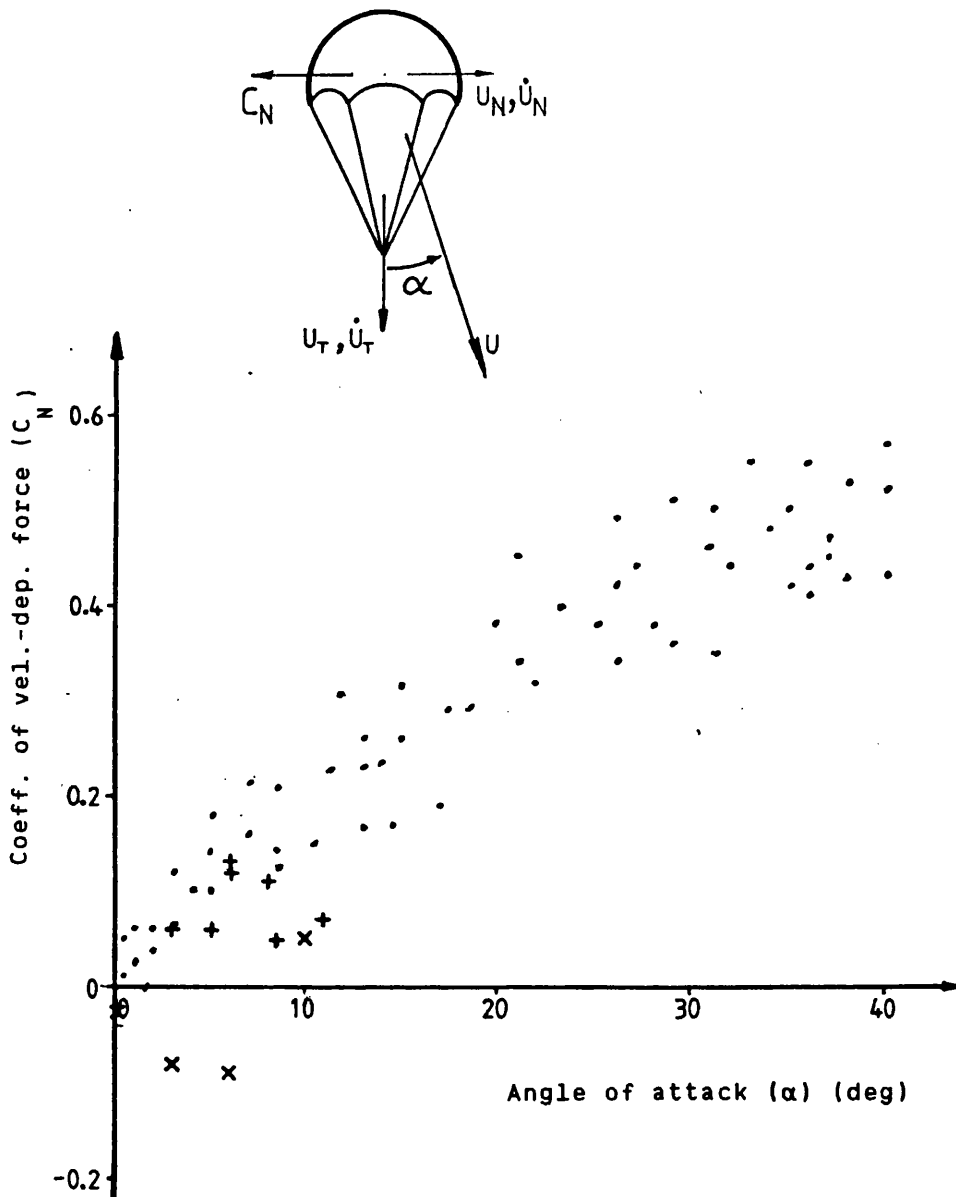
Figure 5.33 Coefficient of velocity-dependent force in the lateral (normal) direction (C_N) versus angle of attack (α).

x —— Steady motion
+ —— Oscillations in the direction of motion
• —— Oscillations in the lateral direction

Test model: Ring-slot parachute.
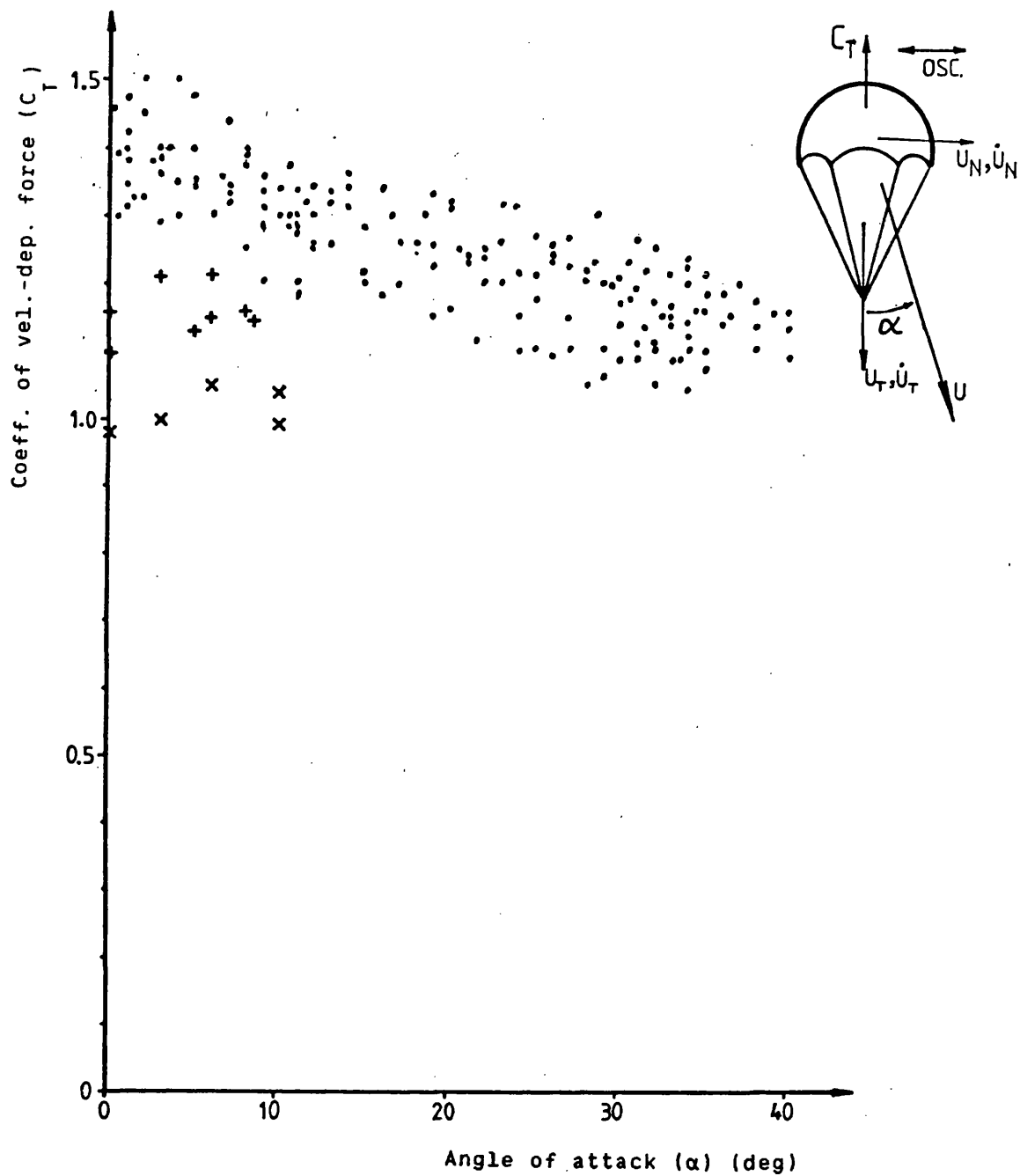
Figure 5.34 Coefficient of velocity-dependent force in the axial direction (C_T) versus angle of attack (α).

x —— Steady motion
+ —— Oscillations in the direction of motion
• —— Oscillations in the lateral direction

Test model: Ring-slot parachute.
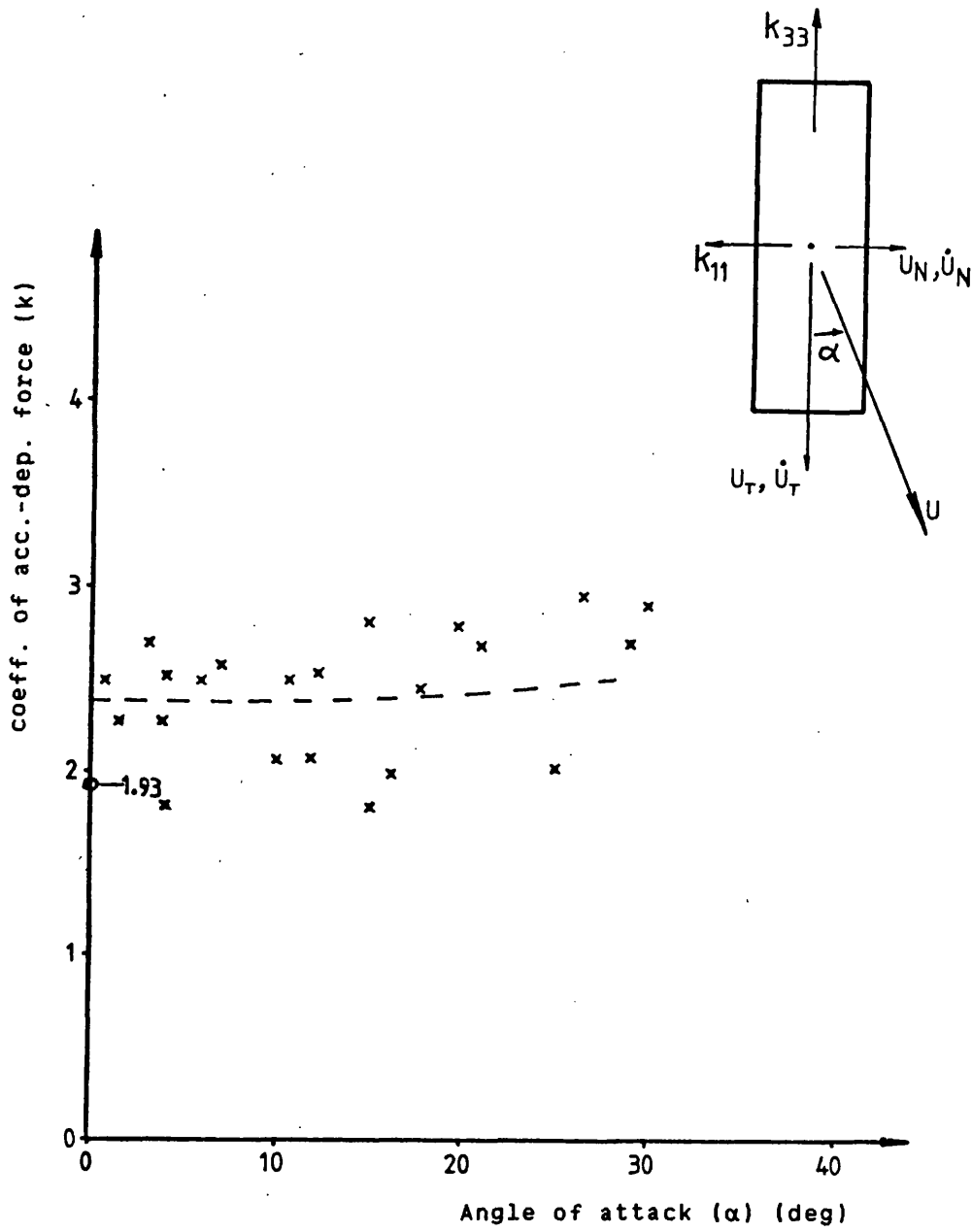
Figure 5.35 Coefficient of acceleration-dependent force (k) versus angle of attack (α).

x ── Normal (lateral) direction (k$_{11}$)
o ── Axial (forward) direction (k$_{33}$)

Test model: Rectangular block of size
457 x 153 x 152.5 mm^3.
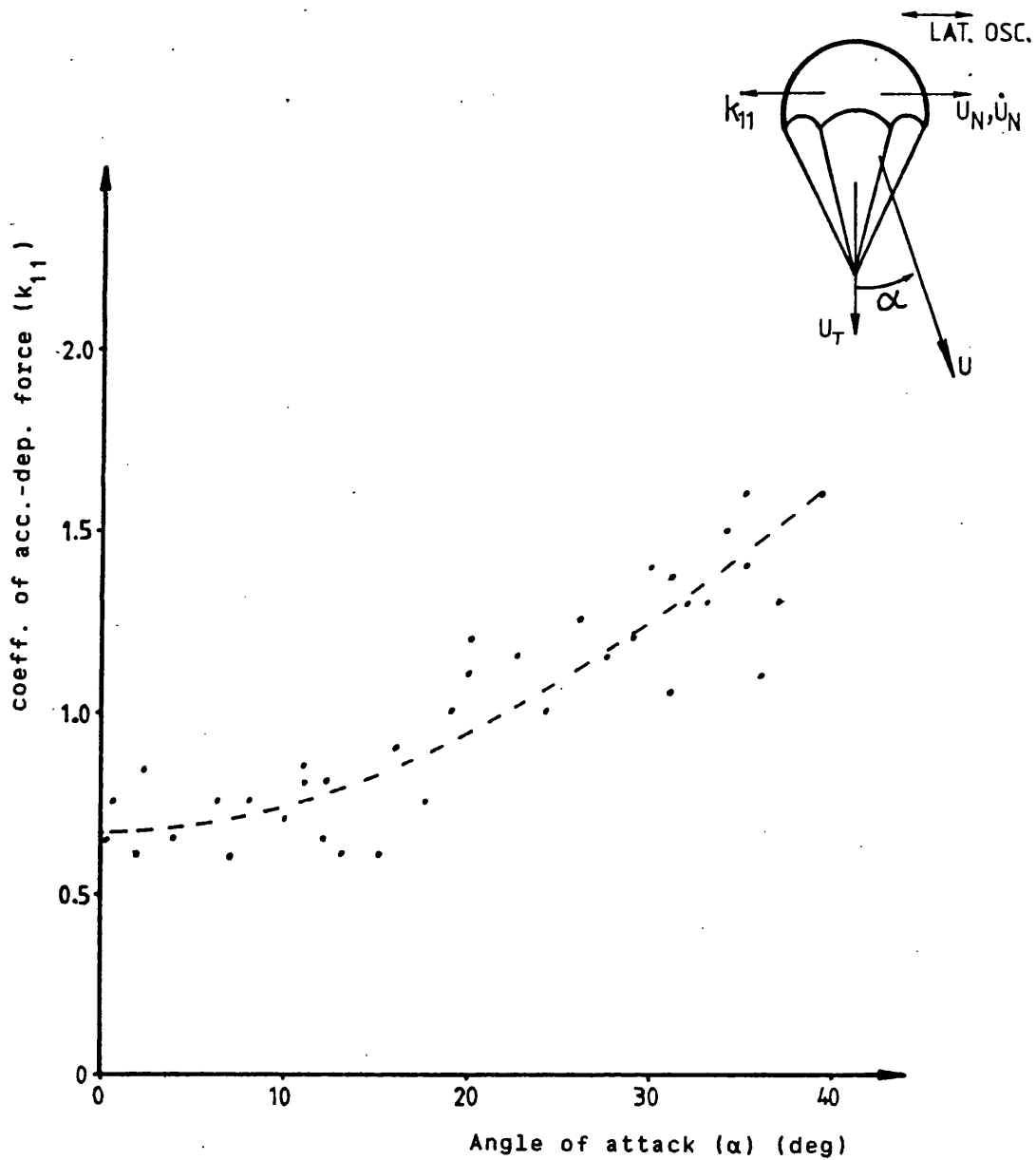
Figure 5.36 Coefficient of acceleration-dependent
force in the lateral (normal) direction (k_{11}) versus
angle of attack (α).

Test model: Cruciform parachute with arm
ratio of 4:1.
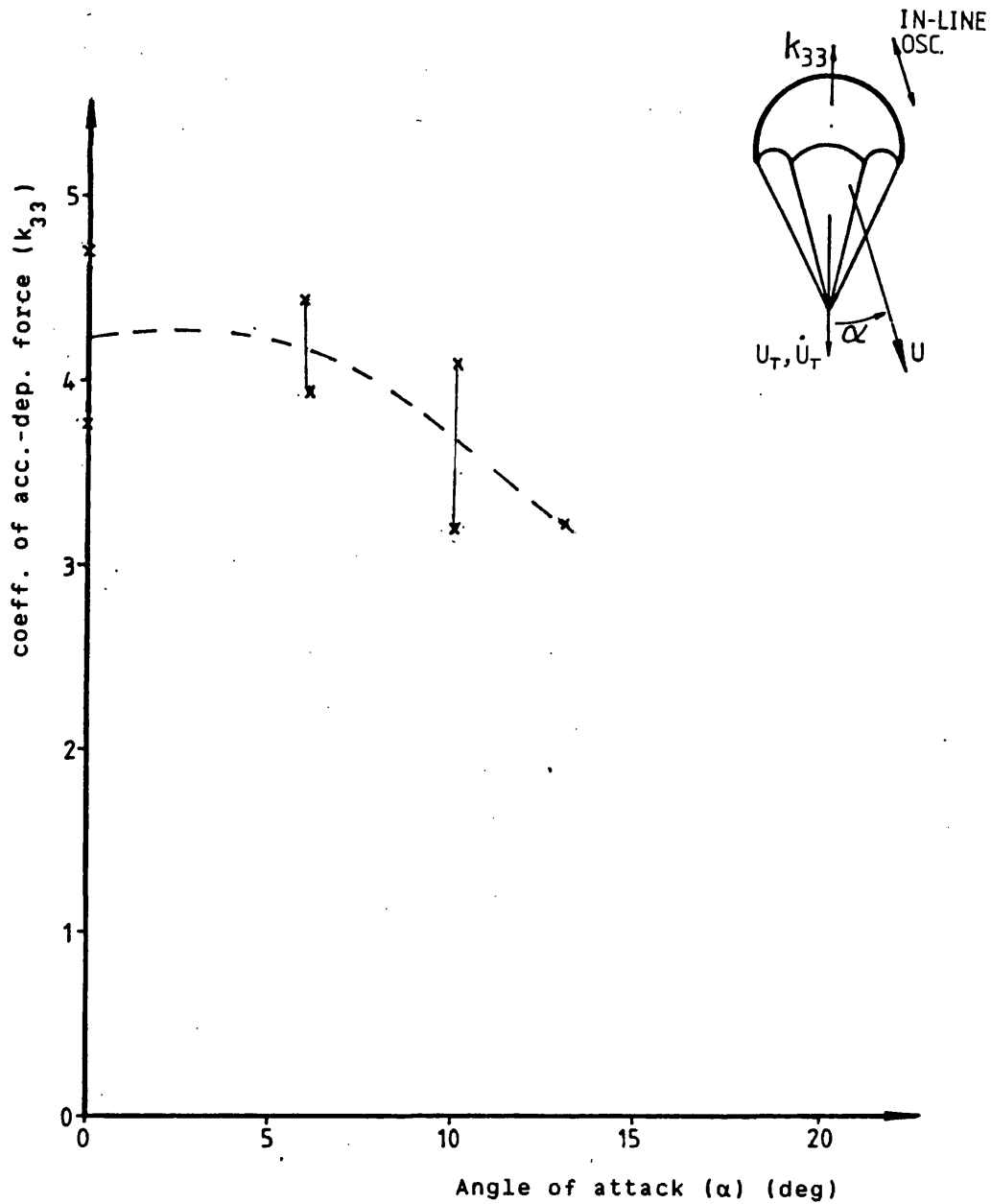
Figure 5.37 Coefficient of acceleration-dependent force in the axial direction (k_{33}) versus angle of attack (α).

Test model: Cruciform parachute with arm ratio of 4:1.
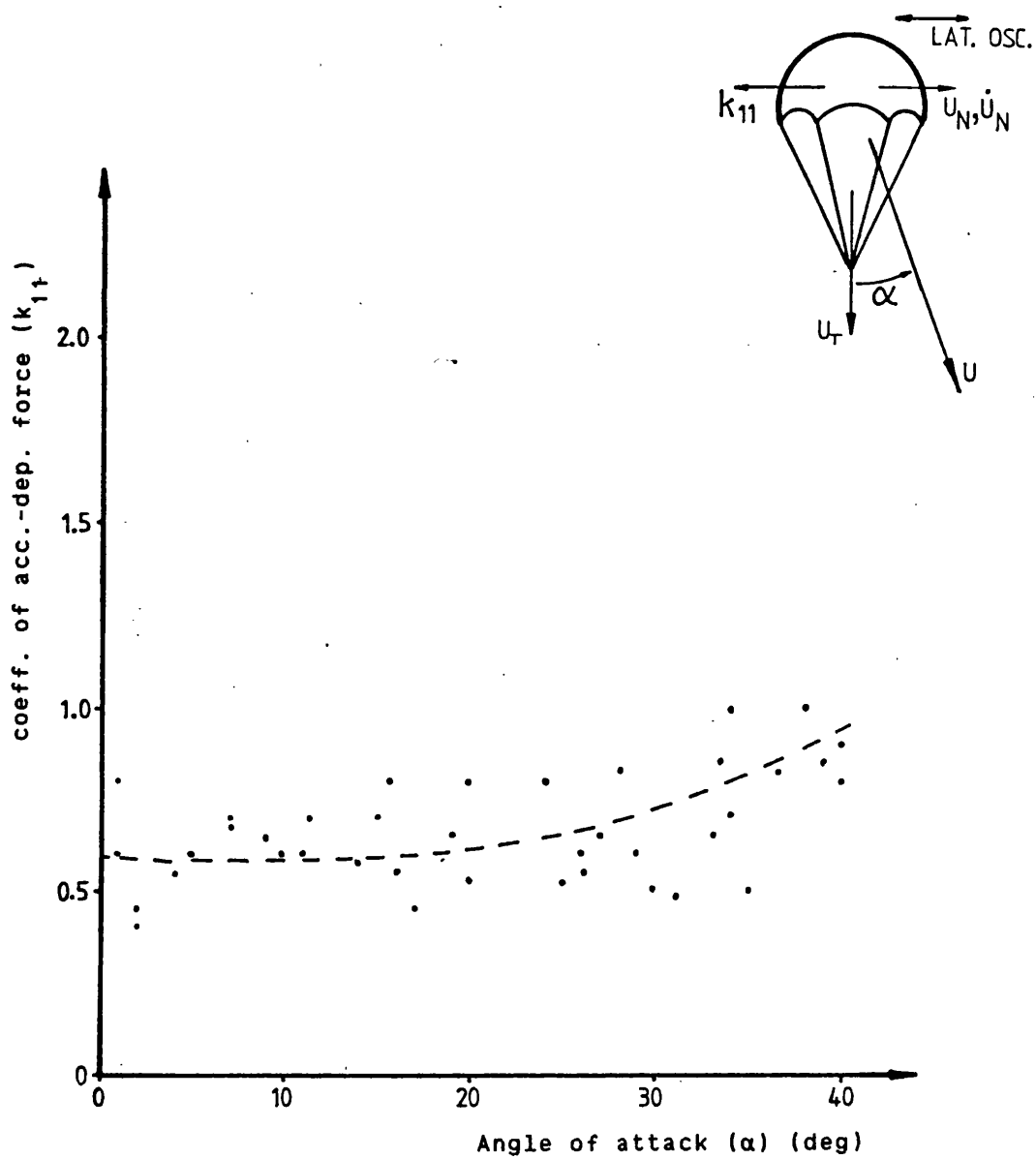
Figure 5.38 coefficient of acceleration-dependent force in the lateral (normal) direction (k_{11}) versus angle of attack (α).

Test model: Ring-slot parachute
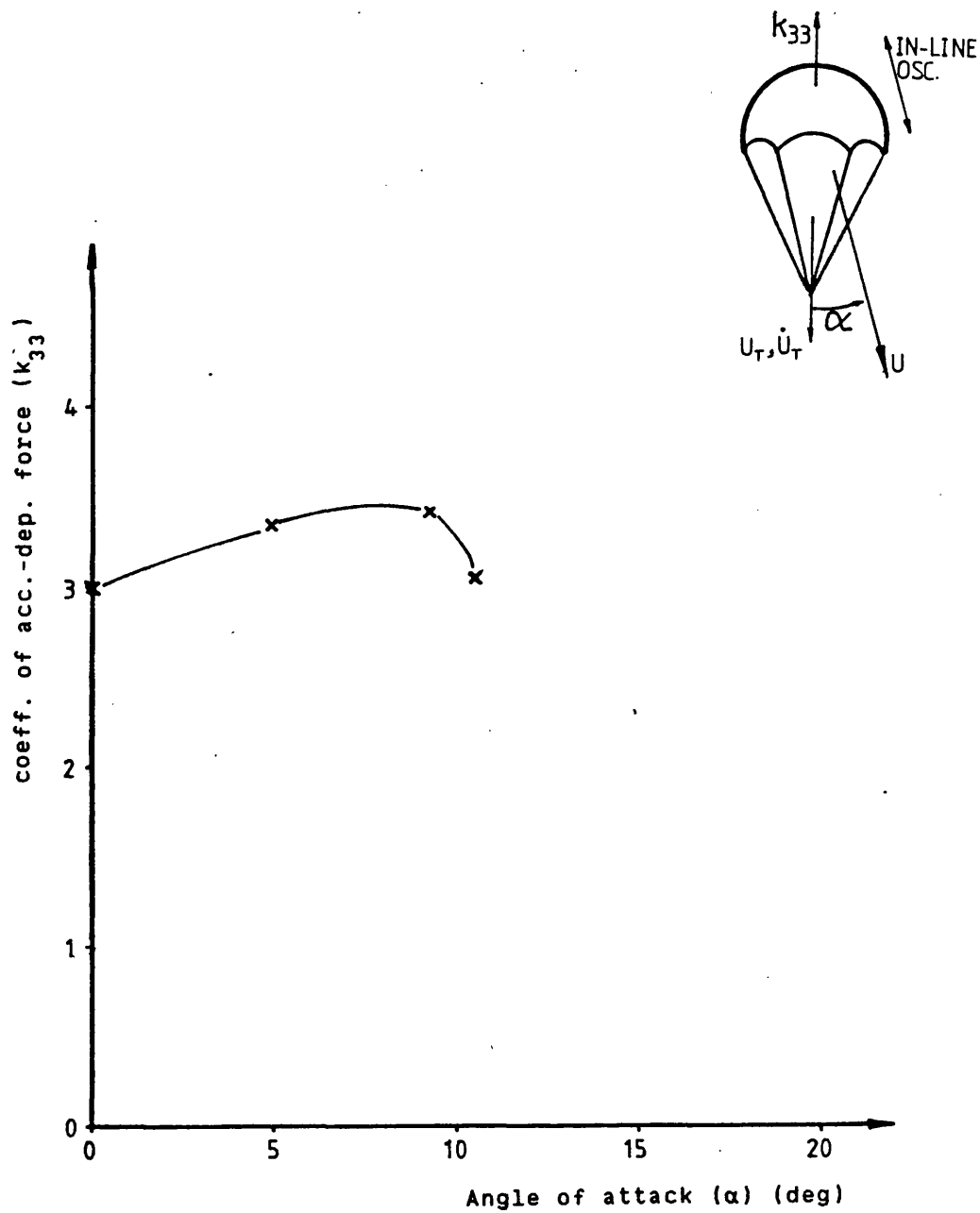
Figure 5.39 Coefficient of acceleration-dependent force in the axial direction (k_{33}) versus angle of attack (α).

Test model: Ring-slot parachute
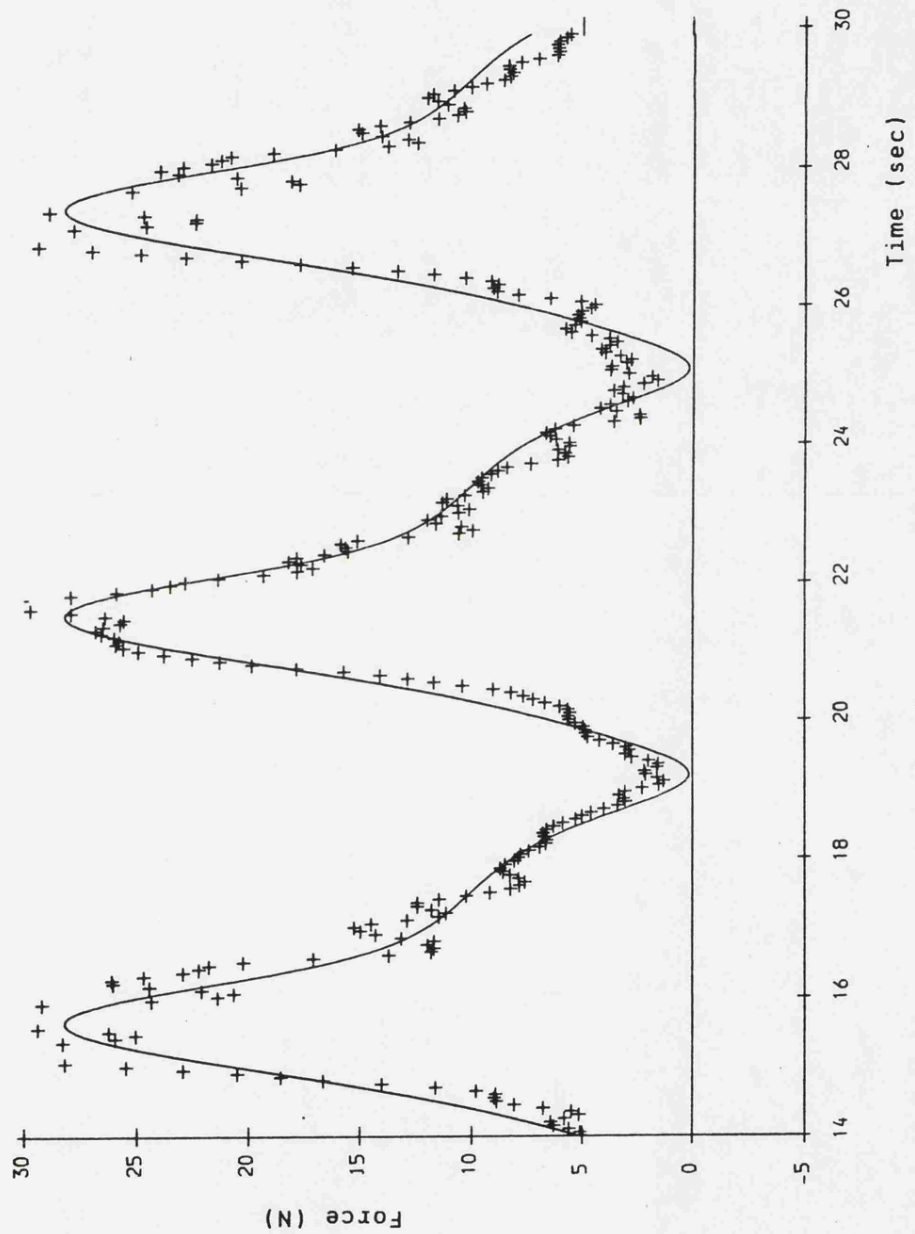
Figure 5.40 Forces on the circular cylinder in in-line oscillation.

+ + + +   experimental
_____   equation (5.1)
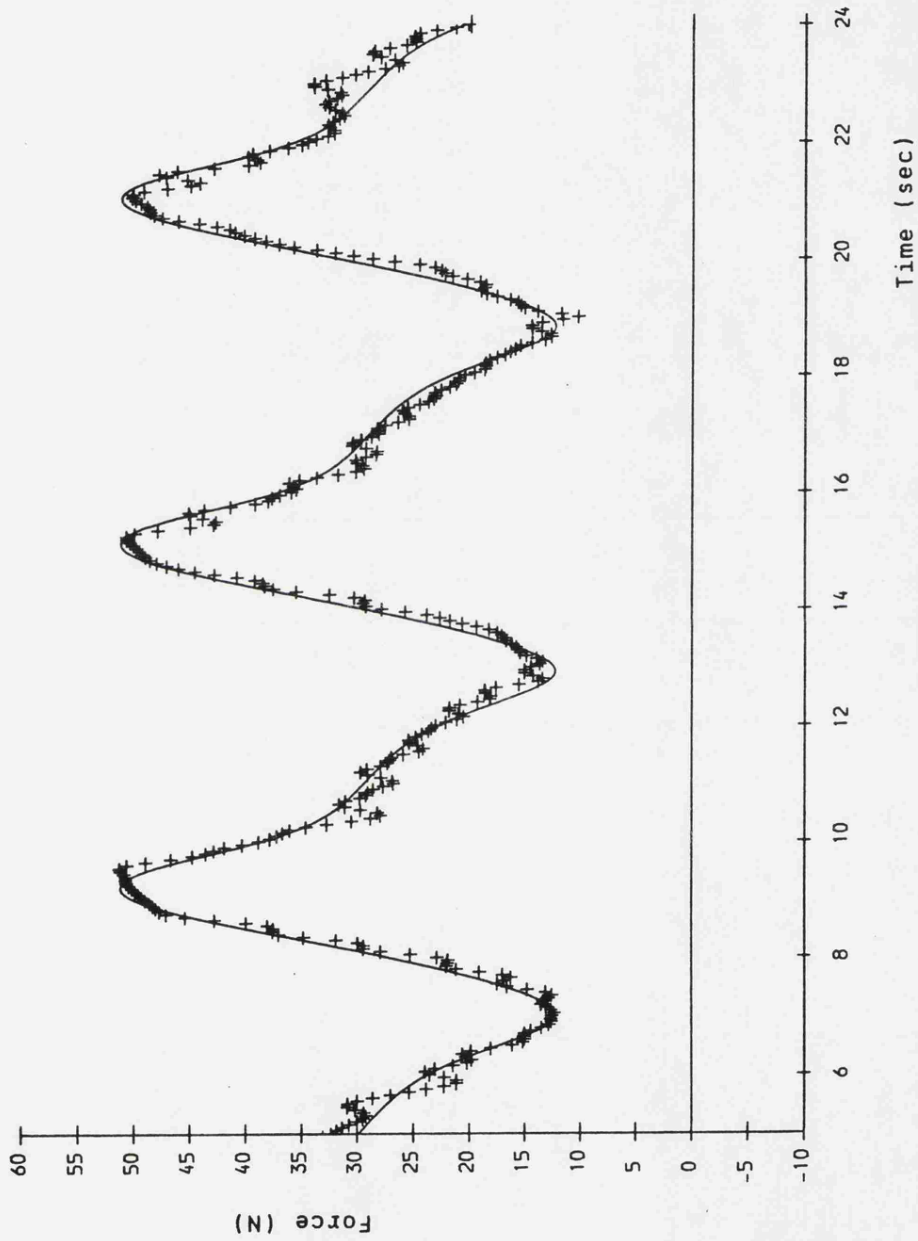
Figure 5.41 Forces on the rectangular block in in-line oscillation.

+ + + +   experimental

———   equation (5.1)

Figure 5.42 Forces on the cruciform parachute in lateral oscillation.

+ + + + +   experimental
_____ equation (5.1)

Figure 5.43 Forces on the ring-slot parachute in lateral oscillation.

+ + + +   experimental

—————   equation (5.1)
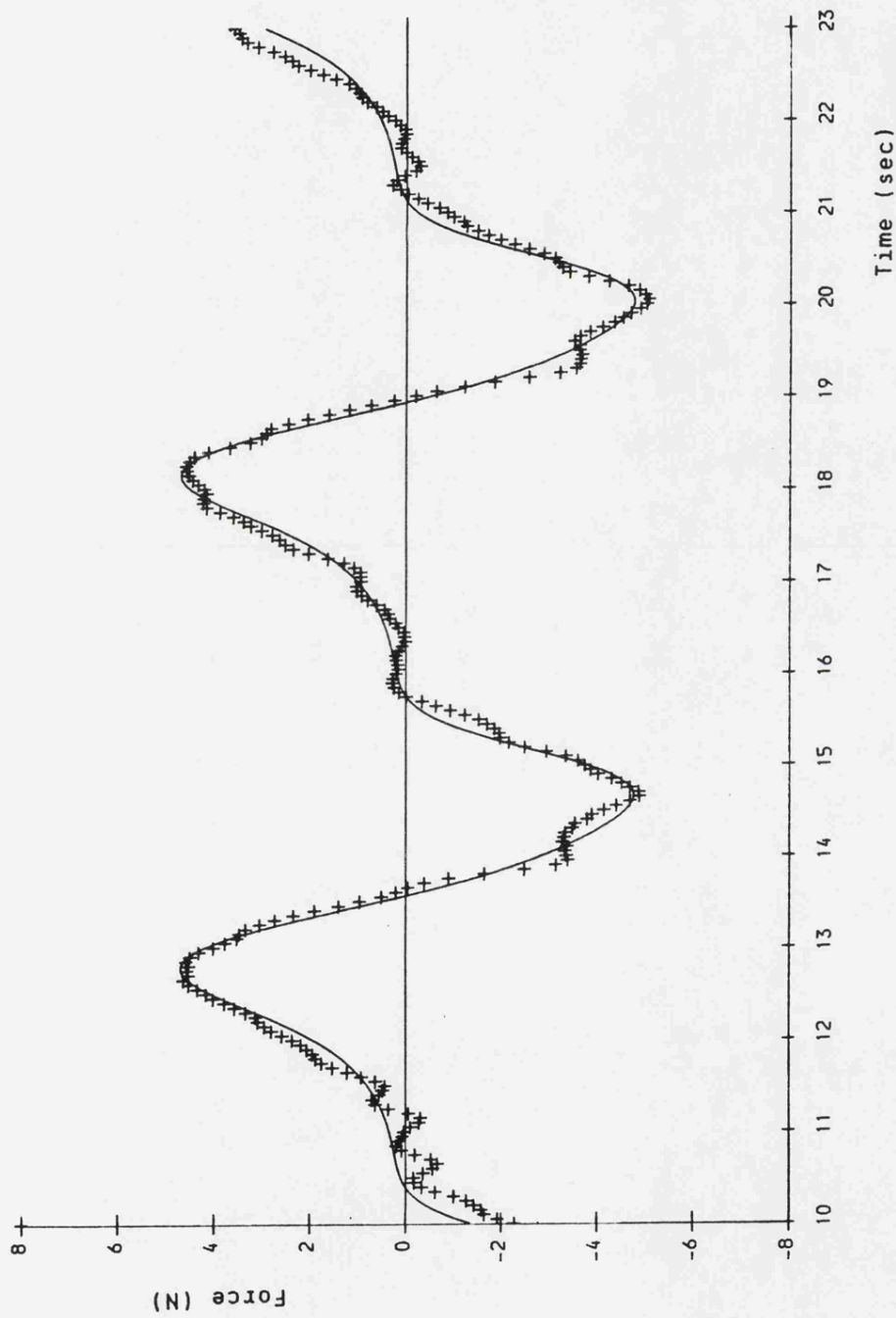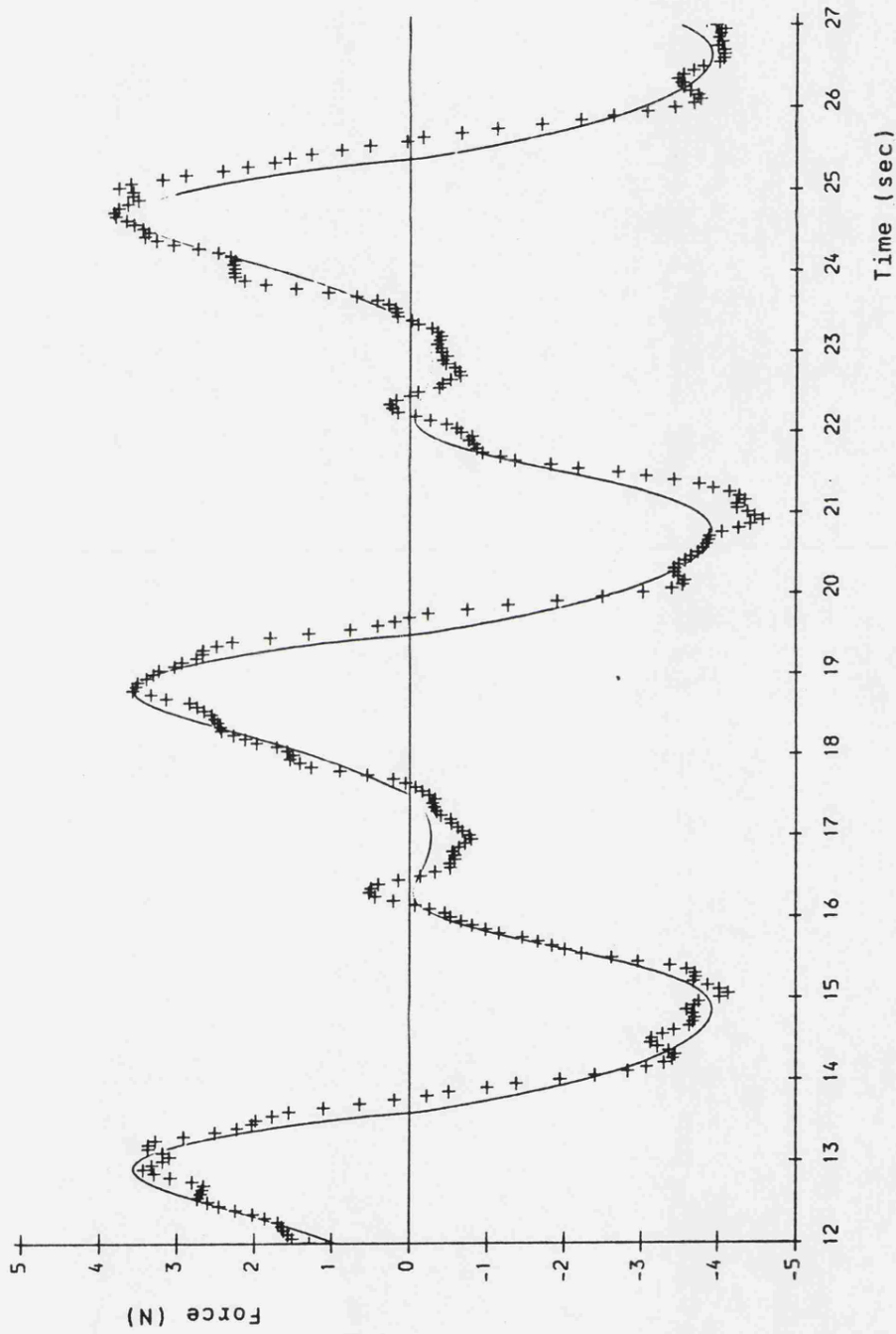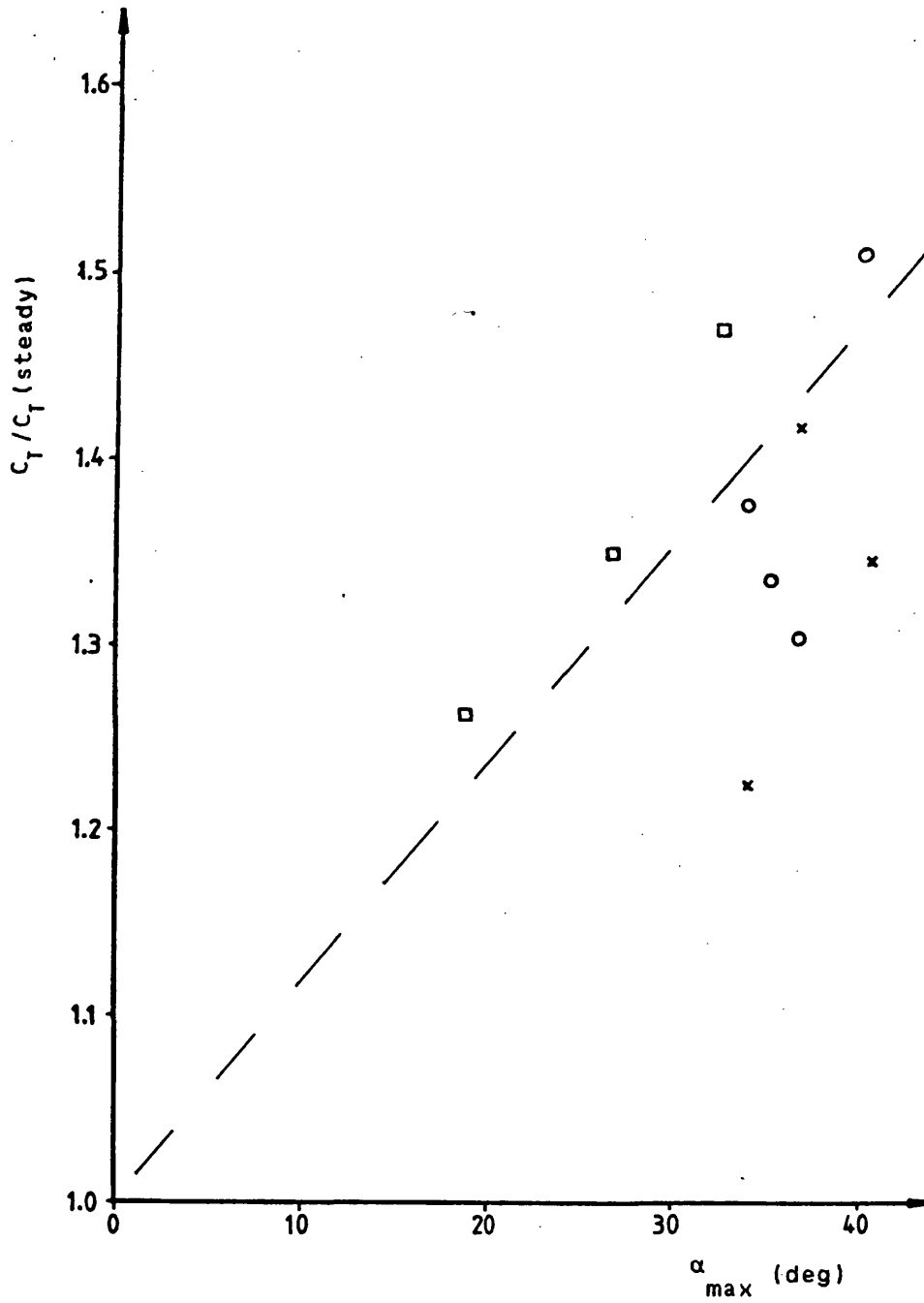
Figure 5.44 Effect of maximum angle of attack imposed by lateral oscillation on the coefficient of the velocity-dependent axial force.

□ ——— Rectangular block
x ——— Cruciform parachute
o ——— Ring slot parachute
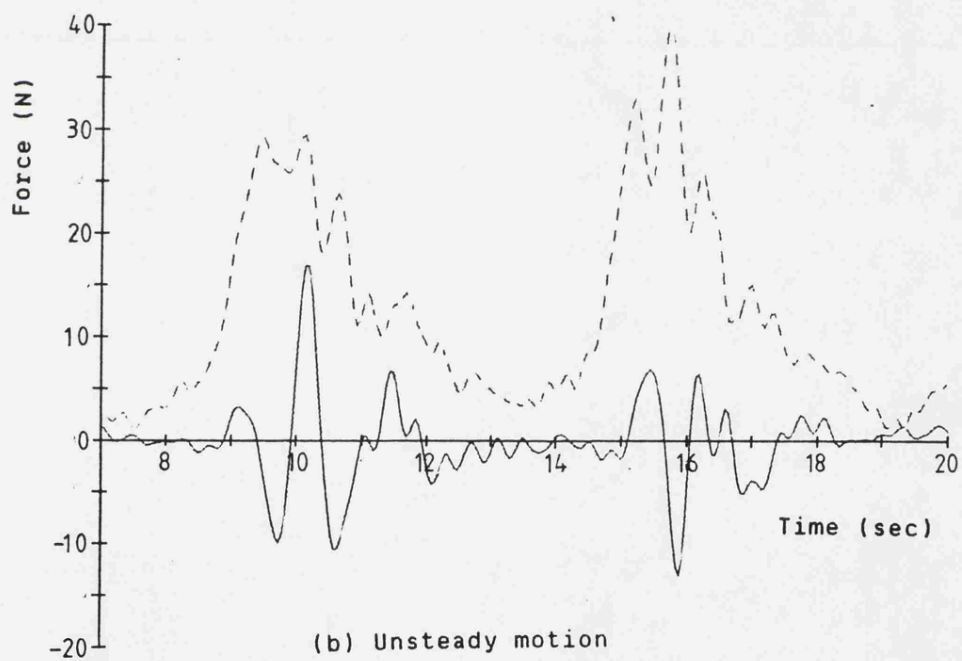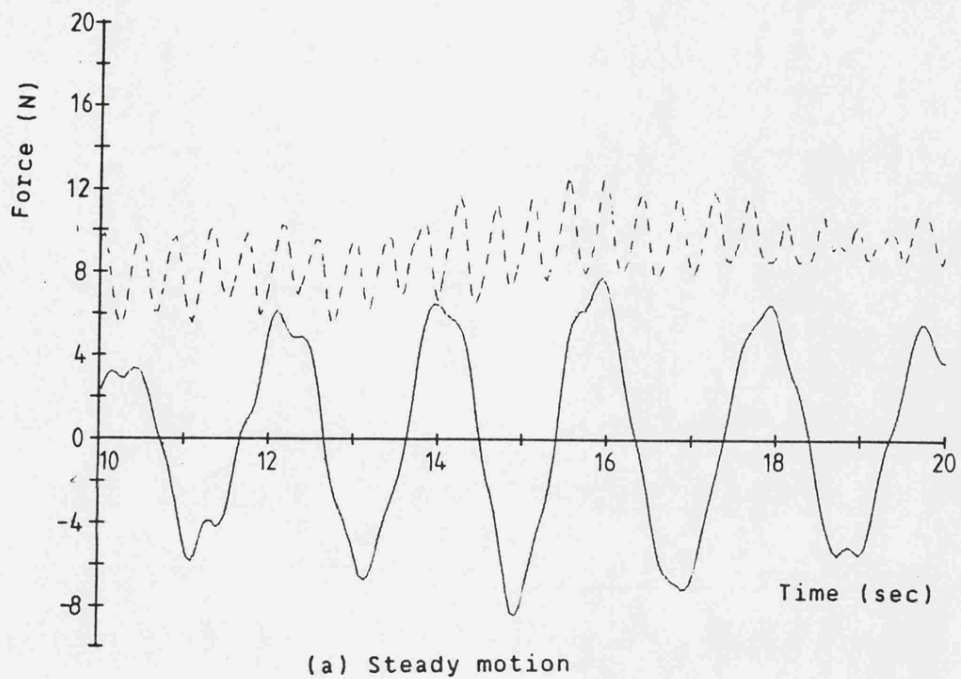
Figure 5.45 Lateral force on circular cylinder in steady motion and in unsteady motion.

——————— lateral force
- - - - - in-line force
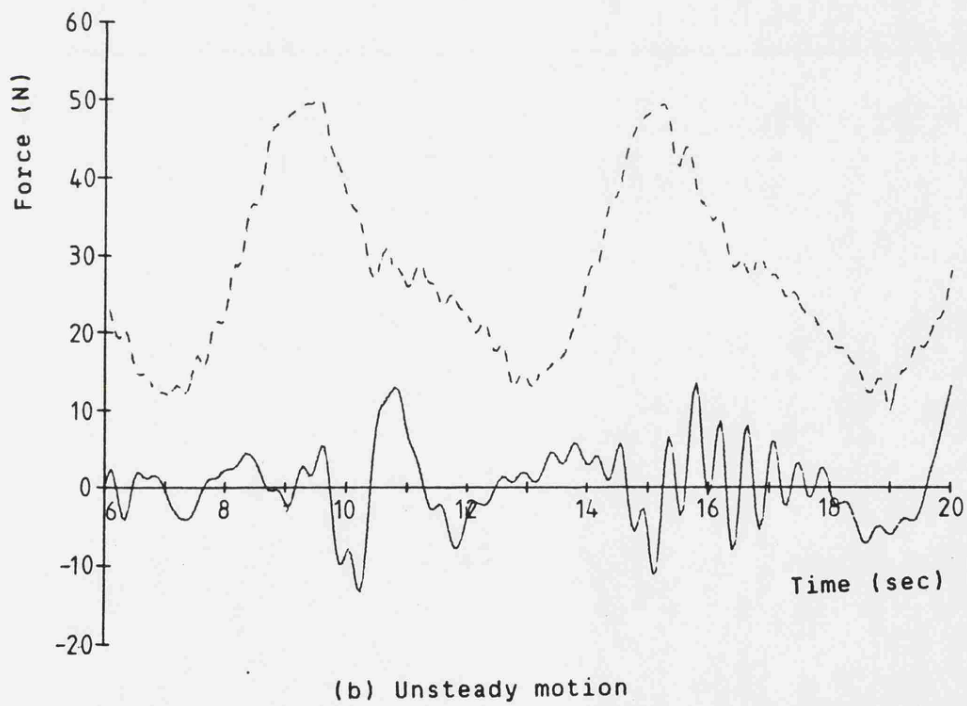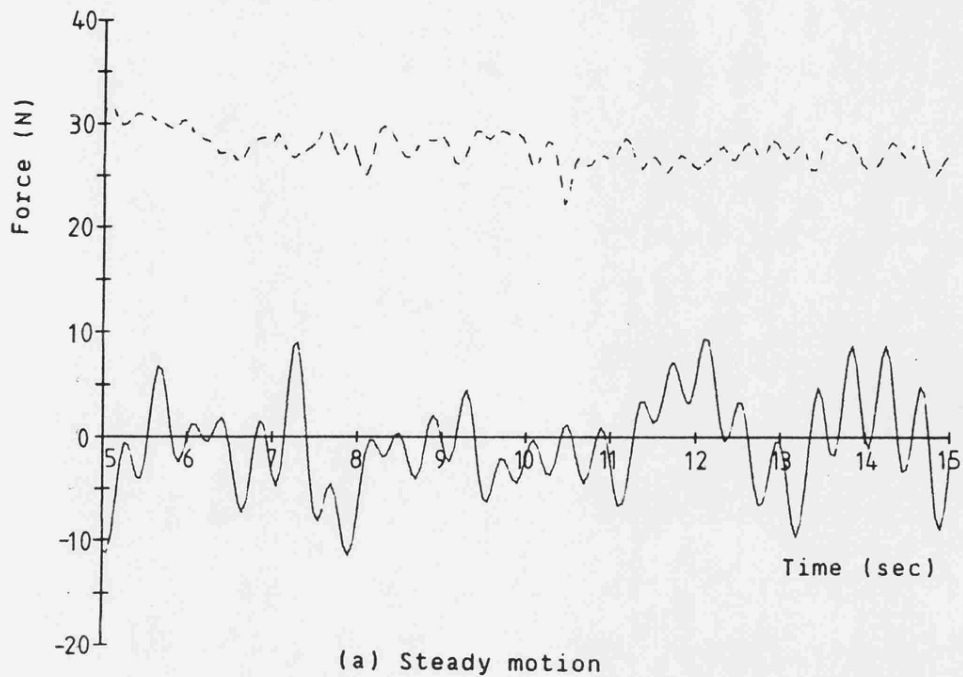
Figure 5.46 Lateral force on rectangular block at zero angle of attack in steady motion and in unsteady motion.

lateral force
axial force
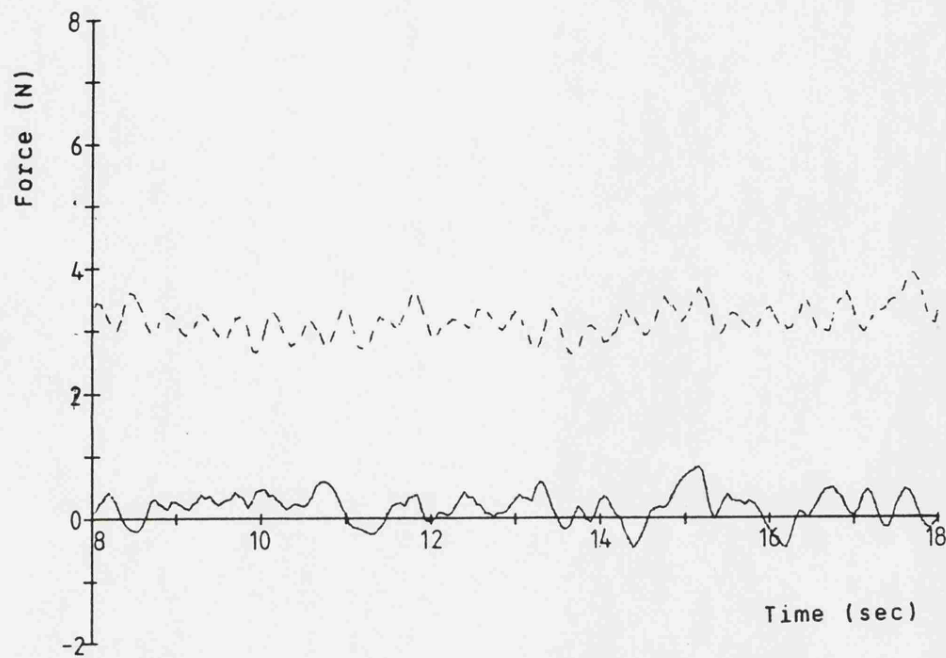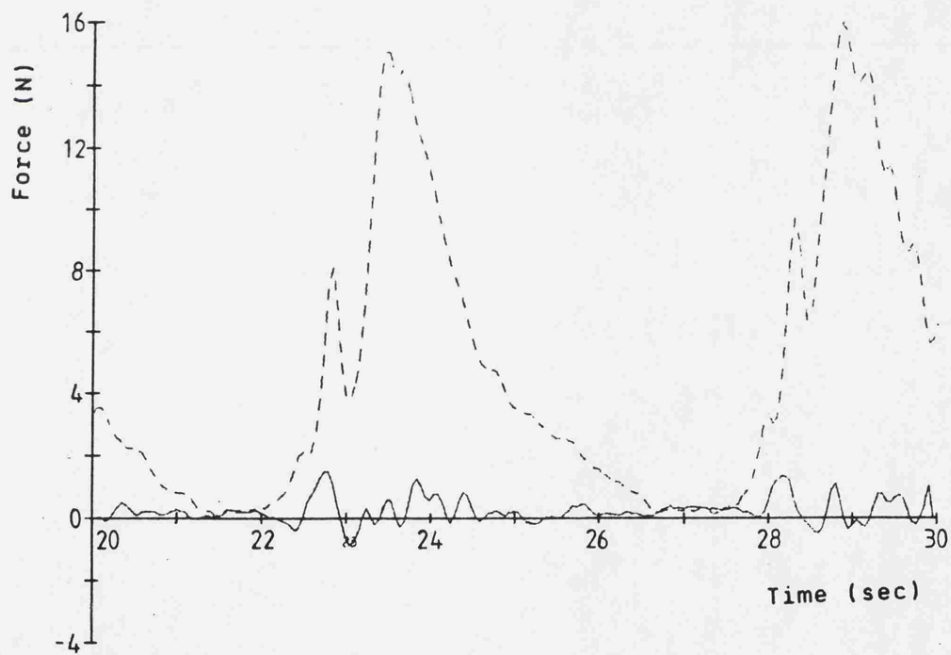
(a) Steady motion

(b) Unsteady motion

Figure 5.47   Lateral   force on cruciform parachute at zero angle of attack in steady motion and in unsteady motion.

————————   lateral force
— — — — —   axial force
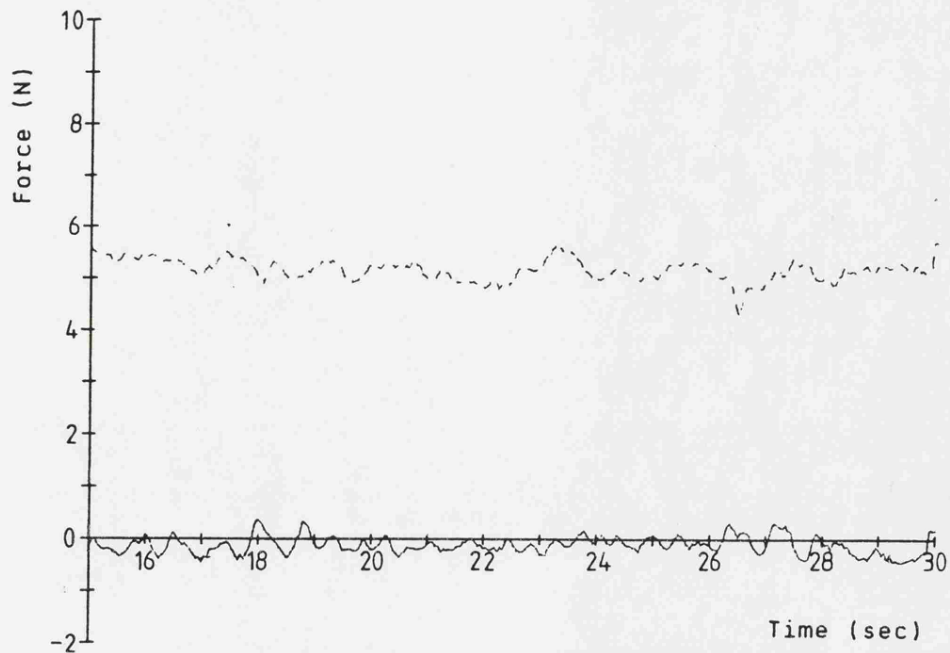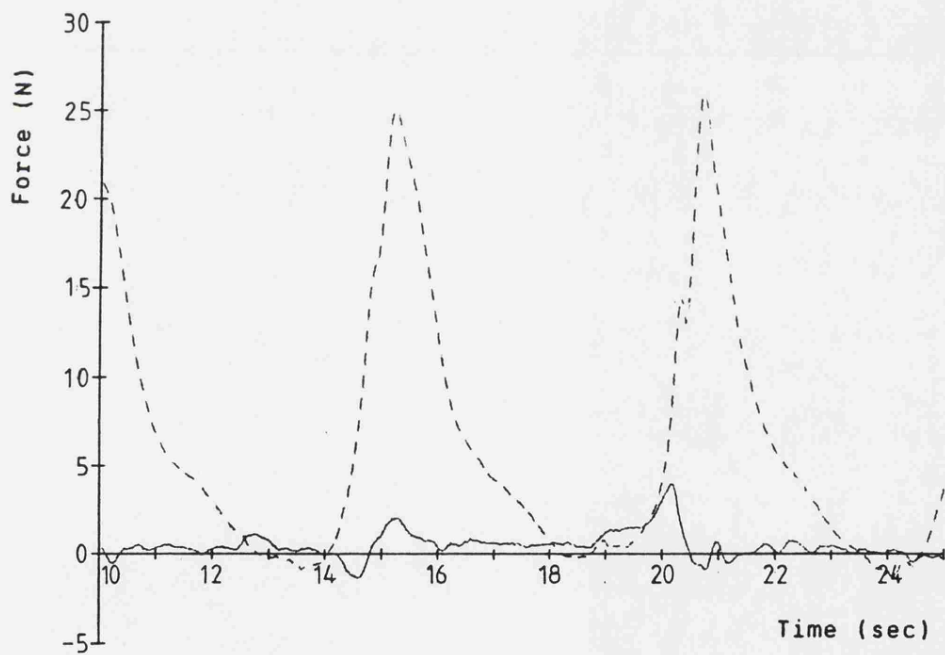
(a) Steady motion

(b) Unsteady motion

Figure 5.48 Lateral force on ring-slot parachute at zero angle of attack in steady motion and in unsteady motion.

——————— lateral force
- - - - - axial force

CHAPTER SIX

RECOMMENDATIONS FOR FUTURE STUDIES
AND CONCLUSIONS

RECOMMENDATIONS FOR FUTURE STUDIES

AND CONCLUSIONS

6.1 RECOMMENDATIONS FOR FUTURE EXPERIMENTAL WORK

(1)   The author is unaware of any other experimental research programme by which unsteady fluid dynamic force on a submerged body has been related to the velocity and the acceleration of the body, in the form given by equation (5.1). It is recommended that independent investigations should be conducted in order to understand more about the phenomenon of time-delay (τ) associated with the unsteady fluid dynamic forces.

(2)   Further experiments are also required for non-dimensionalising τ. Parameters the author considers relevant are discussed in Section 5.7 of Chapter Five. The first stage of such experiments should include test models of the same shape but of different sizes. Fluids with different densities and different viscosities are recommended for further investigations. Such experiments could be used to understand the effect on the model given by equation (5.1) due to scaling of submerged bodies.

(3)   The empirical model form given by the equation (5.1) has been derived exclusively from experiments in which the test models are oscillated in either lateral or in-line

directions while they are being translated at uniform speed. These experiments were designed bearing in mind that a primary applications of the results would be in dynamics of fully inflated descending parachutes. It is suggested that the studies should be conducted for other modes of motion also (e.g. non-periodic unsteady flow), to investigate the possibilities of extending the application of the model. An immediate area of interest is studying the effects of angular velocities and angular accelerations of bluff bodies on their added moments of inertia.

(4) Experimental results show that the fluid dynamic force on a steadily moving submerged body is substantially increased when lateral oscillations are superimposed on this motion. The correlation between the increase in the coefficient of velocity-dependent axial force and the maximum angle of attack (α_{max}) imposed by lateral oscillations, shown in figure 5.44, could be improved by further experiments. In these experiments variations of both the frequency and the amplitude of the oscillations should be included. The level of uncertainty shown in figure 5.32 could be reduced by repeating these experiments.

6.2 CONCLUSIONS

(1)   Existing empirical relationships in which unsteady
fluid dynamic forces on submerged bodies are related to
instantaneous velocity and instantaneous acceleration, are
considered as inadequate. Such inadequacies occur due two
reasons:

(a) At   the   stage   of   analysing   these   forces   the
components of the total force that are dependent on
the velocity and the acceleration are inadequately
defined.   Thus, certain components of the total
force that are velocity-dependent can be often
erroneously considered as acceleration-dependent,
or vice versa.

(b) The history of the motion of real fluids is known to
play an important role in the magnitude and the
direction of the fluid dynamic force.

During the present investigation the author has
related the fluid dynamic forces on submerged bodies to the
entire history of their periodic motion, to obtain the
empirical relationship

$$F(t) = C_R \ 0.5 \ \rho A U(t-\tau) |U(t-\tau)|$$
$$+ \ k \ \rho \forall \dot{U}(t-\tau)$$

where the 'time-delay' τ is a time constant which is found
to be independent of the frequency of oscillation. The
coefficients of forces in this model, C_R and k are found to

be constants, i.e. independent of the acceleration number $(\dot{U}L/U^2)$, if the attitude of the body remains unchanged. Since they are also considered to be independent of Reynolds number in the given range (Section 5.6), the variations in these coefficients can be regarded as due to the variations in the attitude of motion (or, the angle of attack.) Experimentally derived values of these coefficients for various shapes of bodies are given in Tables 5.3 and 5.4 and in figures 5.29 to 5.39. These data together with equation (5.1) represent an effective model for deriving unsteady fluid dynamic forces on bluff bodies.

(2)   As shown in Tables 5.3 and 5.4, data for the coefficient of velocity-dependent force (C_R) and the coefficient of acceleration-dependent force (k) show that

(a) The magnitude of C_R for unsteady flow is not unlike that in steady flow provided that the motion of the submerged body persists in the same direction all the time. Lateral oscillations however increase this force coefficient because the width of the wake downstream of the body is made larger by the lateral movements.

(b) When the flow around bluff bodies is fully developed, the experimental values of k can reach values as much as 2.5 times larger than the corresponding potential flow values. These additional components of the coefficient of acceleration-dependent force are due to the mass of

the fluid involved in the boundary layer and in the wake downstream of the body.

(3)   In the relationship given above which was obtained by relating the fluid dynamic force on submerged bodies to the entire history of the velocity and of the acceleration, coefficients of force components that are dependent on the velocity and on the acceleration remain substantially constant.   The method decsribed in Section 5.4 can be used to identify the two components of the total force separately, thus evaluating the coefficients of these component forces, namely C_R and k, made very effective.

(4)   The values of C_R calculated from the experimental results show that the fluid dynamic force in any particular direction increases substantially when lateral oscillations are superimposed on linear translations. The increase in the coefficient of the velocity-dependent force in the direction of linear translation is related in figure 5.44 to the maximum angle of attack (α_{max}) imposed by the lateral oscillations.   From the limited number of data points given in figure 5.44 it can be seen that the increase in the coefficient of the velocity-dependent force is greater for larger values of α_{max}.

(5)   It is required to established the non-dimensional form of τ so that the model given by equation (5.1) could be used for bodies scaled up to full size. Such work has already been recommended by the author for future

investigations.   The   group $U\tau/L$ is suggested (see Section
5.7   of   Chapter Five) as a suitable non-dimensional form of
τ,   where   U   is   a   reference   velocity.   However,   firm
conclusions with respect to such non-dimensional term cannot
be made without further experimental investigation.

REFERENCES

REFERENCES

1. Basset A.B.

    On the Motion of a Sphere in a Viscous Liquid.

    Philosophical Transactions of the Royal Society;
    Series A; Vol.179; pp 43-63; 1888.

1a. Batchelor G.K.

    An Introduction to Fluid Dynamics.

    Cambridge University Press; 1967.

2. Bearman P.W., Graham J.M.R., Obasaju E.D. and
    Drossopoulos G.M.

    The Influence of corner radius on the Forces
    Experienced by Cylindrical Bluff Bodies in
    Oscillatory FLow.

    Applied Ocean Research; Vol.6; No.2; 1984.

3. Birkhoff G.

    Hydrodynamics.

    Princeton University Press, Princeton, New Jersey;
    1960.

4. Bishop R.E.D., Burcher R.K. and Price W.G.

    The Use of Functional Analysis in Ship Dynamics.

    Proceedings of the Royal Society; Series A; Vol.332;
    pp 23-35; 1973.

5. Bishop R.E.D., Burcher R.K. and Price W.G.

    Application of Functional Analysis to Oscillatory
    Ship Model Testing.

Proceedings of the Royal Society; Series A; Vol.332; pp 37-49; 1973.

6. Bishop R.E.D., Burcher R.K. and Price W.G.

    The Fifth Annual Fairey Lecture: On the Linear Representation of Fluid Forces and Moments in Unsteady Flow.

    The Journal of Sound and Vibration; Vol.29; Part 1; pp 113-128; 1973.

7. Brush Jr. L.M., Ho H-W. and Yen B-C.

    Accelerated Motion of a Sphere in a Viscous Fluid.

    Proceedings of the American Society of Civil Engineers; Journal of the Hydraulic Division; January 1964.

8. Cockrell D.J., Doherr K.-F. and Polpitiye S.J.

    Further Experimental Determination of Parachute Virtual Mass Coefficients.

    AIAA 8th Aerodynamic Decelerator and Balloon Technology Conference; Hyannis,Mass.; April 1984.

8a. Cowley W.L. and Levy H.

    On the Effect of Acceleration on the Resistance of a Body.

    Advisory Committee for Aeronautics; Reports and Memoranda No.612; May 1918.

9. Cummins W.E.

    The Impulse Response Function and Ship Motions.

    David Taylor Model Basin; Washington D.C.; Report No.1661; October 1962.

10. Darwin C.G.

    Notes on Hydrodynamics.

Proceedings of Cambridge Philosopical Society; Vol.49; 1953; pp 342-354.

11. DiStefano III J.J., Stubberud A.R. and Williams I.J.
Feedback and Control Systems. SI(metric) Edition. Schaum's Outline Series; McGraw-Hill Book Company; 1967.

12. Frazer R.A. and Simmons L.F.G.
The Dependence of the resistance of Bodies Upon Acceleration as Determined by Chronograph Analysis. Advisory Committee for Aeronautics; Reports and Memoranda No.590; January 1919.

13. Hoerner S.F.
Fluid - Dynamic Drag
Published by the Author; 1965. (Available from: Hoerner Fluid Dynamics, P O Box 342, Brick Town, N.J. 08723.)

14. Hogben N.
Fluid Loading on Offshore Structures, A State of Art Appraisal: Wave Loads.
Maritime Technology Monograph; Royal Institute of Naval Architects; 1974.

15. Hogben N., Miller B.L., Searle J.W. and Ward G.
Estimation of Fluid Loading on Offshore Structures. Proceedings of the Institution of Civil Engineers; Vol.63; Part 2; pp 515-562; September 1977.

16. Ibrahim S.K.
Apparent Added Mass and Moment of Inertia of Cup-Shaped Bodies In Unsteady Flow.
Ph.D. Thesis; University of Minnesota; Minneapolis; Minnesota; 1965.

17. Iversen H.W. and Balent R.

A Correlating Modulus for Fluid Resistance in Accelerated Motion.

Journal of Applied Physics; Vol.22; No.3; pp 324-328; March 1951.

18. Jorgensen D.S.

Cruciform Parachute Aerodynamics.

Ph.D. Thesis; University of Leicester; 1982.

19. Jorgensen D.S. and Cockrell D.J.

Aerodynamics and Performance of Cruciform Parachute Canopies.

Proceedings of the AIAA 7th Aerodynamic Decelerator and Balloon Technology Conference; Paper No. 81-1919; San Diego, California; October 1981.

20. Karanfilian S.K. and Kotas T.J.

Drag on a Sphere in Unsteady Motion in a Liquid at Rest.

Journal of Fluid Mechanics; Vol.87; Part 1; pp 85-96; 1978.

21. Karman Th. von and Sears W.R.

Aerofoil Theory for Non-Uniform Motion.

Journal of Aeronautical Sciences; Vol.5; No.10; August 1938.

22. Keulegan G.H. and Carpenter L.H.

Forces on Cylinders and Plates in an Oscillating Fluid.

Journal of Research of the National Bureau of Standards; Vol.60; No.5; 1958.

23. Korn G.A. and Korn T.M.

    Mathematical Handbook for Scientists and Engineers.

    McGraw-Hill Book Company, Inc.; 1961.

24. Kreyszig E.

    Advanced Engineering Mathematics.

    3rd Edition (Wiley International Edition); John
    Wiley and Sons, Inc., N.Y.; 1972.

25. Lamb H.

    Hydrodynamics.

    Cambridge University Press; 6th Edition; 1932(1945
    American edition).

26. Maull D.J. and Milliner M.G.

    Sinusoidal Flow Past a Circular Cylinder.

    Coastal Engineering; pp 149-168; 1978.

27. Milne-Thomson L.M.

    Theoretical Hydrodynamics.

    MacMillan and Company Limited; 5th Edition; 1968.

28. Morison J.R., O'Brien M.P., Jonhson J.W. and Schaff
    S.A.

    The Force Exerted by Surface Waves on Piles.

    Transactions of American Institution of Mining and
    Metallurgical Engineers - Petroleum Branch; Vol.189;
    pp 149-157; 1950.

29. Odar F. and Hamilton W.S.

    Forces on a Sphere Accelerating in a viscous Fluid.
    Journal of Fluid Mechanics; Vol.18; pp 302-314;
    1964.

30. Raven F.H.

    Automatic Control Engineering.

    McGraw-Hill Book Company, Inc, N.Y. 1961.

31. Rayleigh Lord

   On the Motion of Solid Bodies Through Viscous Liquid
   Philosophical Magazine and Journal of Science; Sixth
   series; June 1911.

32. Relf E.F. and Jones M.A.

   Measurement of the Effect of Accelerations on the
   Longitudinal and Lateral Motion of an Airship Model.
   Advisory Committee for Aeronautics; Reports and
   Memoranda No.613; June 1918.

33. Robertson J.M.

   Hydrodynamics in Theory and Application.
   Prentice-Hall Inc./Englewood Cliffs, N.J.;1965.

34. Sarpkaya T.

   Lift, Drag and Added Mass Coefficients For a
   Circular Cylinder Immersed in a Time-Dependent Flow.
   Transactions of the American Society of Mechanical
   Engineers; Journal of the Applied Mechanics; Vol.85;
   Series E; pp 13-15; March 1963.

35. Sarpkaya T. and Garrison C.J.

   Vortex Formation and Resistance in Unsteady Flow.
   Transactions of the American Society of Mechanical
   Engineers; Journal of Applied Mechanics; pp 16-24;
   March 1963.

36. Sarpkaya T.

   Separated Flow about Lifting Bodies and Impulsive
   Flow about Cylinders.
   AIAA Journal; Vol.4; No.3; p 414; March 1966.

37. Sarpkaya T.

   An Analytical Study of Separated Flow About Circular
   Cylinders.

Transactions of the American Society of Mechanical Engineers; Journal of the Basic Engineering; Series D; Vol.90; p 511; December 1968.

38. Sarpkaya T. and Isaacson M.

Mechanics of Wave Forces on Offshore Structures.

Van Nostrand Reinhold Company, N.Y.; 1981.

39. Srokosz M.A.

The Submerged Sphere as an Absorber of Wave Power.

Journal of Fluid Mechanics; Vol.95; Part 4; pp 717-741; 1979.

40. Stokes G.G.

On the Effect of the Internal Friction of Fluids on the Motion of Pendulums.

Transactions of Cambridge Philosophical Society; 9; 8; 1851.

41. Verley R.L.P. and Moe G.

The Forces on a Cylinder Oscillating in a Current.

Vassdrags-Og Havnelaboratoriet (VHL) Report STF 60 A79061; The Royal Norwegian Council for Scientific and Industrial Research; 1979.

42. Yavuz T.

Aerodynamics of Parachute and Like Bodies in Unsteady Motion.

Ph.D. Thesis; University of Leicester; 1982.

43. Yavuz T. and Cockrell D.J.

Experimental Determination of Virtual Mass for a Parachute Canopy and Its Significance in Predicting Dynamics Stability Characteristics.

Proceedings of the AIAA 7th Aerodynamic Decelerator

and Balloon Technology Conference; Paper No. 81-1920; San Diego, California; October 1981.

44. Yu Yee-Tack.

Virtual Masses and Moments of Inertia of Discs and Cylinders in Various Liquids.

Journal of Applied Physics; p66; Vol.13; January 1942.

APPENDICES

APPENDIX A

ANALYSIS OF DATA

For each test conducted, a data file is established. Each file contains five channels of data:

1. interruption signals from the switch located on the wheel of the towing carriage,

2. potentiometer output, indicating the position of the crank of the oscillation rig,

3. output from the strain gauge set, for forces in the lateral (normal) direction,

4. output from the strain gauge set, for forces in the axial direction, and

5. output from the strain gauge set for the moment on the test model about the axis perpendicular to the normal and axial directions.

Before any coefficients of forces are calculated, these data are checked for ´unwanted´ signals (noise). After obtaining a ´smooth´ set of data, the net fluid dynamic force is calculated by substracting the drag force on the test sting, and the inertia forces due to moving solid parts. The step-by-step procedure of deriving the force coefficients and the prediction model, for parachute models, is as follows. (Certain steps of this procedure is

by-passed when calculating the force coefficients for cylinder, because of its axisymmetry.)

A.1 VELOCITY AND ACCELERATION OF TEST MODEL

The position of the crank of the oscillation test rig θ, its angular velocity, and angular acceleration are obtained by scanning the output voltage from the potentiometer attached to the crank shaft.
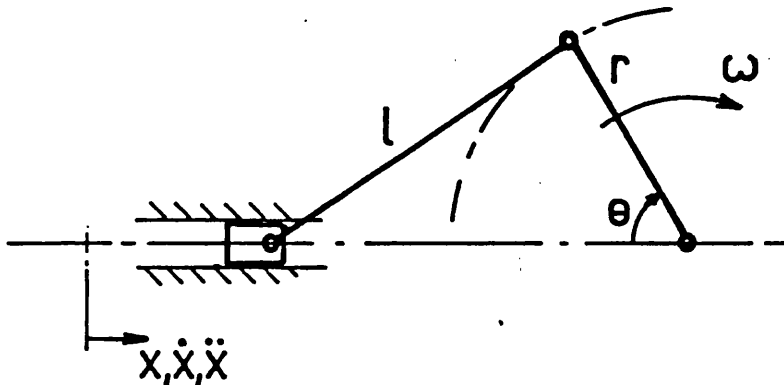
The position of the model, its velocity and acceleration, with respect to the towing carriage are given by,

$$x = (1 + r) - \sqrt{(1^2 - r^2 \sin^2 \theta)} - r\cos\theta$$

$$\dot{x} = \omega r \{ 0.5 \, \frac{r \sin 2\theta}{\sqrt{(1^2 - r^2 \sin^2 \theta)}} + \sin\theta \}$$

$$\ddot{x} = \omega^2 r \{ \frac{r \cos 2\theta}{\sqrt{(1^2 - r^2 \sin^2 \theta)}} + 1/4 \, \frac{r^3 \sin^2 2\theta}{(1^2 - r^2 \sin^2 \theta)^{3/2}} + \cos\theta \}$$

x is vectorially added to the towing carriage speed to obtain the velocity of the model with respect to the earth.

A typical set of time history of motion of the test models appears in figure A.1.

A.2 DATA SMOOTHING

Raw data from experiments contain scatter due to 'electronic noise' of amplifiers, vibration of solid components, etc. Therefore, the results are numerically smoothed before analysing. The smoothing process is carried out in three stages:

1. Scan each channel of data looking for isolated 'spikes'. This is done by comparing each reading with values before and after that. The spikes are identified by 'unusually large' variation between consecutive readings. The overall effect due to removal of these spikes is negligible because the time interval between two consecutive readings is 5 ms.

2. Each reading is compared with the average of eleven readings (five before and five after the concerned reading.) If the difference between the original reading and the average value is greater than two per cent of the full scale deflexion of the A/D converter, the former is replaced by the latter.

3. Each channel of reading is then smoothed by calculating the local average.

The strain gauge output voltage are then converted to to Newtons for forces and to Newton-metres for moment using

calibration formulae obtained by applying static loads on the sting.

A.3 NET FLUID DYNAMIC FORCE ON THE TEST MODELS

It should be noted that the output given by channels 3 and 4 represent the following components:

1. fluid dynamic force on the test model due to its velocity and acceleration,

2. fluid dynamic force on the submerged parts of the test sting, and

3. inertia forces due to the mass of the sting and the mass of the test model.

4. noise due to vibrations etc.

The fluid dynamic force on the test sting is derived from the data obtained by towing the sting without any test model attached to its end, along the length of the ship tank. The inertia forces of the test sting and the test model are obtained using Newton's second law motion. The net fluid dynamic force, therefore, is equal to the total force indicated by the strain gauge output less the fluid dynamic force on the test sting and the inertia force of the test sting and the test model.

A.4 FIRST APPROXIMATION OF QUASI-STEADY MODEL

Having calculated the velocity and acceleration of the test model, and their directions, the first approximation of the quasi-steady model is written by using

the steady flow value of the velocity-dependent force
coefficient and the potential flow value of the acceleration
dependent force coefficient, in equation (1.3). The Fourier
series of the quasi-steady model and that of the
experimental results are used to obtain the moduli and the
arguments of Impulse Response Function associated with the
convolution integral. The 'time-delay' in the IRF is used
to re-estimate the force coefficients.

The process is repeated until the values of force
coefficients and Impulse Response Function for the best fit
on experimental results are obtained. The flow chart
illustrating the process of analysing data is given below.

```
                    ( START )
                        |
                        v
        +-------------------------------+
        | Scan  channel  1  and         |
        | obtain  the  speed of         |
        | the towing carriage           |
        +-------------------------------+
                        |
                        v
        +-------------------------------+
        | Scan channel 2 and obtain the |
        | frequency of oscillation of the|
        | test rig.    The potentiameter |
        | output recorded in this channel|
        | gives the position of the crank|
        | angle, which  is  then used to |
        | calculate  the  velocity  and  |
        | acceleration of the model.     |
        +-------------------------------+
                        |
                        v
        +-------------------------------+
        | Check  each  number in channels|
        | 3,4  &  5  individually  by    |
        | comparing  with  numbers before|
        | and  after  that.  Remove from |
        | the data file any 'noise' given|
        | as spikes.                     |
        +-------------------------------+
                        |
                        v
        +-------------------------------+
        | Smooth data channels 3,4 & 5 by|
        | calculating   local   average |
        | values.                        |
        +-------------------------------+
                        |
                        v
        +-------------------------------+
        | Convert raw data into forces(N)|
        | or            moments(Nm),     |
        | correspondingly,         using |
        | calibration formulae.          |
        +-------------------------------+
                        |
                        v
        +-------------------------------+
        | Calculate    velocity     and  |
        | acceleration of the test model,|
        | in   the   normal   and   axial|
        | directions,  and  its  angle of|
        | attack.                        |
        +-------------------------------+
                        |
                        v
        +-------------------------------+      +-------------------------+
        | Substract,  from  the  recorded|      | Read            first   |
        | force,  the  drag  force on the|      | approximations of the   |
        | test sting,  and the force due |      | force coefficients.     |
        | to   inertia  of  moving solid |      +-------------------------+
        | parts.                         |                   |
        +-------------------------------+                   |
                        |                                   |
                        v<----------------------------------+
        +-------------------------------+
        | Calculate   the   terms   on  the|
        | left-hand-side of eq.3.3a using |
        | available    values       of   |
        | coefficients.                  |
        +-------------------------------+
                        |
                        v
        +-------------------------------+
        | Obtain Fourier series  of the  |
        | actual  force  and  the Fourier|
        | series of the terms in eq. 3.3a|
        | & 3.3b.                        |
        +-------------------------------+
                        |
                        v
        +-------------------------------+
        | Calculate the modulus          |
        | and  the  phase angle          |
        | cf the IRF using,              |
        |                                |
        |            B  cos(nωt+Ψ )      |
        |            n            n      |
        | G(inω) = ---------------       |
        |            A  cos(nωt+φ )      |
        |            n            n      |
        +-------------------------------+
                        |
                        v
```

$$G(in\omega) = \frac{B_n \cos(n\omega t + \Psi_n)}{A_n \cos(n\omega t + \phi_n)}$$

```
                    │                                              ▲
                    ▼                                              │
┌─────────────────────────────┐                                   │
│ Plot modulus and phase angle │                                  │
│ of IRF, against the frequency│                                  │
│ of excitation.               │                                  │
└─────────────────────────────┘                                   │
                    │                                              │
                    ▼                                              │
┌─────────────────────────────┐                                   │
│ Derive the value of          │                                  │
│ time-delay (τ) from          │                                  │
│ these graphs (given          │                                  │
│ by the gradient of           │                                  │
│ phase v. freq. plot)         │                                  │
└─────────────────────────────┘                                   │
                    │                                              │
                    ▼                                              │
┌─────────────────────────────┐                                   │
│ Re-write          the        │                                  │
│ empirical                    │                                  │
│ relationship  for the        │                                  │
│ force.                       │                                  │
└─────────────────────────────┘                                   │
                    │                                              │
                    ▼                                              │
┌─────────────────────────────┐                                   │
│ Plot, for each test          │                                  │
│                              │                                  │
│         F(t)                 │                                  │
│   ──────────────────         │                                  │
│   1/2ρAU(t-τ)|U(t-τ)|        │                                  │
│                              │                                  │
│   versus                     │                                  │
│                              │                                  │
│       ρ∀U(t-τ)               │                                  │
│   ──────────────────         │                                  │
│   1/2ρAU(t-τ)|U(t-τ)|        │                                  │
└─────────────────────────────┘                                   │
```

$$\frac{F(t)}{1/2\rho AU(t-\tau)|U(t-\tau)|}$$

versus

$$\frac{\rho \forall U(t-\tau)}{1/2\rho AU(t-\tau)|U(t-\tau)|}$$

From these graphs, obtain C_M, C_T, k_{11} & k_{33} as functions of α

Calculate C_T v. α from lateral oscillations tests.

Do you want to improve the value of τ?   —— yes / no

Use latest data for C_M & C_T, to re-calculate k_{11} & k_{33} as functions of α & A_n.

Use latest data for k_{11} & k_{33} to re-calculate C_M & C_T.

Write the empirical relationship for the force in unsteady motion.

Does the prediction model agree with the actual force?   —— poor correlation

good correlation

(STOP)

Figure A.1   History of motion in typical tests.

APPENDIX B

NATURAL FREQUENCIES OF VIBRATION,

AND VORTEX SHEDDING FREQUENCIES

It can clearly be seen from figures 5.1, 5.2, 5.3 and 5.4 that the strain gauge output signals represent not only the fluid dynamic forces and moments, but vibrations due to natural frequencies, vortex shedding, electronic noise etc.

B.1 NATURAL FREQUENCIES OF VIBRATION

An approximate analysis of the vibrations in the linear and angular directions are included in this section.

B.1.1 Vibration for Bending (of the sting)

With a model of mass M at the end of the sting, the natural frequency of vibration in air is given by

$$\omega = \sqrt{\frac{k}{(M_1 + M) + 0.23m}}$$

where, k = the stiffness of the test-sting-rod $(3EI/L^3 = 13.15 \times 10^3$ N/m)

E = Young's modulus $(200 \times 10^9$ N/m$^2)$

I = second moment of area of sting cross section($\pi\{d_o^4-d_i^4\}/64$ = $1.76\text{x}10^{-8}$ m^4)

L = length of the test sting

m = mass per unit length of sting (1.22 kg/m run)

M_1 = mass of the extension piece for supporting the model (see figure 4.4)

Therefore,

$$\omega = \sqrt{\frac{13.15\text{x}10^3}{0.523 + M}} \quad \text{rad/sec.}$$

e.g. for a circular cylinder with mass of 10.775 kg the natural frequency in air:

$$\omega = 34.12 \text{ rad/sec.} = 5.43 \text{ Hz.}$$

Figure 5.9b gives an added mass coefficient of 2.4 (therefore, 25.9 kg.) Neglecting damping effects the natural frequency in water is given by

$$\omega' = 18.8 \text{ rad/sec.} = 3 \text{ Hz.}$$

The lowest frequency of vibration in water for each test model using average coefficients of acceleration-dependent force (from figures 5.27 to 5.31) are:

Rectangular block: ≈ 3.2 Hz.

Cruciform parachute: ≈ 4.2 Hz.

Ring-slot parachute: ≈ 3.5 Hz.

B.1.2 Torsional Vibration:

The moment of inertia of the cylinder = 0.1043 M

= 1.124 kg m^2 (in air)

Torsional inertia of M_1 = 0.0202 kg m^2

Angular stiffness of sting = GJ/L

= 2.92x10^3 Nm/rad

where, G is the rigidity modulus(77x10^9 N/m^2) of sting and J the polar second moment of area ($\pi(d_o^4 - d_i^4)/32$ = 3.527x10^{-8} m^4)

$$\omega = \sqrt{\frac{k}{0.0202 + 0.1043 M}}$$

where M = 10.775 kg.

The natural frequency of torsional vibration in air is 8.04 Hz and that in water (with added mass = 25.9 kg) is 4.4 Hz.

B.2 VORTEX SHEDDING FREQUENCY

e.g.   Cylinder in laminar (steady) flow:

Strouhal No. = nD/U ≈ 0.2

where, n is the vortex shedding frequency, D the diameter of the cylinder and U the free-stream velocity.

Therefore, n ≈ 1.8U   (for D=0.114m)

For an average speed of 0.35 m/sec. the vortex shedding frequency is 0.6 per second.

B.3 REMARKS

The analysis outline above give only approximate frequencies because the damping effects have not been taken into account. The actual frequencies of vibration are expected to be slightly less than these values.

APPENDIX C

IMPULSE RESPONSE FUNCTION

C.1 CONVOLUTION INTEGRAL

An arbitrary input (e.g. the velocity function of a flow field) of a system, given by $I(t)$, can approximately be expressed by a series of impulse functions as $I_1(t)$, $I_2(t)$, $I_3(t)$,..... having impulse widths Δt_1, Δt_2, Δt_3,..... respectively (Fig. C.1). Using the convolution integral the response $R(t)$ at any instant t, due to this input (e.g. force on a submerged body due to the velocity function) can be written as

$$R(t) = R_1(t) + R_2(t) + R_3(t) + \ldots \ldots \quad (C.1)$$

where,

$$R_1(t) = \int_{-t_1}^{t} G(t-\tau)\, I_1(\tau)\, d\tau$$

$$R_2(t) = \int_{-t_2}^{t} G(t-\tau)\, I_2(\tau)\, d\tau \qquad \text{etc.}$$

are the responses due to each impulse $I_1(t)$, $I_2(t)$,..... respectively. The function $G(t)$ is the Impulse Response Function of the system.

In the convolution integral method, the initial values of the problem are taken into account by the limits of the integration; i.e. $I(t) = 0$ for $t < t_1$ etc. In the case of $I(t)$ sustained over long period of time, $t \to -\infty$.

The integral also implies that 'future' values of $I(t)$ cannot affect 'earlier' values of $R(t)$. It also reflects that for a physically realizable system, the instantaneous effects of the output $R(t)$ are ruled out.
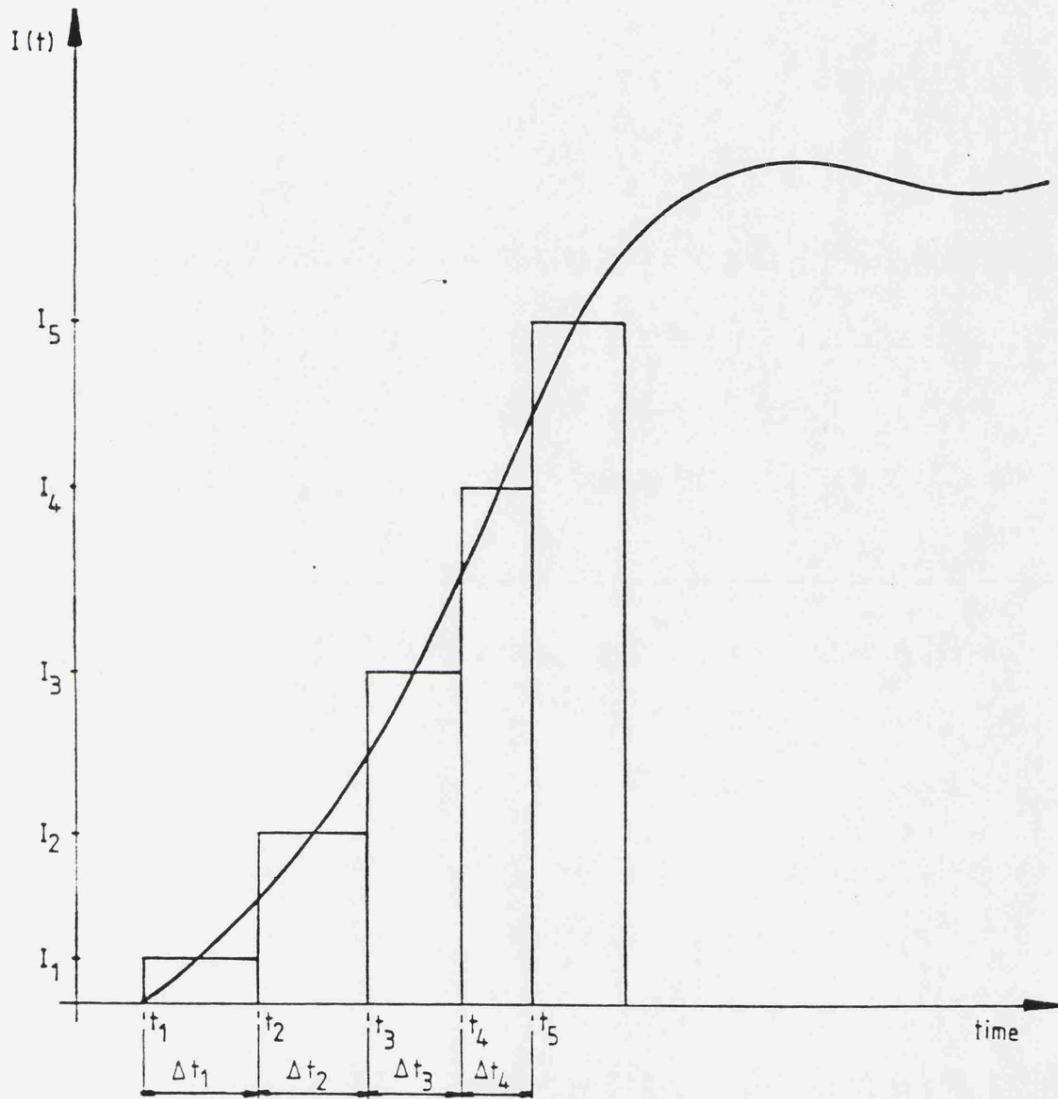
Figure C.1   An arbitrary function I(t) described
by a series of impulses.

APPENDIX D

ANALYSES OF UNCERTAINTIES

D.1 FOURIER SERIES PRESENTATION OF DATA

As described in Chapter 3, the Impulse Response Function (IRF) of a bluff body, moving unsteadily in a fluid, is evaluated by transforming the time series of the effects due to the motion, and the time series of the measured force due to this motion into two Fourier series. The IRF is derived by considering the harmonic frequencies, of both motion and fluid dynamic force, one at a time. It is realised from the figures 5.5, 5.6, 5,7 and 5.8 that the IRF can be expressed as a delayed impulse only for frequencies up to about 3 rad/sec. For higher frequencies the behaviour of the IRF is quite arbitrary. Therefore, the prediction model, given by equation (5.1) is representative only for low frequencies. Thus equation (5.1) can effectively be applied to predict unsteady fluid dynamic forces only if the components of the total force due to high frequencies are negligible.

Given in Table D.1 are the percentages of high frequency components in the total fluid dynamic force derived using equation (5.1).

D.2 STRENGTH OF SIGNAL CARRIED BY VORTEX SHEDDING, NATURAL

FREQUENCY VIBRATIONS ETC.

The vortex shedding frequencies, as discussed in Appendix B, are of the order of about O.6 Hz. (about 3.5 rad/sec) The natural frequencies of vibration have effects beginning from about 3 Hz. The individual effects cannot be separately because the forces due to natural vibrations can occur at their harmonic frequencies as well. Any form of recorded force with frequencies above 3 rad/sec is regarded as due to vortex shedding, or natural frequencies of vibration, or system noise. They are separated from what is considered as the main fluid dynamic force, using Fourier series, simply by discarding the higher order terms. The magnitude of these high frequency forces, as percentages of the total measured forces, are given in Table D.1.

D.3 UNCERTAINTY OF EXPERIMENTAL METHODS

The experimental uncertainty during the present investigation is regarded as due to two reasons: (a) the 'noise' associated with the apparatus and (b) uncertainty due to inconsistency in the repeated measurements.

D.3.1 Noise Level of the Equipmemts

The average noise level produced by the equipment used for amplifying and recording data is estimated by the variation of the recorded readings for a given steady input signal.

$$\frac{\text{noise}}{\text{signal}} = \sum_{i=1}^{n} |X_i - \bar{X}| \ / \ \text{F.S.D.}$$

Where X_i is the ith reading,

$\bar{X}$ is the average of X_i and

F.S.D. is the full scale deflexion.

The average 'noise/signal' ratio, as a percentage of the full scale deflexion is found to be 0.63%. The maximum value of the noise/signal ratio recorded was 0.8%.

D.3.2 Experimental Uncertainty

The experimental uncertainty is derived by considering the measurements repeated under the same conditions. The uncertainty is expressed as $\sigma_{n-1}/\bar{X}$ where σ_{n-1} and $\bar{X}$ are the sample standard deviation and the mean value of n number of repeated readings. The sample standard deviation associated with of each test model is given in Table D.2.

D.4 DEVIATION OF THE PREDICTION MODEL

Once the prediction model is established in the form given by equation (5.1), the experimentally measured forces are compared with the forces reproduced by equation (5.1), so that the success of the application of this model can be assessed. The reliability to which the model can be applied is given by the deviation of the modelled force from the experimentally measured force (as a percentage of measured force). This 'error' is defined in the form of the sum of the deviation per unit force as:

$$\text{Deviation} = \sum_{i=1}^{n} |X_i(t) - X_i'(t)| \; / \; \sum_{i=1}^{n} |X_i(t)|$$

where,

n is the number of experimental reading considered,

$X_i(t)$ is the actual fluid dynamic force on the test model, and

$X_i'(t)$ is the force estimated by the prediction model (eq. 5.1)

The deviations of the forces modelled for each body are given in Table D.1.

D.5 BLOCKAGE EFFECTS

The blockage effect on each test model, is defined as the ratio of cross sectional area of the test model to that of the ship tank. These ratios are given in Table D.3.

D.6 FREE SURFACE EFFECTS

The submerged Froude number $\{U/\sqrt{(gh)}\}$ the test model is approximately equal to 0.13, where U is the average speed of the test model, g the acceleration of gravity and h the distance from the free surface to the model. The ratio of L/2h where L is the characteristic length of each test model, is given in Table D.3.

Test Model	direction of force	high frequency components as % of total force	high frequency components of measured force	deviation of predicted force	lateral osc. force / in-line force
circular cylinder (in-line oscillations)	lateral				45%
	in-line	4%	11%	17%	
rectangular block (lateral oscillations)	lateral	14%	17%	11%	
	axial	7%	9%		
rectangular block (in-line oscillations)	lateral				5%
	axial	6%	10%	13%	
cruciform parachute (lateral oscillations)	lateral	12%	17%	14%	
	axial	9%	13%		
cruciform parachute (in-line oscillations)	lateral	5%	24%*	22%	2%
	axial	7%	17%		
ring-slot parachute (lateral oscillations)	lateral	8%	14%	19%	
	axial	8%	9%		
ring-slot parachute (in-line oscillations)	lateral	6%	46%*	24%	2%
	axial	8%	13%		

Table D.1 The effect of high frequency force components, and the deviation of the modelled forces from the measured forces.

* Lateral forces for in-line oscillations at small angles of attack.

Test model	Sample Standard deviation
	Arithmetical mean
Circular Cylinder	0.18
Rectangular Block	0.11
Cruciform Parachute	0.10
Ring-slot Parachute	0.05

Table D.2 Experimental uncertainty of measurements.

Test Model	Blockage	L/2h
Circular Cylinder	0.017	0.08
Rectangular Block	0.004	0.1*
Cruciform Parachute	0.008	0.17
Ring-slot Parachute	0.012	0.22

Table D.3 Blockage and distance from free surface.

* Using the height of the test model as L.

APPENDIX E

OPTIMISING FORCE COEFFICIENTS WITH τ=0

E.1 INTRODUCTION

In periodic motion, the acceleration of the body always leads the velocity. Thus, if large values of accleration-dependent forces are derived to satisfy the characteristics of the measured forces, shown in figures 5.40 to 5.43, this inevitably leads to a phase-lead, or time-lead in the modelled force, hence requiring a term similar to τ as a compensating parameter. Conversely, if the relative magnitude of the acceleration-dependent force is low, the value of ι becomes smaller. The velocity-dependent force under these circumstances may require adjustment to obtain the necessary magnitude of the total force. Thus by applying suitable values of (C_R/k) one may be able to make τ equal to zero, and optimise only the values of C_R and k. Although this method would produce a less satisfactory fit to the experimental results, it has the advantage of dealing with equation (1.3) which includes only two experimentally determined parameters.

E.2 OPTIMISING WITH ONLY TWO FORCE COEFFICIENTS

The effect due to lowering the acceleration-dependent force is achieved by suitably deviding the coefficients of acceleration-dependent force (k) given in figures 5.35 to 5.39 by a constant p, where p=2,4,8 & ∞. This method would show the effect on the fluid dynamic force for a range of values of k. For p=∞ the acceleration-dependent force is zero, thus the fluid dynamic force is modelled based on a single coefficient as C_R 1/2ρA U|U|. The velocity-dependent force coefficients shown in figures 5.29 to 5.34 are suitably increased during this process to allow for the reduction in the acceleration-dependent force. Hence, the unsteady fluid dynamic forces are modelled using equation (1.3) by varying the ratio of (C_R/k) in order to obtain the best fit to the experimental results. The deviation of the forces thus modelled, for p = 2,4,8 and ∞ are shown in Table E.1. Examples of forces produced using these optimised values of C_R and k are shown in figures E.1 to E.4.

The agreement between the measured force and the force modelled using equation (1.3) can be improved by suitably adjusting the magnitudes of C_R and k. The deviation of the modelled force from the measured force appears to increase for high values as well as very low values of the acceleration-dependent forces.

It can be seen in Table E.1 that the agreement between the measured forces and the forces modelled using equation (1.3) with optimised C_R and k is less satisfactory

than the agreement obtained by introducing the time delay term τ. This may well be due to the fact that the measured force has a noticeable second order harmonic behaviour near the mean value, as can be seen clearly in figures 5.42 and 5.43. These characteristics represent high values of acceleration-dependent forces which consequently lead to a time-lead in the part of the modelled force. Hence a better fit to the experimental results can be achieved by using the term τ which represents the time-delay of the measured force relative to the modelled force.

It can also be seen in Table E.1 that the improvements made by equation (5.1) in modelling unsteady forces for in-line oscillation is rather small because the velocity-dependent forces in these cases are much larger than the acceleration-dependent forces. Hence the effect of the acceleration-dependent force on the total fluid dynamic force is very low. Nevertheless, for lateral oscillation the unsteady forces modelled by equation (5.1) appear to be much better than those modelled by equation (1.3).

(a) for p=2.8

(b) for p=8.0

Figure E.1 Forces on circular cylinder modelled by equation (1.3).

+ + + + +　　　　experimental
―――――　　　　equation (1.3)

Figure 5.40 Forces on the circular cylinder in in-line oscillation.

+ + + + +　　　　experimental
―――――　　　　equation (5.1)
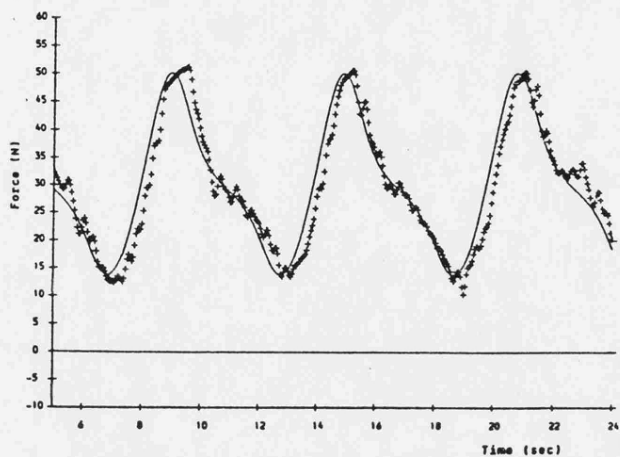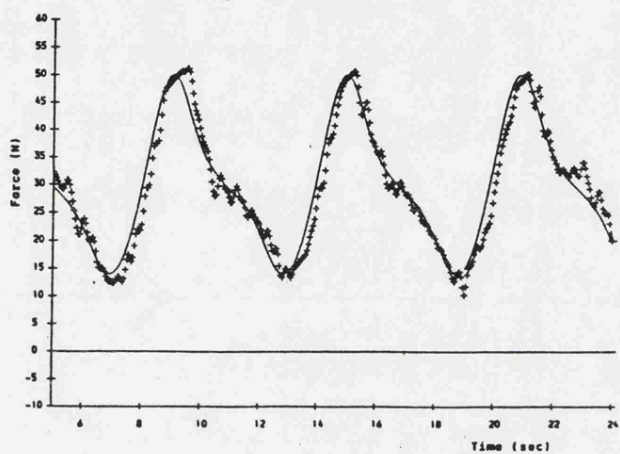
(a) for p=2.0

(b) for p=8.0

Figure E.2 Forces on rectangular block modelled by equation (1.3).
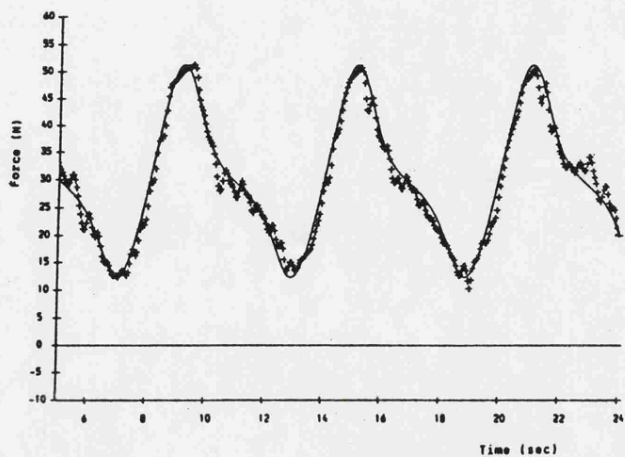
+ + + + + experimental
——————— equation (1.3)

Figure 5.41 Forces on the rectangular block in in-line oscillation.

+ + + + + experimental
——————— equation (5.1)
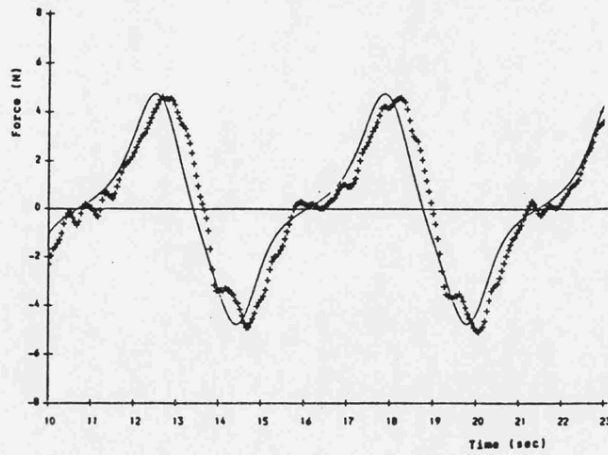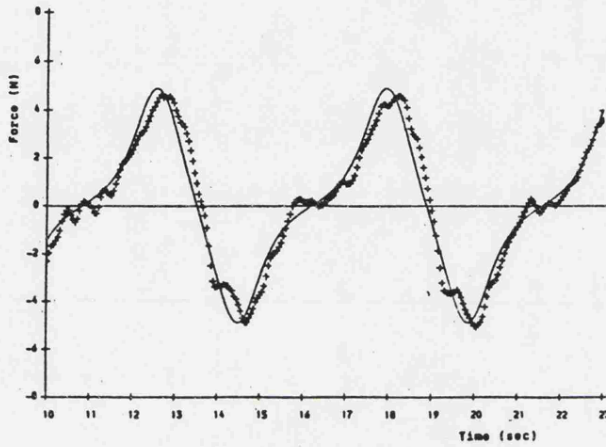
(a) for p=2.0

(b) for p=8.0

Figure E.3 Forces on cruciform parachute modelled by equation (1.3).
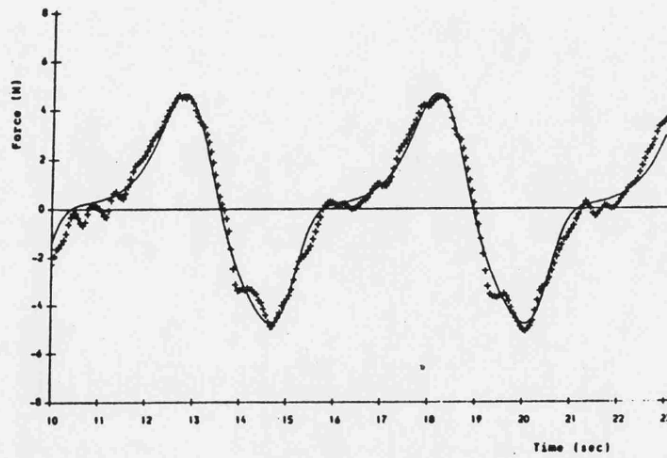
+ + + + +   experimental
————————   equation (1.3)

Figure 5.42 Forces on the cruciform parachute in lateral oscillation.

+ + + + +   experimental
————————   equation (5.1)
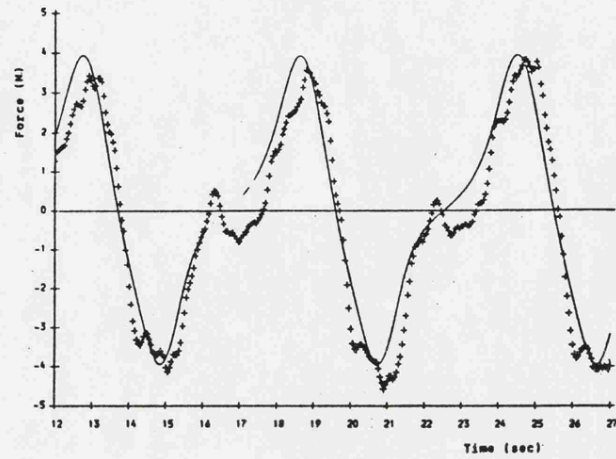
(a) for p=2.0
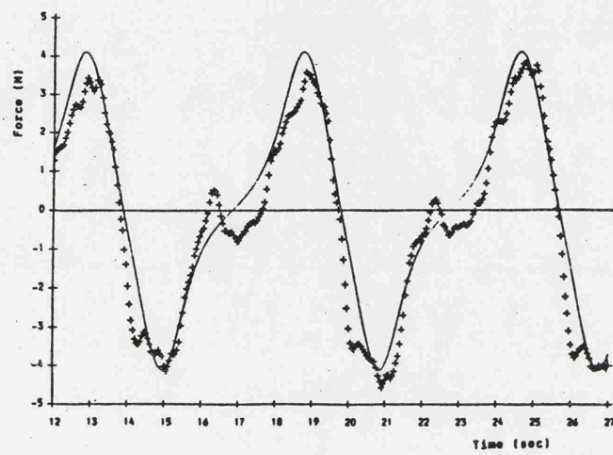

(b) for p=8.0

Figure E.4 Forces on ring-slot parachute modelled by equation (1.3).
+ + + + +   experimental
————————   equation (1.3)
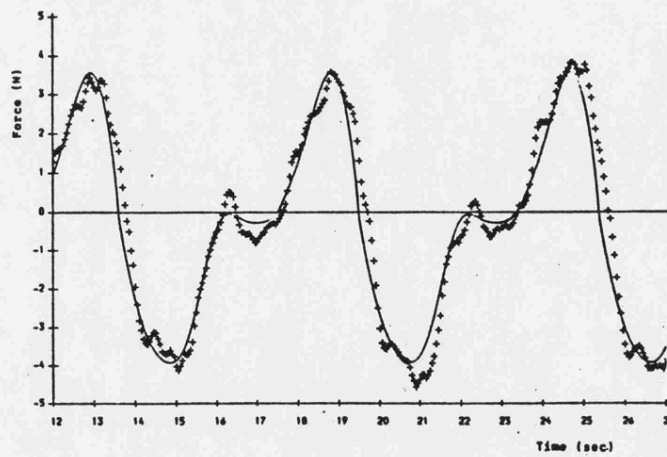
Figure 5.43 Forces on the ring-slot parachute in lateral oscillation.
+ + + + +   experimental
————————   equation (5.1)

Test model	Mode of motion	p (factor by which acc-dep. forces are decreased)*				forces modelled by eq. (5.1)
		2	4	8	∞	
Circular Cylinder	in-line osc.	18%	17.8%	17.7%	17.8%	17.1%
Rectangular Block	lateral osc.	26%	24.9%	24.2%	24.1%	11%
	in-line osc.	14.4%	14.3%	14.2%	14.2%	13.2%
Cruciform Parachute	lateral osc.	29%	23.6%	19%	19.5%	14%
	in-line osc.	25.4%	24.9%	24.8%	25.1%	22%
Ring-Slot Parachute	lateral osc.	32%	29.6%	28.1%	30.2%	19%
	in-line osc.	27.4%	27%	27.9%	28.1%	24%

Figure E.1   Deviation of the forces modelled using equation (1.3) by optimising C_R and k, from the experimentally measured forces.
*p is the factor by which the coefficients in figures 5.35 to 5.39 are devided in order to obtain a range of values of the ratio (C_R/k)

UNSTEADY FLUID FLOW AROUND CERTAIN BLUFF BODIES
by   S.J. Polpitiye

ABSTRACT

It is shown in this thesis that fluid dynamic forces on unsteadily moving bluff bodies depend on the history of motion as much as on the velocity and acceleration of motion. An empirical relationship between the motion of the body and the resulting force is obtained by analysing the effect of the history of motion on the fluid dynamic force at any instant.

The fluid dynamic force, velocity and acceleration are obtained as functions of time, by oscillating test models in water while they are being towed at constant speed. The test models used are:
1. a two-dimensional circular cylinder,
2. a rectangular block with square frontal area and fineness ratio of 3:1,
3. a cruciform parachute canopy with arm ratio of 4:1, and
4. a ring-slot parachute canopy.

The functions by which the history of flow affects the future forces, are evaluated by using the Convolution Integral. The results show that the effects due to history of both velocity and acceleration are by no means negligible, that is the velocity and the acceleration at a specific time prior to any instant is so domineering that the fluid dynamic force can approximately be expressed as being delayed by this period of time. This 'time-delay', or time lag (as opposed to phase-lag) in the part of the measured force is found to be independent of the frequency of excitation. In the light of this evidence, a prediction model is suggested for estimating unsteady fluid forces. The data required for the application of this prediction model are obtained experimentally.

Chapter One of this thesis gives a brief explanation of the historical background of unsteady fluid dynamics. The effects of acceleration on the fluid dynamic force, in both ideal and real fluids, are discussed in Chapter Two. Explained in Chapter Three are the techniques used for building the force prediction model, and data acquisition. The experimental procedure is explained in Chapter Four. Chapter Five gives the empirical form of the prediction model, and some data that are used in association with this model.